การเพิ่มหมู่ฟังก์ชันบนพื้นผิวคาร์บอนนาโนฮอร์น และการประยุกต์ใช้งานเป็นตัวเร่งปฏิกิริยา

นางสาวชมพูพิชญ์ เติมวิชชากร

วิทยานิพนธ์นี้เป็นส่วนหนึ่งของการศึกษาตามหลักสูตรปริญญาวิศวกรรมศาสตรดุษฎีบัณฑิต
สาขาวิชาวิศวกรรมเคมี ภาควิชาวิศวกรรมเคมี
คณะวิศวกรรมศาสตร์ จุฬาลงกรณ์มหาวิทยาลัย
ปีการศึกษา 2560

Functionalization of carbon nanohorns and their catalysis applications

Miss Chompoopitch Termvidchakorn

A Dissertation Submitted in Partial Fulfillment of the Requirements
for the Degree of Doctor of Engineering Program in Chemical Engineering
Department of Chemical Engineering
Faculty of Engineering
Chulalongkorn University
Academic Year 2017

Thesis Title	Functionalization of carbon nanohorns and their catalysis applications
By	Miss Chompoopitch Termvidchakorn
Field of Study	Chemical Engineering
Thesis Advisor	Associate Professor Tawatchai Charinpanitkul, D.Eng.
Thesis Co-Advisor	Kajornsak Faungnawakij, D.Eng.
	Professor Noriaki Sano, Ph.D.

Accepted by the Faculty of Engineering, Chulalongkorn University in Partial Fulfillment of the Requirements for the Doctoral Degree

.....Dean of the Faculty of Engineering
(Associate Professor Supot Teachavorasinskun, D.Eng.)

THESIS COMMITTEE

.....Chairman
(Associate Professor Varong Pavarajarn, Ph.D.)

.....Thesis Advisor
(Associate Professor Tawatchai Charinpanitkul, D.Eng.)

.....Thesis Co-Advisor
(Kajornsak Faungnawakij, D.Eng.)

.....Thesis Co-Advisor
(Professor Noriaki Sano, Ph.D.)

.....Examiner
(Assistant Professor Apinan Soottitantawat, D.Eng.)

.....Examiner
(Chalida Klaysom, Ph.D.)

.....External Examiner
(Nawin Viriya-empikul, D.Eng.)

ชมพูพิชญ์ เติมวิชชากร : การเพิ่มหมู่ฟังก์ชันบนพื้นผิวคาร์บอนนาโนฮอร์น และการประยุกต์ใช้งานเป็นตัวเร่งปฏิกิริยา (Functionalization of carbon nanohorns and their catalysis applications) อ.ที่ปรึกษาวิทยานิพนธ์หลัก: รศ. ดร. ธวัชชัย ชรินพาณิชกุล, อ.ที่ปรึกษาวิทยานิพนธ์ร่วม: ดร. ขจรศักดิ์ เฟื่องนวกิจ, ศ. ดร. โนริเอกิ ซะโน, หน้า.

งานวิจัยนี้มุ่งศึกษาการเพิ่มหมู่ฟังก์ชันบนพื้นผิวคาร์บอนนาโนฮอร์นซึ่งผลิตโดยวิธีการอาร์คไฟฟ้าในน้ำ ในงานวิจัยนี้ประสบความสำเร็จในการเพิ่มหมู่ฟังก์ชันของโลหะ(นิกเกิล ทองแดง เหล็ก แพลเลเดียม และแพลทินัม) หมู่ฟังก์ชันของโลหะผสม (นิกเกิลทองแดง นิกเกิลเหล็ก นิกเกิลแพลเลเดียม และ นิกเกิลแพลทินัม) รวมถึงการปรับพื้นผิวด้วยการให้ความร้อนและการเพิ่มหมู่ฟังก์ชันของกรดลงบนพื้นผิวคาร์บอนนาโนฮอร์น ผลของการปรับเปลี่ยนปริมาณโลหะที่เติมลงไปและเงื่อนไขของการเพิ่มหมู่ฟังก์ชันต่อวัสดุผสมที่ได้นั้นถูกนำไปวิเคราะห์สมบัติโดยใช้กล้องจุลทรรศน์อิเล็กตรอนแบบส่องผ่าน, เทคนิคเอกซเรย์สเปคโตรสโคปแบบกระจายพลังงาน เทคนิคการเลี้ยวเบนรังสีเอกซ์ เทคนิคการดูดซับก๊าซไนโตรเจน เทคนิคฟูเรียร์ทรานส์ฟอร์มอินฟราเรดสเปคโตรสโคปี และเทคนิคการคายซับก๊าซแอมโมเนียด้วยโปรแกรมอุณหภูมิ อีกทั้งยังมีการศึกษาการนำวัสดุผสมดังกล่าวไปใช้เป็นตัวเร่งปฏิกิริยาใน 3 ปฏิกิริยาที่ต่างกันคือ การเปลี่ยนน้ำตาลไซโลสเป็นสารประกอบเฟอร์ฟูรัลโดยปฏิกิริยาการควบแน่น การเปลี่ยนกรดเลวูลินิคเป็นเอทิลเลวูลิเนทโดยปฏิกิริยาเอสเทอริฟิเคชันและการเปลี่ยนเมททิลเลวูลิเนทเป็นสารแกมมาวาริโลแลคโตนโดยปฏิกิริยาการเติมไฮโดรเจน โดยพิจารณาด้านคุณภาพและเสถียรภาพของตัวเร่งปฏิกิริยารวมไปถึงหน้าที่ของตัวเร่งปฏิกิริยาดังกล่าวในแต่ละปฏิกิริยาอีกด้วย

ภาควิชา	วิศวกรรมเคมี	ลายมือชื่อนิสิต .....
สาขาวิชา	วิศวกรรมเคมี	ลายมือชื่อ อ.ที่ปรึกษาหลัก .....
ปีการศึกษา	2560	ลายมือชื่อ อ.ที่ปรึกษาร่วม .....
		ลายมือชื่อ อ.ที่ปรึกษาร่วม .....

5671408021 : MAJOR CHEMICAL ENGINEERING
KEYWORDS: CARBON NANOHORNS / FUNCTIONLIZATION / CATALYST / HYBRIDIZED / ACID TREATMENT / DEHYDRATION / HYDROGENATION / ESTERIFICATION

CHOMPOOPITCH TERMVIDCHAKORN: Functionalization of carbon nanohorns and their catalysis applications. ADVISOR: ASSOC. PROF. TAWATCHAI CHARINPANITKUL, D.Eng., CO-ADVISOR: KAJORNSAK FAUNGNAWAKIJ, D.Eng., PROF. NORIAKI SANO, Ph.D., pp.

Carbon nanohorns (CNHs) synthesized by gas-injected arc-in-water method were functionalized in this study. Metal (Ni, Cu, Fe, Pd, and Pt) and their alloy (NiCu, NiFe, NiPd, and NiPt) hybridized with CNHs were successfully produced. In addition, thermal and acid treatment was applied on the hybridized materials. Effect of metal loading and functionalizing conditions on characteristics of CNHs and functionalized CNHs was examined based on transmission electron microscope (TEM), energy-dispersive X-ray spectroscopy (EDX), X-ray diffraction (XRD), N_2 sorption, Raman spectroscopy, Fourier transform infrared (FT-IR) spectrometer, temperature programmed desorption of ammonia (NH_3-TPD) analysis. The functionalized CNHs were applied as a catalyst in 3 difference reactions, namely dehydration of xylose to furfural, esterification of levulinic acid to ethyl levulinate, and transfer hydrogenation of methyl levulinate to γ-valerolactone. Performance and stability of the catalyst was investigated. Moreover, role of the catalyst in each reaction were also discussed.

Department:	Chemical Engineering	Student's Signature .....
Field of Study:	Chemical Engineering	Advisor's Signature .....
Academic Year:	2017	Co-Advisor's Signature .....
		Co-Advisor's Signature .....

ACKNOWLEDGEMENTS

I would like to express my sincere gratitude to my advisor, Associate Professor Dr. Tawatchai Charinpanitkul, for his kindness, guidance and supported to me, and to my thesis co-advisor, Dr. Kajornsak Faungnawakij, for his kindness, invaluable suggestion, comments and support. Furthermore, I also would like to express my sincere gratitude to another co-advisor, Professor Dr. Noriaki Sano who kindly take care, supported, and suggested me during and after research in Kyoto university, Japan.

I am also gratefully thank to Associate Professor Dr. Varong Pavarajarn, Assistant Professor Dr. Apinan Soottitantawat, Dr. Chalida Klaysom, and Dr. Nawin Viriya-Empikul for their useful comments and participation as the thesis committee.

In addition, I would like to thank Ms. Pusanisa Patrachotesawate, all of previous and present members of Center of Excellence in Particle Technology (CEPT) CU, and all members of Nanomaterials for Energy and Catalysis Laboratory (NEC) NSTDA for their help, suggestion and warm collaborations.

Furthermore, for the financial support from Doctoral Degree Chulalongkorn University 100th Year Birthday Anniversary scholarship, Overseas Research Experience Scholarship for Graduate Student, Graduate School, Chulalongkorn University, National Nanotechnology Center (NANOTEC), National Science and Technology Development Agency and the Collaboration Hubs for International Program (CHIRP) of Strategic International Collaborative Research Program (SICORP), Japan Science and Technology Agency (JST) and the JASTIP program–WP2 (NSTDA-Kyoto University collaboration) are also acknowledged.

Finally, I would like to express my greatest gratitude to my parents for their continuous support, encouragement, and understanding during the whole period of my education.

CONTENTS

Page
THAI ABSTRACT iv
ENGLISH ABSTRACT v
ACKNOWLEDGEMENTS vi
CONTENTS vii
LIST OF TABLES xi
LIST OF FIGURES xiii
Chapter I INTRODUCTION 1
1.1 Background and motivation 1
1.2 Objective of the research 3
1.3 Scopes of the research 3
1.4 Expected benefit 4
Chapter II FUNDAMENTAL THEORY AND LITERATURE REVIEW 5
2.1. Carbon nanomaterial 5
2.1.1. Carbon nanohorns (CNHs) 7
2.2. Gas-injected arc-in-water technique 8
2.3. Bimetallic material 8
2.4. Functionalization 9
2.4.1. Alloy loading 9
2.4.1.1. Ni-base alloy 9
2.4.1.2. PtPd alloy 9
2.4.1.3. Metal/alloy supported on CNHs 12
2.4.2. Acid treatment 13
2.5. Catalytic biomass conversion 15
2.5.1. Carbon material as catalyst and catalyst support for converting biomass to valuable products. 16
Chapter III EXPERIMENTAL 18
3.1. Chemicals & Materials 18
3.2. Methods 19

Page

3.2.1. Synthesis and functionalization of CNHs....19
3.2.1.1. Synthesis of CNHs....19
3.2.1.2. Mono-functional group....20
3.2.1.1.1. Hybridized with metal/alloy....20
3.2.1.1.1.1. Metal (Ni, Cu, Fe, Pd, Pt) hybridized with CNHs....20
3.2.1.1.1.2. Alloy (NiCu, NiFe, NiPd, NiPt, PdPt) hybridized with CNHs....21
3.2.1.1.2. Oxidation in air....22
3.2.1.1.3. Acid treatment....22
3.2.1.3. Multi-functional groups....24
3.2.1.1.1. Oxidation in air on metal/alloy hybridized with CNHs....24
3.2.1.1.2. Acid treatment on metal hybridized with CNHs....24
3.2.2. Post-treatment process....24
3.2.3. Characterization....24
3.2.3.1. Morphology by field-emission scanning electron microscope (FE-SEM)....24
3.2.3.2. Morphology by Transmission electron microscope (TEM)....25
3.2.3.3. Composition of the sample by energy-dispersive X-ray spectroscopy (EDX)....26
3.2.3.4. Phase and crystal structure by X-ray diffraction (XRD)....26
3.2.3.5. Specific surface area and pore structure by N_2 sorption combined with Brunauer-Emmett-Teller (BET) and pore analysis approaches....27
3.2.3.6 Carbon atom arrangement by Raman spectroscopy....27
3.2.3.7. Surface functional groups by Fourier transform infrared (FT-IR) spectrometer....28
3.2.3.8. Acidity by temperature programmed desorption of ammonia (NH_3-TPD)....28
3.2.3.9. Alloy loading by thermogravimetric analysis (TGA)....29

Page

3.2.3.10. Metal leaching by inductively coupled plasma mass spectrometry (ICP-MS) 30
3.3. Catalysis applications 30
3.3.1. Dehydration of xylose to furfural 30
3.3.1.1. Parr reactor 31
3.3.1.2. In-house batch reactor 32
3.3.2. Esterification of levulinic acid to ethyl levulinate 32
3.3.3. Transfer hydrogenation of Methyl levulinate to *γ*-valerolactone 33
3.4. Analytical instruments 34
3.4.1. High performance liquid chromatography (HPLC) 34
3.4.2. Gas chromatography (GC) 35
Chapter IV RESULTS AND DICUSSION 36
4.1. Synthesis and functionalization of CNHs 36
4.1.1. Synthesis of CNHs 36
4.1.2. Mono-functional group 39
4.1.2.1. Metal/Alloy hybridized with CNHs 39
4.1.2.2. Oxidation in air 54
4.1.2.3. Acid treatment 56
4.1.3. Multi-functional groups 59
4.1.3.1. The thermal treatment (oxidation and reduction) on Ni/CNHs, Cu/CNHs and NiCu/CNHs samples 59
4.1.3.2. The acid treatment by sulfuric acid on Pd/CNHs sample 61
4.2. Catalysis applications 62
4.2.1. Dehydration of xylose 63
4.2.1.1. Parr-reactor 63
4.2.1.2. In-house batch reactor 64
4.2.2. Esterification of levulinic acid to ethyl levulinate 66
4.2.3. Transfer hydrogenation of methyl levulinate to *γ*-valerolactone 68
Chapter V CONCLUSIONS AND RECOMMENDATIONS 72

Page

5.1. Conclusions 72
5.2. Recommendations 73
REFERENCES 74
APPENDIX A BASIC PROPERTIES OF METAL AND ACID 85
APPENDIX B CALIBRATION DATA 87
APPENDIX C CHROMATOGRAM DATA 95
APPENDIX D RAMAN SPECTRA DATA 98
APPENDIX E QUANTITATIVE DATA 100
APPENDIX F SAMPLING SIZE CALCULATION 104
APPENDIX G PUBLICATIONS 105
VITA 107

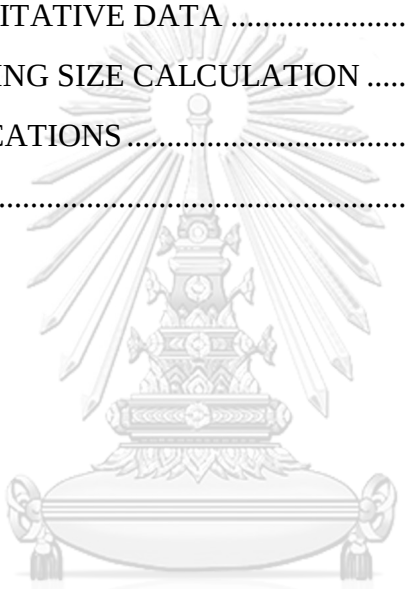

LIST OF TABLES

Table 2.1 Summarized techniques to synthesis carbon nanomaterial.....6
Table 2.2 Literature reviews about supported alloys as a catalyst.....10
Table 2.3 Literature reviews about metal/alloy supported on CNHs.....12
Table 2.4 Literature reviews about acid treatment techniques on carbon material 14
Table 2.5 Literature reviews about catalytic applications of carbon material for biomass conversion.....17
Table 3.1 Sample code of metal hybridized with CNHs samples.....20
Table 3.2 Sample code of alloy hybridized with CNHs samples 21
Table 3.3 Sample code of acid functionalized CNHs 23
Table 4. 1 Average crystalline size of Ni/CNHs and Cu/CNHs by XRD.....40
Table 4. 2 Average crystalline size of NiCu/CNHs by XRD 41
Table 4.3 Composition of the samples by EDX 52
Table 4.4 Specific surface area, total pore volume, and average pore diameter of metal hybridized with CNHs 54
Table 4.5 Specific surface area, total pore volume, and average pore diameter of SA-CNHs and AA-CNHs 57
Table 4.6 I_G to I_D ratio of acid treated CNHs.....58
Table 4.7 Acidity of acid treated CNHs by NH_3-TPD.....59
Table 4.8 Weight change of samples after thermal treatment process 61
Table 4.9 Specific surface area, total pore volume, and average pore diameter of Pd/CNHs and SA-Pd/CNHs.....62
Table A.1 Basic properties of metal 85
Table A.2 Atomic radius of metal.....85
Table A.3 Basic properties of sulfuric acid and acetic acid.....86
Table E.1 Dehydration of xylose in parr reactor at 170 °C, reaction time=4 h, and initial P=15 bar.....100
Table E.2 Dehydration of xylose in in-house batch reactor at 170 °C, reaction time=4 h, and initial P=15 bar 100

Table E.3 Transfer hydrogenation of ML to GVL at 200°C, reaction time=3 h 101

Table E.4 Effect of reaction temperature on transfer hydrogenation of ML to GVL, reaction time=3 h 101

Table E.5 Reusability of catalyst in transfer hydrogenation of ML to GVL at 200°C, reaction time=3 h 102

Table E.6 Effect of amount of catalyst on esterification of LA to EL at reaction temperature= 140 °C, reaction time = 90 min, initial LA:EtOH=1:5 102

Table E.7 Effect of reaction temperature on esterification of LA to EL at 15 mg of catalyst, reaction time = 90 min, initial LA:EtOH=1:5 102

Table E.8 Effect of reaction temperature on esterification of LA to EL at 15 mg of catalyst, at reaction temperature= 140 °C, reaction time = 90 min 103

LIST OF FIGURES

Figure 2.1 Carbon nanohorns structure 7
Figure 2.2 Experimental apparatus for gas-injected arc-in-water 8
Figure 2.3 Roadmap for conversion of lignocellulose 15
Figure 3.1 a) Schematic diagram of GI-AIW, b) Arc discharge process, c) Floating product on the top of water surface 19
Figure 3.2 Quartz tube reactor 22
Figure 3.3 a) Ultrasonic bath (GT-2013 QTS, GT SONIC), b) The suspension of CNHs in acid solution 23
Figure 3.4 Field-emission scanning electron microscope 25
Figure 3.5 Transmission electron microscope 25
Figure 3.6 Energy-dispersive X-ray spectroscopy 26
Figure 3.7 X-ray diffraction analyzer 26
Figure 3.8 N_2 sorption analyzer 27
Figure 3.9 Raman spectroscopy 27
Figure 3.10 Fourier transform infrared (FT-IR) spectrometer 28
Figure 3.11 Chemisorption analyzer 29
Figure 3.12 Thermogravimetric analyzer 29
Figure 3.13 Inductively coupled plasma mass spectrometry 30
Figure 3.14 Parr reactor 31
Figure 3.15 In-house batch reactor 32
Figure 3.16 High performance liquid chromatography 34
Figure 3.17 Gas chromatography 35
Figure 4.1 XRD pattern of CNHs 36
Figure 4.2 TEM images of CNHs at a)x120k, b)x250k, c) x400k 37
Figure 4.3 a) Adsorption-desorption isotherm of CNHs, b) pore size distribution of mesopores by BJH 37
Figure 4.4 Raman spectra of CNHs 38
Figure 4.5 TGA curve of CNHs 39

Figure 4.6 XRD patterns of a)Ni/CNHs-10, b)Ni/CNHs-1,4,6,10, c)Cu/CNHs-10, d)Cu/CNHs-1,4,6,10 40

Figure 4.7 XRD patterns of NiCu/CNHs with Ni:Cu = a.1)8:2, a.2)6:4, a.3)4:6, a.4)2:8, b.1)4:4, b.2)2:2, b.3)1:1 41

Figure 4.8 XRD patterns of a) Fe/CNHs-10, b.1)NiFe/CNHs-7:3, b.2)NiFe/CNHs-5:5, b.3)NiFe/CNHs-3:7, b.4)Fe/CNHs-10 42

Figure 4.9 XRD patterns of a) Pd/CNHs-4, b.1)NiPd/CNHs-9:1, b.2)NiPd/CNHs 8:2, b.3)NiPd/CNHs-7:3 42

Figure 4.10 XRD patterns of a) Pt/CNHs-4, b.1)NiPt/CNHs-9:1, b.2)NiPt/CNHs 8:2, b.3)NiPt/CNHs-7:3 43

Figure 4.11 XRD patterns of PdPt/CNHs at Pd:Pt = a)1:3, b)2:2, c)3:1 44

Figure 4.12 TEM images of a)Ni/CNHs-1, b)Ni/CNHs-4, c)Ni/CNHs-6, and d)Ni/CNHs-10 45

Figure 4.13 TEM images of a)Cu/CNHs-1, b)Cu/CNHs-4, c)Cu/CNHs-6, and d)Cu/CNHs-10 46

Figure 4.14 TEM images of a)NiCu/CNHs-8:2, b)NiCu/CNHs-6:4, c)NiCu/CNHs-4:6, d)NiCu/CNHs-2:8 48

Figure 4.15 TEM images of a)NiCu/CNHs-1:1, b)NiCu/CNHs-2:2, c)NiCu/CNHs-4:4 49

Figure 4.16 TEM images of a)Fe/CNHs-10, b)Pd/CNHs-4, and c)Pt/CNHs-4 50

Figure 4.17 TGA curve of Ni/CNHs a.1)Ni/CNHs-10, a.2)Ni/CNHs-6, a.3)Ni/CNHs-4, a.4)Ni/CNHs-1 and Cu/CNHs b.1)Cu/CNHs-10, b.2)Cu/CNHs-6, b.3)Cu/CNHs-4, b.4)Cu/CNHs-1 51

Figure 4.18 TEM images of oxd-CNHs at a)x150k and b)x300k 55

Figure 4.19 a) Adsorption-desorption isotherm of oxd-CNHs, b) pore size distribution of mesopores by BJH 55

Figure 4.20 Adsorption-desorption isotherm of a) SA-CNHs and b) AA-CNHs 56

Figure 4.21 FT-IR spectra of acid treated CNHs a)SA-CNHs and b)AA-CNHs 58

Figure 4.22 XRD patterns of thermal treatment on a)Ni/CNHs-10, b)Cu/CNHs-10, and c)NiCu/CNHs-5:5 60

Figure 4.23 XRD patterns of a)Pd/CNHs, b)SA-Pd/CNHs 61

Figure 4.24 Performance of the catalysts in dehydration of xylose in Parr reactor at 170 °C, reaction time=4 h, and initial P=15 bar 64

Figure 4.25 Performance of Ni/CNHs Cu/CNHs and NiCu/CNHs with or without thermal treatment catalysts on dehydration of xylose in in-house batch reactor at 170 °C, reaction time=4 h, and initial P=15 bar 66

Figure 4.26 Effect of amount of catalyst on esterification of LA to EL at reaction temperature= 140 °C, reaction time = 90 min, initial LA:EtOH=1:5 67

Figure 4.27 Effect of reaction temperature on esterification of LA to EL at 15 mg of catalyst, reaction time = 90 min, initial LA:EtOH=1:5 67

Figure 4.28 Effect of initial LA:EtOH molar ratio on esterification of LA to EL at 15 mg of catalyst, at reaction temperature= 140 °C , reaction time = 90 min 68

Figure 4.29 Performance of Ni/CNHs Cu/CNHs and NiCu/CNHs with or without thermal treatment catalysts on transfer hydrogenation of ML at 200°C, reaction time=3h 69

Figure 4.30 Effect of reaction temperature for ML to GVL conversion (reaction time of 3 h, catalyst loading of 0.1 g) 70

Figure 4.31 Reusability of red-oxd-Ni/CNHs for ML-to-GVL conversion. Reaction conditions: reaction temperature of 200 °C, reaction time of 3 h, catalyst loading of 0.1 g 71

Figure B.1 Calibration curve of xylose for HPLC analysis @Nanotechnology center (NSTDA) 87

Figure B.2 Calibration curve of furfural for HPLC analysis @Nanotechnology center (NSTDA) 88

Figure B.3 Calibration curve of xylose for HPLC analysis @Kyoto University 89

Figure B.4 Calibration curve of furfural for HPLC analysis @Kyoto University 90

Figure B.5 Calibration curve of methyl levulinate for GC analysis 91

Figure B.6 Calibration curve of methyl levulinate for GC analysis 92

Figure B.7 Calibration curve of levulinic acid for HPLC analysis 93

Figure B.8 Calibration curve of ethyl levulinate for HPLC analysis 94

Figure C.1 Chromatogram of dehydration of xylose to furfural by HPLC (UV detector) 95

Figure C.2 Chromatogram of dehydration of xylose to furfural by HPLC (RID detector) 95

Figure C.3 Chromatogram of transfer hydrogenation of methyl levulinate to γ-valerolactone by GC 96

Figure C.4 Chromatogram of esterification of levulinic acid to ethyl levulinate by HPLC (UV detector) 96

Figure C.5 Chromatogram of esterification of levulinic acid to ethyl levulinate by HPLC (RID detector) 97

Figure D.1 Raman spectra of acid treated CNHs by sulfuric acid (SA-CNHs) with difference ultrasonicating time 98

Figure D.2 Raman spectra of acid treated CNHs by acetic acid (AA-CNHs) with difference ultrasonicating time 99

Chapter I
INTRODUCTION

1.1 Background and motivation

Recently, nanomaterials have become well-known in everyday life. Carbon nanomaterial is one of widely material which was used in many applications. There are many structures of carbon nanomaterial such as graphene, carbon nanofibers, fullerenes, carbon nanodiamonds, carbon nanotubes and carbon nanohorns [1, 2]. Each of them has unique properties which would exhibit both advantages and drawbacks with respect to specific applications to be targeted [3]. For the synthesis of carbon nanomaterial, many techniques, for example, chemical vapor deposition, arc discharge, laser ablation have been explored [4]. Controlling their structure and size has been one of the most challenging issues for research works in the material science field [2].

Among various carbon nanostructures, carbon nanohorn (CNH) is one of the most interesting carbon nanostructures because of its unique morphology. The CNHs is carbon nanostructure with a cone-shaped single-layered graphitic aggregate with approximately 40–50 nm in length and approximately 2 and 3 nm in diameter [5, 6]. It should be noted that the structure of a single cone-shaped single-layered graphitic aggregate is derived from a single-walled carbon nanotube (SWCNT) and ended by a five-pentagon conical cap. Based on the assembly or aggregating form, CNHs can be classified as Dahlia-like, bud-like, and seed-like structures with diameters of approximately 80–100 nm [2, 4, 6]. Interestingly, CNHs possess very high specific surface area and pore volume [2, 4]. Their unique morphology would accommodate gas and liquid species to permeate, be easy for functionalization, and provide good electrical and thermal conductivities, leading to high potential to be used for gas storage, bio-sensing, drug delivery, catalyst, catalyst support and so on [2, 7]. CNHs can be synthesized by various methods, such as arc discharge and laser ablation. Among those methods, arc discharge seems to be a simple, cost effective and scalable technique [4, 5, 8-11]. With the arc discharge method, CHNs can be produced without using any catalysts, resulting in high purity of carbon and no requirement of post-purification [8].

It is also well recognized that effective utilization of carbon nanomaterials as an active catalyst or catalyst support would require an additional processing. Functionalization and metal loading of carbon nanomaterials are common methods to modify their surface to gain such catalytic property. Based on some previous works, acid functionalized carbon nanomaterials can present a better catalyst activity when compared to its pristine condition [12, 13]. The modification of CNHs by acid treatment could alter their natural inertness and hydrophobic properties [14]. It is also recognized that functionalization of CNHs can be accomplished through chemical oxidation and thermal oxidation which would attach some specific functional groups onto the surface of CNHs [14]. Meanwhile, metal nanoparticles embedded in carbon nanomaterials have shown promising properties for catalysis [7]. Therefore, research works for attaching metal nanoparticles onto the surface of carbon nanomaterials have also been reported. The catalytic activity and stability of such carbon nanomaterials hybridized with metal nanoparticles are inherently dependent on the structure and proportion of carbon nanomaterials and metal nanoparticles [7]. However, only a few reports, especially those relevant with CHNs and CNHs hybridized with metal nanoparticles are available.

Therefore, synthesis of CNHs by the arc discharge method and their functionalization by metal nanoparticle hybridization as well as acid treatment would be recognized as good motivation for research. In order to understand the effect of functionalizing parameters on properties of CNHs and CNHs hybridized with metal nanoparticles, design of systematic experimental works would be worth for exploring. Furthermore, investigation of application of such nanomaterials for conversion of sugar and their derivatives to valuable bio-chemical products would potentially provide new tangible evidences on their usefulness.

The thesis is divided in 5 main chapters as shown below:

Chapter I gives motivation and introduction of this work.

Chapter II describes fundamental knowledge and theory of carbon nanomaterials and its functionalization (hybridized material with metal/alloy, oxidized in air, and acid treatment). Moreover, catalytic reactions of converting sugar and their

derivatives to valuable bio-chemical products are presented. Literature review of previous work related to this work is also provided in this chapter.

Chapter III provides chemicals, synthesis and functionalization methods, characterization methods and catalytic reactions (dehydration, transfer hydrogenation, and esterification) procedure.

Chapter IV describes experimental results and discussion of this research.

Chapter V gives overall conclusions and recommendations of this work.

1.2 Objective of the research

The objective of this research was to examine properties of carbon nanohorns (CNHs) which were synthesized by gas-injected arc-in-water method and then functionalized by metal/alloy nanoparticle hybridization, oxidation in air, and acid treatment. In addition, catalysis applications of such nanomaterials were also examined and discussed.

1.3 Scopes of the research

1.3.1 Synthesis and functionalization of CNHs by gas-injected arc-in-water method

- Synthesis of CNHs
- Mono-functional group
    - Hybridized with metal/alloy
        - Type of metal/alloy hybridization with CNHs
        - Metal loading and alloy composition in hybridized materials
    - Oxidation in air
    - Acid treatment
        - Type of acid solution
        - Treatment time

- Multi-functional groups
    - Oxidation in air on metal/alloy hybridized with CNHs
    - Acid treatment on metal hybridized with CNHs

The properties of all synthesized products were investigated by field-emission scanning electron microscope (FE-SEM), transmission electron microscope (TEM), energy-dispersive X-ray spectroscopy (EDX), X-ray diffraction (XRD), N_2 sorption, Raman spectroscopy, Fourier transform infrared (FT-IR) spectrometer, temperature programmed desorption of ammonia (NH_3-TPD), thermogravimetric analysis (TGA), inductively coupled plasma mass spectroscopy (ICP-MS).

1.3.2 Catalysis applications

- Dehydration of xylose to furfural
    - Parr reactor
    - In-House reactor
- Esterification of levulinic acid to ethyl levulinate
- Transfer hydrogenation of methyl levulinate to γ-valerolactone

Selective reaction for each material was perform in batch reactor. High performance liquid chromatography (HPLC) or gas chromatography (GC) were used to measure the catalyst activities.

1.4 Expected benefit

Expected benefits to be obtained from this research would be the knowledge in functionalization of CNHs by metal nanoparticle hybridization, oxidation in air, and acid treatment. New alternative materials will be introduced as a catalyst in conversion of sugar and their derivatives to valuable bio-chemical products.

Chapter II
FUNDAMENTAL THEORY AND LITERATURE REVIEW

2.1. Carbon nanomaterial

Carbon nanomaterial is a carbon which have at least one dimension in the nanometer range. Nano-size provide them novel and special properties such as a high surface-to-volume ratio, unique thermal, chemical, mechanical or electronic properties [1]. The basic members of carbon nanomaterial are graphene, carbon nanofibers, fullerene, carbon nanodiamonds, carbon nanotubes, carbon nanohorns and so on [1, 13].

For the synthesis of carbon nanomaterial, many techniques provide carbon nanomaterial for example: chemical vapor deposition, arc discharge, laser ablation etc. [4]. Each of techniques would product difference structure of carbon nanomaterial as shown in Table 2.1. With the same technique but changing the control condition also gives a different structure and size distribution of product.

Table 2.1 Summarized techniques to synthesis carbon nanomaterial [16]

Structure / Technique	SWCNT	MWCNT	CNHs	Fullerene	Amorphous	Graphene
Arc discharge	x	o	o	o	o	x
Arc discharge with Catalyst	o	o	x	o	o	x
Laser deposition	x	x	o	o	o	x
Laser deposition with Catalyst	o	o	x	o	o	x
CVD (Pyrolysis)	x	x	x	x	o	x
CVD with catalyst	o	o	x	x	o	o
CVD (Plasma with catalyst)	o	o	x	-	o	o

o: Can be synthesized by this method
x: Cannot be synthesized by this method

2.1.1. Carbon nanohorns (CNHs)

Carbon nanohorns (CNHs) is a new interesting member in carbon nanomaterial family which was discovered in 1999 from the soot prepared by CO_2 laser vaporization of pure carbon rod in an atmospheric pressure of Ar [8].

They have a unique structure with a horn-shaped sheath aggregate of graphene sheets with approximately 40–50 nm in tubule length and approximately 2 and 3 nm in diameter. The structure is derived from a single walled carbon nanotube (SWCNT) and ended by a five-pentagon conical cap with a cone as shown in Figure 2.1. They are classified based on the assembly of the individual [4]. CNHs can be aggregated together to form Dahlia-like, bud-like, and seed-like structures with diameters of approximately 80–100 nm [2, 4, 6]. From structure as describe above, CNHs have a very high surface area, pore volume, chemical resistance, thermal stability, and hydrophobic surface property [2, 4, 15].

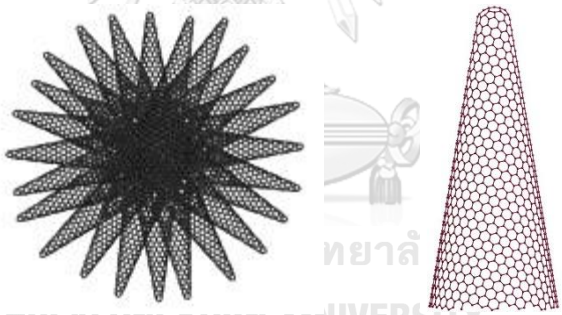

Figure 2.1 Carbon nanohorns structure [16]

CNHs can be synthesized by arc discharge and laser ablation method while arc discharge seems to be a simple, cost effective and scalable technique [4, 5, 8-10]. CHNs can be produced without using any catalysts which result in high purity of carbon [8]. They are also easy for the gas and liquid to permeate to the inside, easy to functionalization, and good electrical and thermal conductivities which afford more potential to be used for gas storage, gas sensor, drug delivery, catalyst support and drug carrier [2, 7, 9].

2.2. Gas-injected arc-in-water technique

Gas-injected arc-in-water (GI-AIW) is one of the arc discharge method [11]. This method can provide SWCNHs by injecting N_2 gas into arc zone within a hollow cavity of a cathode submerged in water. Water acted like liquid N_2 quenching the carbon vapor to form carbon nanoparticle. For a modified arc-in-liquid method, the GI-AIW method has a benefit about its simplicity and capability for synthesizing various nanomaterials including metallic and carbonaceous particles [9]. The simple experimental apparatus for GI-AIW was shown in Figure 2.2**.**

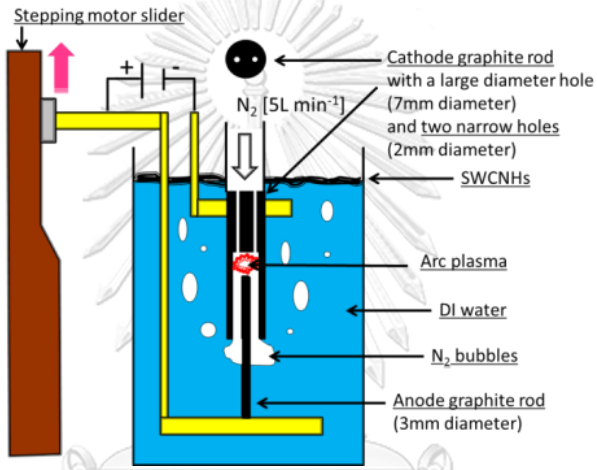

Figure 2.2 Experimental apparatus for gas-injected arc-in-water [9]

2.3. Bimetallic material

Bimetallic material consists of two metal atoms which bond to each the other. There are three types of bimetallic: physically-mixed, core-shell, and alloy [17]. For supported bimetallic in catalyst application, it usually showed an increasing of catalyst performance, activity, selectivity, and/or stability comparing to the supported monometallic catalysts [18-21]. These enhancement of catalyst properties are cause by the synergistic combination of the two metals. There are several studies reported that not only the surface composition but also the particle size of the alloy particles is important for the reaction [22, 23].

2.4. Functionalization

Modification of carbon by surface functionalization or doping with heteroatoms before using seems to be a common alternative to adjust carbon properties for many application including catalytic application [12, 13].

2.4.1. Alloy loading

The properties of alloy such as their components, compositions, crystal structures, uniformity, and other characteristics are significantly effect on their catalytic performance. Therefore, optimization of these parameters is essentially important for the development of alloy catalysts with high catalytic performance [22]. There are many methods to synthesize bimetallic with small particle size distribution [24].

2.4.1.1. Ni-base alloy

Pristine Ni is well known for its high hydrogenation activity for a wide range of hydrogenation reaction. However, one major problem for Ni catalyst is the deactivation with time due to carbon deposition, nickel sintering and phase transformation [25]. To overcome this problem, many Ni-base alloy including NiCu, NiCo, NiPd, NiFe alloy catalysts were introduced. The literature reviews about Ni-base alloy as a catalyst are shown in Table 2.2.

2.4.1.2. PtPd alloy

Supported noble metal catalysts are well known for their high hydrogenation activity at low reaction temperatures and moderate hydrogen pressures, and their low resistance to sulfur poisoning [26]. It has been reported earlier that bimetallic catalysts such as PtPd alloy show higher activity, stability, and metal dispersion than Pt alone [27]. To overcome this problem, PtPd alloy catalysts were introduced. The literature reviews about PtPd alloy as a catalyst are also shown in Table 2.2.

Table 2.2 Literature reviews about supported alloys as a catalyst

No.	Catalysts	Method of synthesis	Reactions	Type of study	Ref.
1	$NiCu/Al_2O_3$	Wet impregnation	Catalytic partial oxidation of methane	To study NiCu-based catalysts for catalytic partial oxidation of methane process.	[25]
2	$NiCu/ZrO_2–SiO_2$	Wet impregnation	Hydrodeoxygenation of guaiacol to hydrocarbons	To study catalysts performances.	[28]
3	$NiCu/ZrO_2–SiO_2$	Sol–gel	Hydrotreatment of Bio-oil using guaiacol	To study the effect of phosphorus and molybdenum as modifying additives on the stability and activity of Ni-based catalysts.	[29]
4	$NiCu–SiO_2$	Decomposition of metal salts with subsequent stabilization	Hydrodeoxygenation of anisole	To study the effect of Ni/Cu ratio on the selectivity of product formation in anisole conversion.	[30, 31]
5	Ni-Pd/γ-Al_2O_3	Impregnation	Partial oxidation and steam reforming of hydrocarbons	To study the effects Pd adding on catalyst performance.	[32]
6	$Ni-Pd/SIO_2$	Co-impregnation	Total hydrogenation of furan derivatives	To study the effects of the Ni/Pd ratio on catalyst performance.	[33]

Table 2.2 Literature reviews about supported alloys as a catalyst (cont.)

No.	Catalysts	Method of synthesis	Reactions	Type of study	Ref.
7	Ni–Fe/palygorskite, Ni–Fe/MgO–Al_2O_3	Impregnating	Tar cracking	To study the effects of NiFe loading on catalyst performance.	[34, 35]
8	Ni–Fe/SiO_2	Incipient wetness co-impregnation	Hydrogenation of	To study the effects of on catalyst performance.	[33]
9	Pt-Pd/Silica-alumina, Pt-Pd/ß-zeolite	Wet impregnation	furanic compounds	To study the effect of bimetallic and support material on catalytic performance.	[26]
10	Pt-Pd/Al_2O_3	Impregnation	Hydrogenation of aromatics	To study the effects of the Pt/Pd ratio on catalyst performance.	[27]
11	PtPd/C	Impregnation	Competitive hydrogenation of poly-aromatic hydrocarbons	To study the effects of the Pt/Pd ratio on catalyst performance.	[36]

According to Table 2.2, Ni-based alloy on support materials could be used as a catalyst in various catalytic reactions such as oxidation reaction, hydrogenation reaction or hydrothermal reaction. Conventional methods to synthesize Ni-based alloy are impregnation and sol-gel method which were a multi-step method. In addition, these methods required many chemical reagents during the synthesis which could result in contamination of synthesized products.

2.4.1.3. Metal/alloy supported on CNHs

There are many studies reported about using CNHs as a metal/alloy support in various catalytic reaction. The major advantages of CNHs are high surface area and purity. CNHs consist of two types of pore, one is internal pore and the other is spaces between particles from aggregation. From those advantages, metal/alloy nanoparticles seem to have high dispersion when deposit on CNHs. The literature reviews about metal/alloy supported on CNHs are shown in Table 2.3.

Table 2.3 Literature reviews about metal/alloy supported on CNHs

No.	Materials	Doping method	Application	Ref.
1.	Pt/CNHs	Colloidal method	Fuel cell	[37]
2.	Pd/CNHs	Chemical reduction (PVP as stabilizer)	-	[38, 39]
3.	Pt/CNHs	One-step synthesis by arc plasma in liquid nitrogen	Fuel cell	[40]
4.	Pd/CNHs,	Single-step synthesis by GI-AIW method	-	[9]
	Pd-Ni alloy/CNHs,		-	[10]
	Fe/CNHs		-	[41]

CNHs were used as a supported material for noble metals such as Pd and Pt in fuel cell application as shown in Table 2.3. Non-noble metals were recently hybridized with CNHs using a single step synthesis process by Sano's team. However, application of CNHs was mostly focused on fuel cell or electronic devices. Only few works reported in the application of CNHs as support or hybrid material.

2.4.2. Acid treatment

Generally functional groups and delocalized electrons of the graphitic structure define the acid and hydrophilic/hydrophobic character of the carbon surface [42, 43]. Treatment can be done through many methods such as chemical methods by liquid phase oxidation with concentrated acids (ex. H_2SO_4, HNO_3, H_3PO_4, H_2O_2 etc.) or gas phase thermal oxidation processes (ex. air, CO_2) [44]. Carbon based catalysts are attractive for applications in the field of valuable bio-chemical production from sugar and their derivatives due to their structural integrity in aqueous environments [45]. The literature reviews about acid treatment in liquid phase techniques on carbon material are shown in Table 2.4.

From Table 2.4, for liquid phase treatment, H_2OS_4 and HNO_3 were selected as an acid solution to treat carbon material. Method, treatment temperature, and treatment time were varied upon each work. Comparing to gas phase treatment, lower treatment temperature was used in liquid phase. While equal or longer treatment time were applied for liquid phase treatment.

Table 2.4 Literature reviews about acid treatment techniques on carbon material

No.	Material	Method of treatment	Temperature (°C)	Time	Treated by	Ref.
1	CNTs	Ultrasonication	100	1-24 h	HNO_3	[46]
2	CNTs	Ultrasonication	-	8 h	H_2SO_4/HNO_3	[47]
3	CNHs	Stirring	110	15, 30 min, 1, 2, and 4 h	HNO_3	[14]
4	CNTs	Suspension	-	35 min	H_2SO_4/HNO_3	[48]
5	CNHs	Exposing	500	30 min	Air	[15]
6	AC	Stirring	At boiling point of reagent	10 min	H_2SO_4, HNO_3	[45]
7	CNFs	Suspension	120	2 h	H_2SO_4	[42]

2.5. Catalytic biomass conversion

Due to decreasing of fossil fuel resources while increasing of environmental concern, the development of renewable and sustainable energy source become a very interesting issue [49-51]. Many research teams have been studied in using renewable biomass resources instead of fossil fuel. Biomass is a highly abundant and carbon–neutral renewable energy resource, Lignocellulose is the major non-food component of biomass comprising three main fractions, namely cellulose (40–50%), hemi-cellulose (25–35%) and lignin (15–20%) [51]. Roadmap for conversion of lignocellulose has been reported as shown in Figure 2.3.

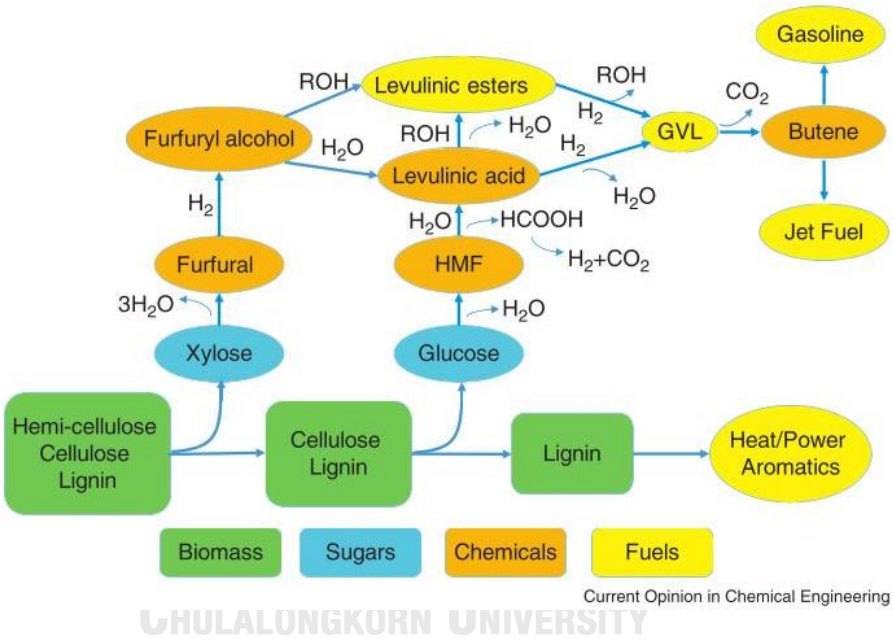

Figure 2.3 Roadmap for conversion of lignocellulose [52]

Biomass conversion usually involves in hydration, dehydration, and hydrogenation reaction. According to many problems in homogenous catalyst system, solid catalyst system was introduced [51]. Those reactions required bi or multifunctional catalysts including acidic sites and metallic sites so that solid-supported Brønsted or Lewis acid reagent catalysts, acid-modified amorphous carbon, layered transition metal oxides, and acidic resins were reported for using as a catalyst in biomass conversion. Besides, improvement of catalyst activity, selectivity, and stability should be considered.

2.5.1. Carbon material as catalyst and catalyst support for converting biomass to valuable products.

Carbon material can be used as catalysts or catalyst supports for biomass conversion reactions. Due to good properties of carbon material, large specific surface area, high porosity, relative chemical inertness [53]. Moreover, carbon material can be prepared from residual biomass which is the outstanding advantage of carbon. Summarizing of using carbon material as catalysts or catalyst supports for biomass conversion were reported in Table 2.5.

Table 2.5 Literature reviews about catalytic applications of carbon material for biomass conversion

No.	Catalysts	Reactions	Ref.
1	Sulfonated carbon	Conversion of cellulose into high yields of methyl glucosides	[54]
2	Carbon-supported Ru	Conversion of cellulose to sugar alcohols	[55]
3	Ru/CNT	Conversion of cellulose into sorbitol	[56]
4	Graphene, graphene oxide, sulfonated graphene, sulfonated graphene oxide	Dehydration of xylose to furfural in water	[57]
5	Sulfonic acid-functionalized CNTs, CNFs	Conversion of fructose into 5-hydroxymethylfurfural and alkyl levulinates	[58]
6	Pt supported on reduced graphene oxide	Selective conversion of cellulose or cellobiose to sorbitol	[59]
7	Sulfonated carbon	Esterification of long chain fatty acids to high grade biodiesel	[60]
8	Ru, Pt, Pd supported in carbon	Selective hydrogenation of levulinic acid to γ-valerolactone	[61]
9	Ru/AC	Hydrogenation of alkyl levulinate to γ-valerolactone	[62]
10	Sulphonated MWCNTs	Esterification of palm fatty acid	[63]
11	Sulfonated CNHs	Biodiesel production by esterification of palmitic acid	[15]

Chapter III
EXPERIMENTAL

3.1. Chemicals & Materials

3.1.1. Graphite rod (99.9995%, Alfa Aesar)

3.1.2. Nickel wire (99+%, Nilaco corporation)

3.1.3. Copper wire (99.9%, Nilaco corporation)

3.1.4. Iron wire (99.5%, Nilaco corporation)

3.1.5. Palladium wire (99.95%, Nilaco corporation)

3.1.6. Platinum wire (99.98%, Nilaco corporation)

3.1.7. Sulfuric acid 96% (96%, CARLO ERBA)

3.1.8. Acetic acid glacial (99.7%, DUKSAN)

3.1.9. D-xylose (99 %, Merck)

3.1.10. Furfural (99%, Sigma-Aldrich)

3.1.11. Methyl levulinate (≥98.0%, Sigma-Aldrich)

3.1.12. ɣ-Valerolactone (99%, Sigma-Aldrich)

3.1.13. 2-propanol (99.98%, Fisher Chemical)

3.1.14. Levulinic acid (98%, Sigma-Aldrich)

3.1.15. Ethyl levulinate (99%, Sigma-Aldrich)

3.1.16. Ethanol (99.9%, ACILabscan)

3.1.17. Membrane filter (PTFE, 0.1µm, diameter 47 mm, ADVANTEC)

3.1.18. Sylinf filter (Nylon, 0.22, diameter 13 mm, Thermo SCIENTIFIC)

3.2. Methods

3.2.1. Synthesis and functionalization of CNHs

3.2.1.1. Synthesis of CNHs

GI-AIW method was used to synthesis CNHs [64-67]. GI-AIW consist of two electrodes made from high purity graphite: cathode (top) and anode (bottom). A 20 mm diameter and 50 mm length of graphite rod with four small holes (diameter 2 mm, length 25 mm) at the top and one large hole at the bottom (diameter 12 mm, length 2 mm) was used as a cathode. Another is a 6 mm diameter and 75 mm length of graphite rod is fixed on a holder connected to the step motor. During the arc discharge, a 10 L/min of N_2 gas flow was supplied through four small holes on the top of the cathode and the anode was moved upward at a rate of 1.3 mm/s using a motor-driven slider. DC supplier generated arc discharge at 80 A. Carbon from an anode was vaporized then quenched by surrounding water. Carbon nanomaterials were formed through self-assembly process. Due to the unique properties of CNHs, CNHs floats on the water surface while other structures of carbon nanomaterials sink at the bottom of the beaker. By collecting only black power floating on the water surface, CNHs was obtained. Arc discharge machine and product after GI-AIW were shown in Figure 3.1.

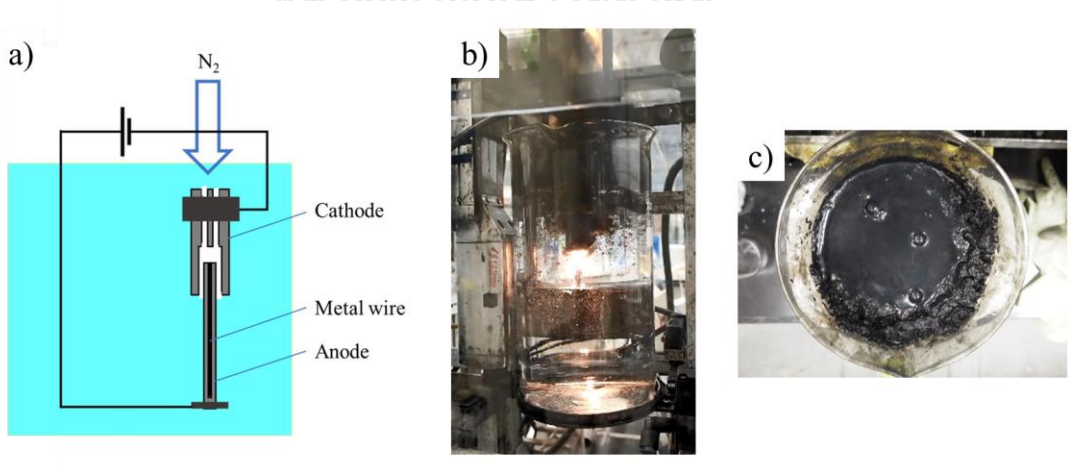

Figure 3.1 a) Schematic diagram of GI-AIW, b) Arc discharge process, c) Floating product on the top of water surface

3.2.1.2. Mono-functional group

3.2.1.1.1. Hybridized with metal/alloy

GI-AIW method was used for synthesis metal/alloy hybridized with CNHs. Graphite rods and various types of metal wires were used for synthesis hybridized materials. Loading of metal in hybridized materials was studied by varying the number of metal wire used.

3.2.1.1.1.1. Metal (Ni, Cu, Fe, Pd, Pt) hybridized with CNHs

Similar to synthesis CNHs, GI-AIW method was used. In addition, an anode was drilled at the center of vertical axis to make a hold (diameter = 1.5 mm, length = 70 mm). A set of 0.03 mm diameter of Ni wire was inserted into a center-hold of graphite anode. Other parameters were set as same as synthesis of CNHs process. Sets of metal wire were set as Ni = 1, 4, 6, 10; Cu = 1, 4, 6, 10; Fe =10; Pd = 4; Pt =4 wires and the products were recorded as XX/CNHs-Y (XX is type of metal and Y is number of metal wire). All of sample's code were shown in Table 3.1.

Table 3.1 Sample code of metal hybridized with CNHs samples

No.	Code	Number of metal wires				
		Ni	Cu	Fe	Pd	Pt
1	Ni/CNHs-1	1	-	-	-	-
2	Ni/CNHs-4	4	-	-	-	-
3	Ni/CNHs-6	6	-	-	-	-
4	Ni/CNHs-10	10	-	-	-	-
5	Cu/CNHs-1	-	1	-	-	-
6	Cu/CNHs-4	-	4	-	-	-
7	Cu/CNHs-6	-	6	-	-	-
8	Cu/CNHs-10	-	10	-	-	-
9	Fe/CNHs-10	-	-	10	-	-
10	Pd/CNHs-4	-	-	-	4	-
11	Pt/CNHs-4	-	-	-	-	4

3.2.1.1.1.2. Alloy (NiCu, NiFe, NiPd, NiPt, PdPt) hybridized with CNHs

For NiCu hybridized with CNHs, the ratio of Ni:Cu (by number of wire) and total number of metal wire were varied. First, ratio of Ni:Cu was varied (fix total number of metal at 10 wires) at 8:2, 6:4, 4:6, and 2:8. The other is to varied total number of metal wire with fix ratio of Ni:Cu. The ratio of Ni:Cu was fix at 1:1 and total number of metal wire were set at 2, 4, 8, 10. The products were coded as NiCu/CNHs-X:Y (X is number of Ni wire and Y is number of Cu wire). A similar method was used as synthesis of metal hybridized with CNHs.

Others alloy hybridized with CNHs, types of metal wire were changed from NiCu to NiFe, NiPd, NiPt, and PdPt. The total number of metal wire was set at 10 wires for NiFe/CNHs, NiPd/CNHs, and NiPt/CNHs. The ratio of metal wire was set at Ni:Fe = 7:3, 5:5 and 3:7; Ni:Pd = 9:1, 8:2, and 7:3; Ni:Pt = 9:1, 8:2, and 7:3. In addition, total number of metal wire for PdPt were set at 4 wired. The Pd:Pt ratio is 3:1, 2:2, and 1:3. All of sample's code were shown in Table 3.2.

Table 3.2 Sample code of alloy hybridized with CNHs samples

No.	Code	Number of metal wires				
		Ni	Cu	Fe	Pd	Pt
1	NiCu/CNHs-8:2	8	2	-	-	-
2	NiCu/CNHs-6:4	6	4	-	-	-
3	NiCu/CNHs-4:6	4	6	-	-	-
4	NiCu/CNHs-2:8	2	8	-	-	-
5	NiCu/CNHs-1:1	1	1	-	-	-
6	NiCu/CNHs-2:2	2	2	-	-	-
7	NiCu/CNHs-4:4	4	4	-	-	-
8	NiCu/CNHs-5:5	5	5	-	-	-
9	NiFe/CNHs-7:3	7	-	3	-	-
10	NiFe/CNHs-5:5	5	-	5	-	-
11	NiFe/CNHs-3:7	3	-	7	-	-
12	NiPd/CNHs-9:1	9	-	-	1	-
13	NiPd/CNHs-8:2	8	-	-	2	-

No.	Code	Number of metal wires				
		Ni	Cu	Fe	Pd	Pt
14	NiPd/CNHs-7:3	7	-	-	3	-
15	NiPt/CNHs-9:1	9	-	-	-	1
16	NiPt/CNHs-8:2	8	-	-	-	2
17	NiPt/CNHs-7:3	7	-	-	-	3
18	PdPt/CNHs-3:1	-	-	-	3	1
19	PdPt/CNHs-2:2	-	-	-	2	2
20	PdPt/CNHs-1:3	-	-	-	1	3

3.2.1.1.2. Oxidation in air

0.2 g of CNHs was put in a ceramic boat and insert in quartz tube reactor as shown in Figure 3.2. CNHs were oxidized in air at 380 °C for 15 min [68]. After the oxidation treatment, about 3-5 wt% weight loss of the product was determined by comparison with the initial weight of CNHs. The resulted product was coded as oxd-CNHs.

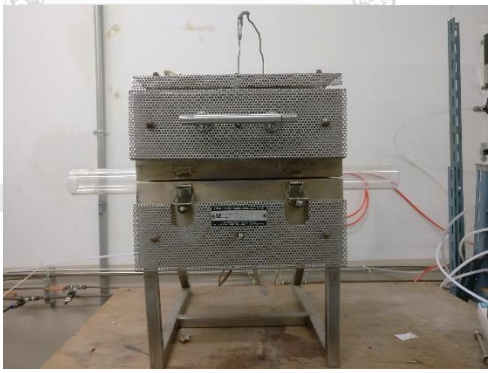

Figure 3.2 Quartz tube reactor

3.2.1.1.3. Acid treatment

0.1 g of CNHs was submerged in 50 ml of H_2SO_4 and sonicated in ultrasonic bath which filled with water as shown in Figure 3.3. Ultrasonicating time was varied from 15, 30, 60, 120, 240 and 360 min. Temperature was controlled at lower 40 °C.

The suspensions were filtrated and neutralized by DI-water using polytetrafluoroethylene (PTFE) membrane. Finally, the solid product was dried in oven at 90 °C for overnight. The resulted solid products were coded as SA-XX-CNHs (SA is sulfuric acid and XX is an ultrasonicating time).

Figure 3.3 a) Ultrasonic bath (GT-2013 QTS, GT SONIC), b) The suspension of CNHs in acid solution

Similar to sulfuric acid, CHNs was treated with acetic acid by above procedure. The resulted solid products were coded as AA-XX-CNHs (AA is acetic acid and XX is ultrasonicating time(min)). All of sample's code were shown in Table 3.3.

Table 3.3 Sample code of acid functionalized CNHs

No.	Code	Acid type		Ultrasonicating time (min)					
		Sulfuric acid	Acetic acid	15	30	60	120	240	360
1	SA-15-CNHs	✓		✓					
2	SA-30-CNHs	✓			✓				
3	SA-60-CNHs	✓				✓			
4	SA-120-CNHs	✓					✓		
5	SA-240-CNHs	✓						✓	
6	SA-360-CNHs	✓							✓
7	AA-15-CNHs		✓	✓					
8	AA-30-CNHs		✓		✓				
9	AA-60-CNHs		✓			✓			
10	AA-120-CNHs		✓				✓		
11	AA-240-CNHs		✓					✓	
12	AA-360-CNHs		✓						✓

3.2.1.3. Multi-functional groups

3.2.1.1.1. Oxidation in air on metal/alloy hybridized with CNHs

Ni/CNHs-10, Cu/CNHs-10, and NiCu/CNHs-5:5 from 3.2.1.2.1.1. and 3.2.1.2.1.2. were oxidized in air by similar procedure as 2.1.2.2. Amount of %burn off were differed in each sample due to properties of metal.

3.2.1.1.2. Acid treatment on metal hybridized with CNHs

Acid functional groups were added to Pd/CNHs-4 from 3.2.1.2.1.2. by acid treatment using H_2SO_4 solution. Similar method as 3.2.1.2.3. was used.

3.2.2. Post-treatment process

Before use as a catalyst, a reduction process was applied to the samples. A reducing process is necessary for reactivity of metal/alloy nanoparticles. Oxidized forms of metal/alloy hybridized with CNHs were changed into metal form and ready to be used as a catalyst. The samples were reduced at 500 °C for 1 h under 10 ml/min of H_2 flow with a heating rate of 10 °C/min.

3.2.3. Characterization

To understand the effect of functionalization on CNHs, physical and chemical properties of the samples were investigated by various characterization techniques.

3.2.3.1. Morphology by field-emission scanning electron microscope (FE-SEM)

Morphology of the samples was investigated by field-emission scanning electron microscope (FE-SEM) (Hitachi, S8030) as shown in Figure 3.4. The dispersion of an aggregated CNHs could be studied by this technique.

Figure 3.4 Field-emission scanning electron microscope

3.2.3.2. Morphology by Transmission electron microscope (TEM)

Morphology and size distribution of metallic species within each sample were studied by a transmission electron microscope (TEM) (JEOL, JEM1010) as shown in Figure 3.5. Size of metallic species was measured through TEM images by using ImageJ processing. More than 330 particles were measured the size and presented as metal particle size distribution histogram.

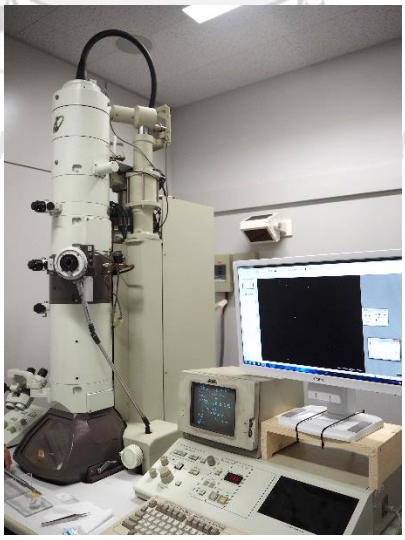

Figure 3.5 Transmission electron microscope

3.2.3.3. Composition of the sample by energy-dispersive X-ray spectroscopy (EDX)

Metal content in each sample was detected by energy-dispersive X-ray spectroscopy (EDX) equipped with SEM (Technex Lab, Tiny SEM/EDX) as shown in Figure 3.6. The sample was put on the top of a molybdenum (Mo) stud and inserted into the machine without any coating.

Figure 3.6 Energy-dispersive X-ray spectroscopy

3.2.3.4. Phase and crystal structure by X-ray diffraction (XRD)

Phase and crystal structure of the samples were measured by a X-ray diffractometer (XRD) (Rigaku, UltimaIV) with CuKα radiation operated at 40 kV and 20 mA with a scanning step of 0.02º /min in a range of 10º to 90º. XRD analyzer was shown in Figure 3.7.

Figure 3.7 X-ray diffraction analyzer

3.2.3.5. Specific surface area and pore structure by N_2 sorption combined with Brunauer-Emmett-Teller (BET) and pore analysis approaches.

BET surface area of the samples was characterized by N_2 sorption (Bel Japan, BELSORP-miniII) as shown in Figure 3.8. Brunauer–Emmett–Teller (BET) equation was used to calculate their specific surface area.

Figure 3.8 N_2 sorption analyzer

3.2.3.6 Carbon atom arrangement by Raman spectroscopy

Crystallinity of the acid-functionalized samples were accomplished using Raman spectroscopy (NTEGA spectro, NT-MDT) as shown in Figure 3.9. Red laser source was used to study the Raman spectra of the samples.

Figure 3.9 Raman spectroscopy

3.2.3.7. Surface functional groups by Fourier transform infrared (FT-IR) spectrometer

Surface functional groups of acid-functionalized samples were studied by Fourier transform infrared (FT-IR) spectrometer (Thermo Scientific, Nicolet 6700) as shown in Figure 3.10. The samples were prepared by mixing dry material into KBr powder and compressed into a thin circular sheet before insert to the machine. The number of scans for the measurement was 64. The frequency range was observed in a range of 500-4000 cm^{-1}.

Figure 3.10 Fourier transform infrared (FT-IR) spectrometer

3.2.3.8. Acidity by temperature programmed desorption of ammonia (NH_3-TPD)

Acidity of acid functionalized samples was measured by a temperature program desorption of ammonia (NH_3-TPD) using chemisorption analyzer (Quantachrome, ChemStar) as shown in Figure 3.11. The samples (30 mg) were put in a U-tube sample cell and removed the moisture at 150 °C for 1 h before NH_3 adsorption at 60 °C for 1 h. After that samples were heated to 900 °C with a heating rate of 5 °C/min to desorb the NH_3 and resulted gas were detected by a thermal conductivity detector (TCD).

Figure 3.11 Chemisorption analyzer

3.2.3.9. Alloy loading by thermogravimetric analysis (TGA)

Compositions of the samples were evaluated by using a thermogravimetric analyzer (TGA) (Shimadzu, TGA-50) as shown in Figure 3.12. The sample was put in an alumina pan and heated from room temperature to 900 °C with a ramp rate of 10 °C/min in air. Then composition of the samples was calculated based on the completely oxidation weight of the sample.

Figure 3.12 Thermogravimetric analyzer

3.2.3.10. Metal leaching by inductively coupled plasma mass spectrometry (ICP-MS)

Metal leaching after acid functionalization were analyzed by inductively coupled plasma mass spectrometry (ICP-MS) (Agilent Technologies, 7900 ICP-MS) as shown in Figure 3.13. Acid solution after acid functionalization were used to analyze by ICP-MS.

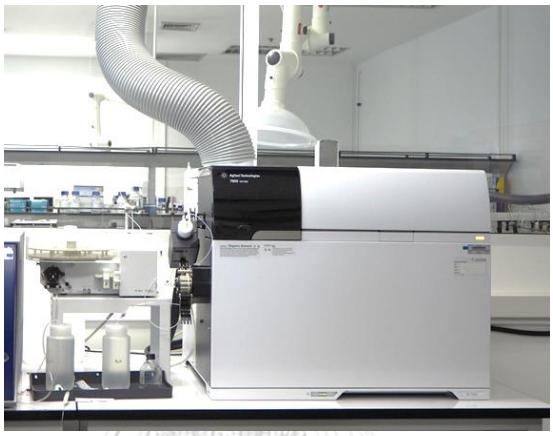

Figure 3.13 Inductively coupled plasma mass spectrometry

3.3. Catalysis applications

The investigation of application of such nanomaterials for converting sugar and their derivatives to valuable bio-chemical products would potentially provide new tangible evidences on their usefulness. The samples were tested by three different reactions. The sections of the catalysts were depended on specific requirement of the catalyst in each reaction.

3.3.1. Dehydration of xylose to furfural

Conversion of xylose to other high value-added products, especially furfural was performed using an autoclave reactor with the presence of CNHs and functionalized CNHs. Composition of resulted products was identified and analyzed for evaluating the catalytic performance. Two sizes of batch reactors were tested.

3.3.1.1. Parr reactor

A 300 ml batch reactor (Parr 4560 mini-series) (Figure 3.14) was selected. 0.1 g of CNHs or oxidized CNHs (oxd-CNHs) was loaded into a reactor. The reactor was pressurized to 15 bar under N_2 atmosphere in prior to being heated to 170 °C. Then 60 ml (0.2 mol/L) of xylose was loaded into the reactor and stirred with a stirring speed of 500 rpm. The resultant product was collected after the elapsed time of 4 h. A nylon syringe filter was used to collect liquid sample for high-performance liquid chromatography (HPLC) analysis. For comparison, commercial CNTs (CNTs) (C 70 P, BAYTUBES) and oxidized CNTs (oxd-CNTs) were also studied with similar conditions. The xylose conversion, furfural yield and selectivity were defined as the following equations:

$$\text{Xylose conversion (\%)} = \frac{\text{Mole of xylose converted (mol)}}{\text{Mole of xylose before reaction (mol)}} \times 100 \qquad (1)$$

$$\text{Furfural yield (\%)} = \frac{\text{Mole of furfural produced (mol)}}{\text{Mole of xylose before reaction (mol)}} \times 100 \qquad (2)$$

$$\text{Furfural selectivity (\%)} = \frac{\text{Mole of furfural produced (mol)}}{\text{Mole of xylose converted (mol)}} \times 100 \qquad (3)$$

Figure 3.14 Parr reactor [69]

3.3.1.2. In-house batch reactor

CNHs, Ni/CNHs-10, Cu/CNHs-10 and NiCu/CNHs-5:5 with and without thermal treatment (oxidation and reduction) were studied as catalysts by using an in-house batch reactor (Figure 3.15). 0.05 g of catalyst and a 30 mL of 0.2 mol/L xylose solution was loaded into the 80 mL autoclave equipped with teflon liner. Magnetic bar was employed for stirring the suspension with a constant speed of 700 rpm. In prior to being heated to 170 °C, N_2 was purged to remove O_2 dissolving in the liquid suspension and to increase the vessel pressure to 15 bar. Resultant product was collected after being held for 4 h. Similar product collection was performed as above procedures. The xylose conversion, furfural yield and selectivity were defined by equation (1), (2), (3):

Figure 3.15 In-house batch reactor

3.3.2. Esterification of levulinic acid to ethyl levulinate

Esterification of levulinic acid (LA) to produce methyl levulinate (ML) in ethanol (EtOH) was studied to evaluate the performance of acid functionalized samples (SA-60-CNHs, SA-60-oxd-CNHs, and SA-60-Pd/CNHs). Effect of amount of catalyst, reaction temperature, and initial molar ratio of LA:EtOH were studied. The amount of catalyst was varied at 0, 15, 20 and 25 mg while the reaction temperature was tested at 100, 120, and 140 °C. The initial molar ratio of LA:EtOH was changed between 1:3, 1:5, and 1:7. The reaction time was set at 90 min. After the reaction, liquid product was separated from solid catalyst by centrifugal and filtrated by syringe filter before

analyzed by HPLC. The LA conversion, EL yield and selectivity were defined as the following equations (4),(5),(6):

$$\text{LA conversion (\%)} = \frac{\text{Mole of LA converted}}{\text{Mole of LA before reaction}} \times 100 \quad (4)$$

$$\text{EL yield (\%)} = \frac{\text{Mole of EL produced}}{\text{Mole of EL before reaction}} \times 100 \quad (5)$$

$$\text{EL selectivity (\%)} = \frac{\text{Mole of EL produced}}{\text{Mole of LA converted}} \times 100 \quad (6)$$

3.3.3. Transfer hydrogenation of Methyl levulinate to *γ*-valerolactone

To evaluate the catalytic performance of catalysts, Ni/CNHs-10, Cu/CNHs-10, and NiCu/CNHs-7:3, NiCu/CNHs-5:5, NiCu/CNHs-3:7 with or without thermal treatment, hydrogenation of methyl levulinate (ML) to *γ*-valerolactone (GVL) in an in-house batch reactor was tested. 0.1 g of the catalyst and 24 cm^3 of 0.2 mol/L methyl levulinate in 2-propanol were mixed under continuous magnetic stirring throughout the whole reaction period. The reaction was heated up to 200 °C with heating rate of 10 °C/min and held at this temperature for 3 h. Then, the liquid product was collected and analyzed by gas chromatography (GC). Moreover, red-oxd-Ni/CNHs-10 was used to further study about effect of reaction temperature and reusability of the catalyst. For effect of reaction temperature, reaction temperature was investigated at 140, 170, and 200 °C. In addition, the reusability of the catalyst was studied as follows: the used catalyst was recovered by filtration and dried overnight in a vacuum oven at 60 °C before testing in the next cycle. The catalyst was tested for 5 repetitive cycles. The ML conversion, GVL yield and selectivity were defined as the following equations (7),(8),(9):

$$\text{ML conversion (\%)} = \frac{\text{Mole of ML converted}}{\text{Mole of ML before reaction}} \times 100 \quad (7)$$

$$\text{GVL yield (\%)} = \frac{\text{Mole of GVL produced}}{\text{Mole of ML before reaction}} \times 100 \quad (8)$$

$$\text{GVL selectivity (\%)} = \frac{\text{Mole of GVL produced}}{\text{Mole of ML converted}} \times 100 \quad (9)$$

3.4. Analytical instruments

3.4.1. High performance liquid chromatography (HPLC)

Liquid products from reactions were analyzed by high performance liquid chromatography (HPLC) (Shimadzu) (Figure 3.16). A refractive index and UV-Vis detectors (210 nm) were used in the analysis process. Liquid product was separated by BIO-RAD Aminex HPX-87H column at 45 °C before went through the detectors. A 5mmol/L of H_2SO_4 solution was used as a mobile phase at a flow rate of 0.6 ml/min.

Figure 3.16 High performance liquid chromatography

3.4.2. Gas chromatography (GC)

Gas chromatography (GC) (Shimadzu, GC-2010 Plus) (Figure 3.17) were used to analyzed liquid products from reactions. Gas chromatography with flame ionization detector (FID) equipped with DB-WAX column were used.

Figure 3.17 Gas chromatography

Chapter IV
RESULTS AND DICUSSION

4.1. Synthesis and functionalization of CNHs

CNHs and metal/alloy hybridized with CNHs were synthesis by GI-AIW method. In addition, surface modification, including thermal treatment, acid functionalization and post treatment on CNHs and metal/alloy hybridized with CNHs were performed. Effect of synthesis conditions and modification of the resulted samples were studied.

4.1.1. Synthesis of CNHs

By using only pure graphite cathode and anode on GI-AIW process, CNHs were synthesized. High purity of CNHs was provided by collected only black particles floating on the top of water surface after the arc discharge process.

Phase and crystallinity of CNHs were investigated by XRD as seen Figure 4.1. From XRD pattern, diffraction peaks were observed at 2θ=26.6°, 42.4°, 44.7°, 54.8° 77.7°, and 83.8° were the reflection of hexagonal graphite namely C(002), C(100), C(101), C(004), C(110), and C(112), respectively.

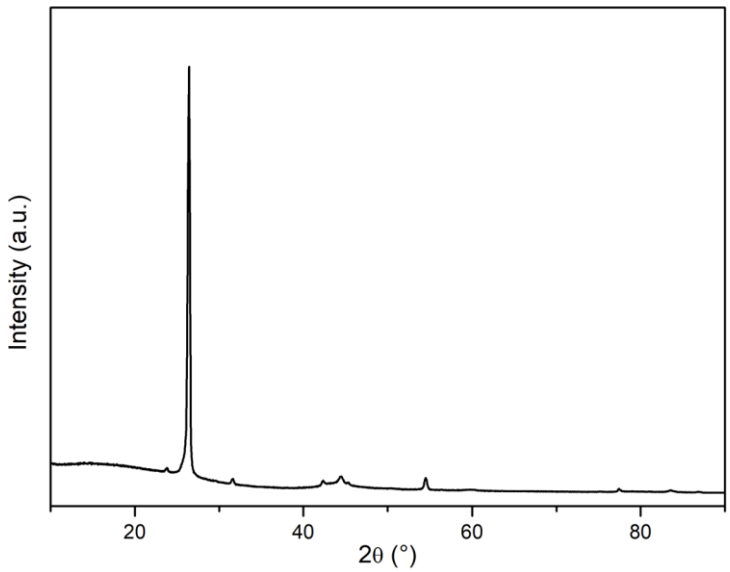

Figure 4.1 XRD pattern of CNHs

The morphology of CNHs was investigated by TEM. Three difference magnification of TEM images were shown in Figure 4.2. The agglomerated of CNHs were presented.

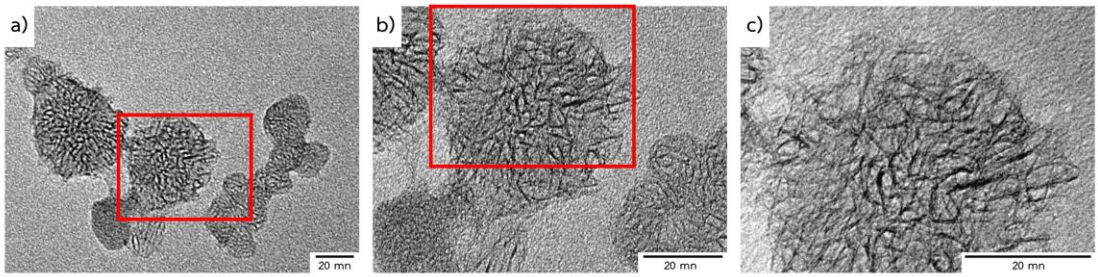

Figure 4.2 TEM images of CNHs at a)x120k, b)x250k, c) x400k

Specific surface area of CNHs was measured by N_2 sorption analyzer and reported in Figure 4.3(a). Specific surface area of CNHs was estimated by the Brunauer-Emmett-Teller (BET) method. CNHs had 162 m^2/g, 0.49 cm^3/g, and 12.20 nm of specific surface area, total pore volume, and average pore diameter, respectively. According to large average pore diameter when compared to diameter of a single horn structure, this can be implied that the majority pore volume in this case was the volume between agglomerated CNHs particles and the minority is the volume in each CNHs particle which could be confirmed by pore size distribution in Figure 4.3(b).

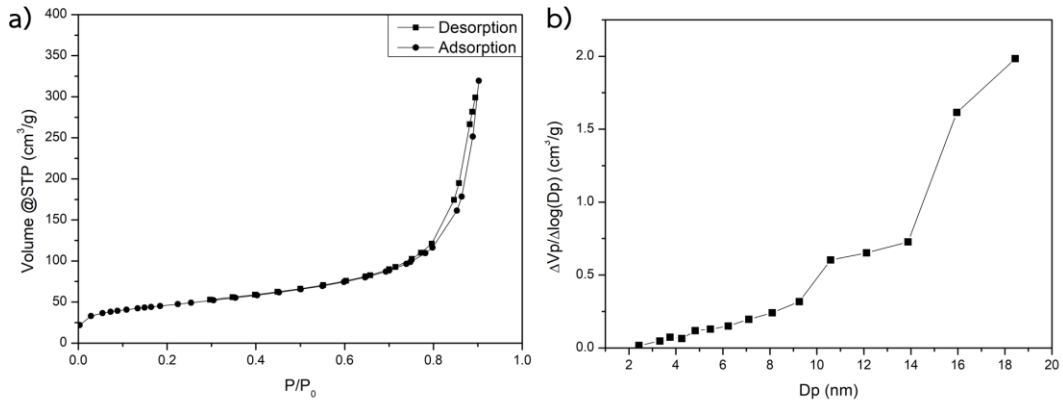

Figure 4.3 a) Adsorption-desorption isotherm of CNHs, b) pore size distribution of mesopores by BJH

Degree of graphitic and disorder carbon of CNHs were investigated by Raman spectroscopy. From Figure 4.4, two peaks were observed which are the representative of D peak (around 1300 cm^{-1}) and G peak (around 1590 cm^{-1}), respectively. The D peak is referred to disorder or amorphous carbon while G peak corresponds to graphitic carbon [70, 71]. The ratio of intensity of D peak and G peak (I_G/I_D) can provide the quality of CNHs. The I_G/I_D ratio of CNHs was 0.80.

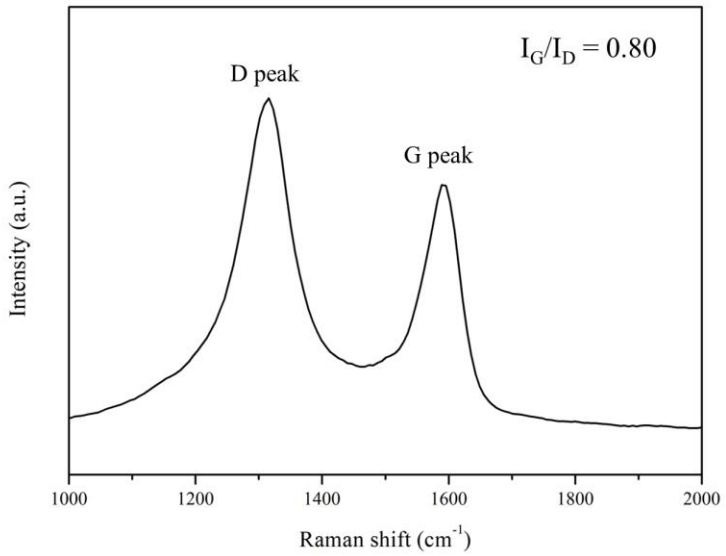

Figure 4.4 Raman spectra of CNHs

Thermal stability of CNHs was investigated by TGA analysis in air environment. From Figure 4.5, CNHs started to decompose at 400 °C. Weight of CNHs was drastically decreased around 500-600 °C. Very high purity of carbon was confirmed from TGA curve.

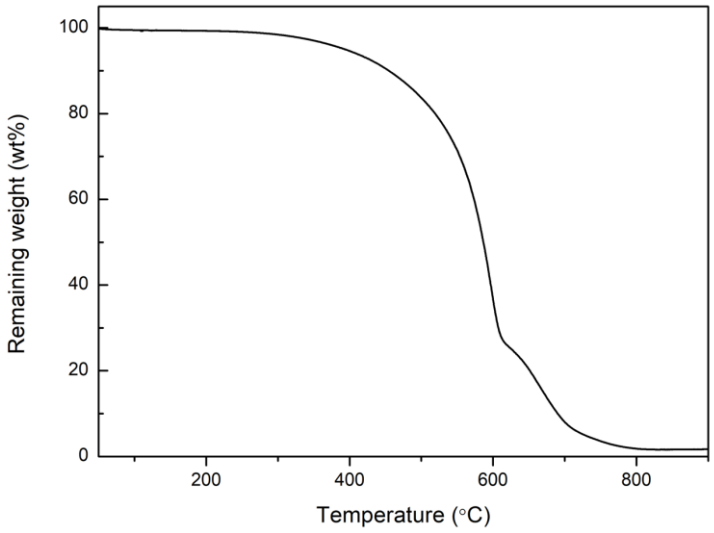

Figure 4.5 TGA curve of CNHs

4.1.2. Mono-functional group

4.1.2.1. Metal/Alloy hybridized with CNHs

Phase and crystallinity of the samples were identified by XRD. For Ni/CNHs and Cu/CNHs samples, XRD patterns between 2θ=10-90° were shown in Figure 4.6(a) and (c) and 2θ =40-53° were shown in and Figure 4.6(b) and (d), respectively. Both Ni/CNHs and Cu/CNHs presented a very shapely peak at 2θ=26.6°, which is the reflection of hexagonal graphite [72]. For all Ni/CHNs samples, peaks at 2θ=44.4°, 51.7° and 76.2° indicated the refraction of face-centered cubic structure (FCC) which are Ni(111), Ni(200), and Ni(220) respectively [30, 73]. The intensity of Ni peak increased with increasing of number of Ni wire which can be implied that when metal loading was increased, intensity of peak also increased. Average crystalline size of the sample was calculated based on Scherrer equation [74] with shape factor = 0.9 and reported in Table 4. 1Table 4. 1 Average crystalline size of Ni/CNHs and Cu/CNHs by XRD. The increasing of the intensity means crystalline size is larger. In case of Cu/CNHs, the peaks at 2θ=43.3°, 50.4°, and 74.1° is the reflection of FCC structure which are Cu(111), Cu(200), and Cu(220), respectively [30, 75, 76]. Increasing of the peak intensity along with the increasing of the number of Cu wire were also reported.

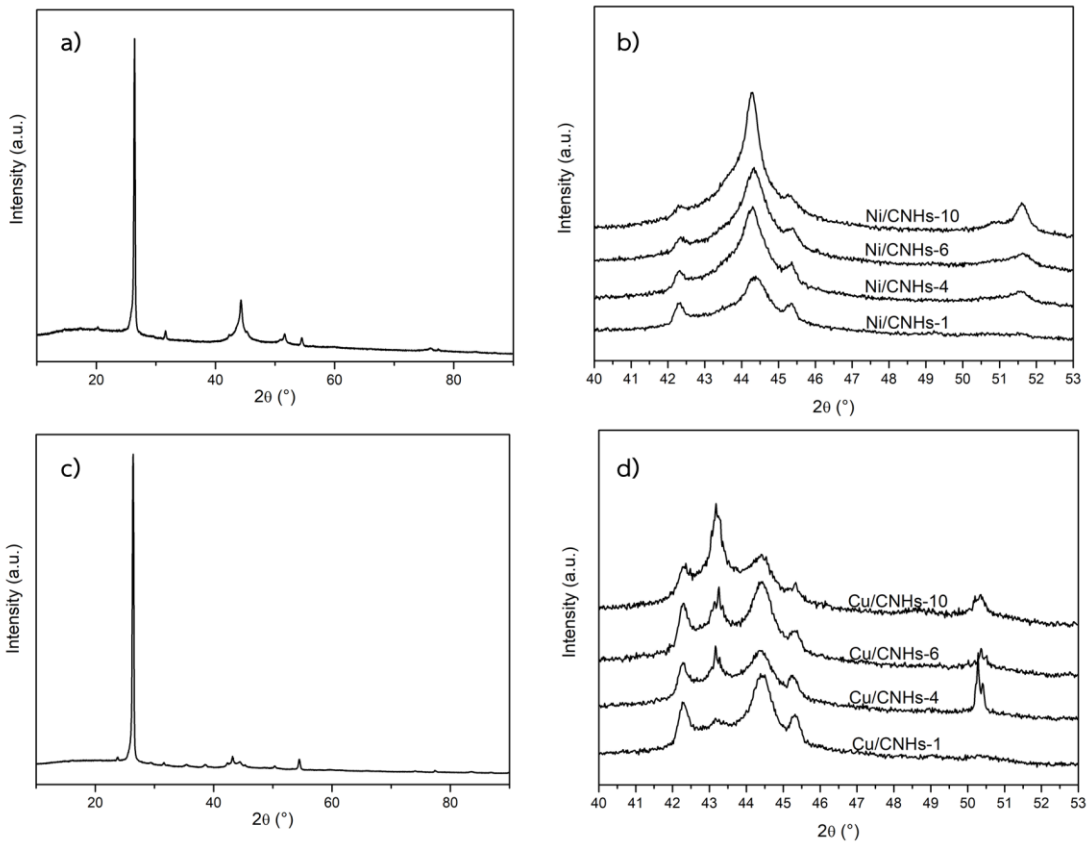

Figure 4.6 XRD patterns of a)Ni/CNHs-10, b)Ni/CNHs-1,4,6,10, c)Cu/CNHs-10, d)Cu/CNHs-1,4,6,10

Table 4. 1 Average crystalline size of Ni/CNHs and Cu/CNHs by XRD

No. of metal wire	Average crystalline size by XRD (nm)	
	Ni/CNHs	Cu/CNHs
1	6.16	5.34
4	6.94	6.60
6	8.23	7.41
10	9.25	10.12

For NiCu/CNHs at total number of wire were 10 wires (Figure 4.7 (a)) and at fix ratio of Ni to Cu (Figure 4.7 (b)), XRD patterns showed two peaks between Cu(111) to Ni(111) and Cu(200) and Ni(200) which can be implied that NiCu alloy were formed in every sample [30, 77-80]. Average crystalline size of NiCu/CNHs samples was reported in Table 4. 2. However, a graphite peak at 2θ = 44.6° is overlapped with

Cu(111) and Ni(111) peaks so the composition of Ni to Cu is difficult to calculate through XRD results.

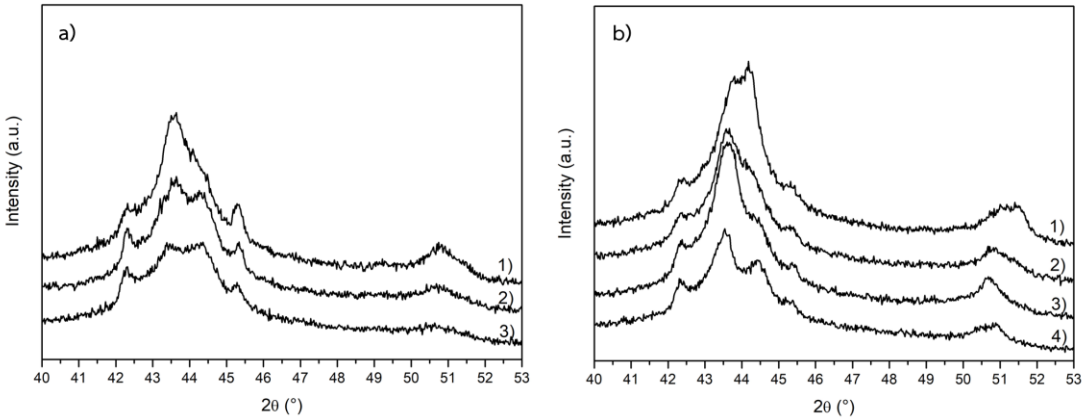

Figure 4.7 XRD patterns of NiCu/CNHs with Ni:Cu = a.1)8:2, a.2)6:4, a.3)4:6, a.4)2:8, b.1)4:4, b.2)2:2, b.3)1:1

Table 4. 2 Average crystalline size of NiCu/CNHs by XRD

Sample	Average crystalline size by XRD (nm)	Sample	Average crystalline size by XRD (nm)
NiCu/CNHs-8:2	7.66	NiCu/CNHs-4:4	7.79
NiCu/CNHs-6:4	8.36	NiCu/CNHs-2:2	6.42
NiCu/CNHs-4:6	10.28	NiCu/CNHs-1:1	2.63
NiCu/CNHs-2:8	6.76		

XRD patterns of Fe/CNHs-10 and other NiFe/CNHs samples were presented in Figure 4.8. A small broad peak at 2θ = 44.5° is identified as Fe(110) in BCC structure [81]. For all of NiFe/CNHs with difference Ni to Fe ratio, peak positions of 2θ were shifted toward smaller angle (compared to Ni/CNHs). This phenomenon confirmed the formation of NiFe alloy in the samples [82]. An increasing of Ni to Fe ratio, the shifting of diffraction peak was closer to Ni(111). Another evidence to support the formation of NiFe alloy is an additional peak around 2θ = 50-52° were presented in XRD pattern of all conditions of NiFe/CNHs.

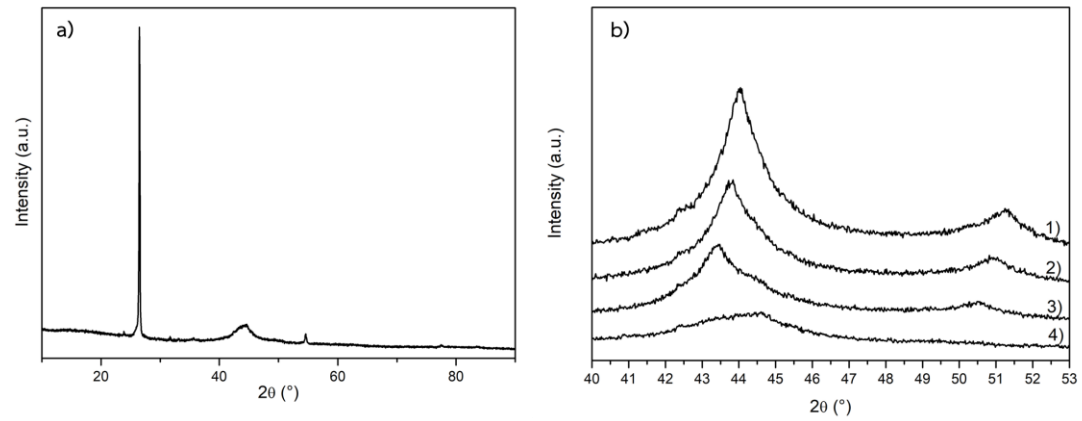

Figure 4.8 XRD patterns of a) Fe/CNHs-10, b.1)NiFe/CNHs-7:3, b.2)NiFe/CNHs-5:5, b.3)NiFe/CNHs-3:7, b.4)Fe/CNHs-10

For Pd/CNHs, diffraction peaks were discovered at 2θ=26.6° from C(002) and at 2θ=40.1°, 46.7°, 68.2°, and 82.2° for Pd(111), Pd(200), Pd(220), and Pd(311), respectively as shown in Figure 4.9 (a). Two peaks which were shifted toward smaller diffraction angle (compared to Ni/CNHs) was observed in every Ni to Pd ratio of NiPd/CNHs (Figure 4.9 (a)), peak around 2θ=44-56° and 2θ=49-52°. The formation of NiPd alloy was confirmed [10]. Larger peaks shifted from Ni(111) were presented with an increasing of Pd loading in the samples.

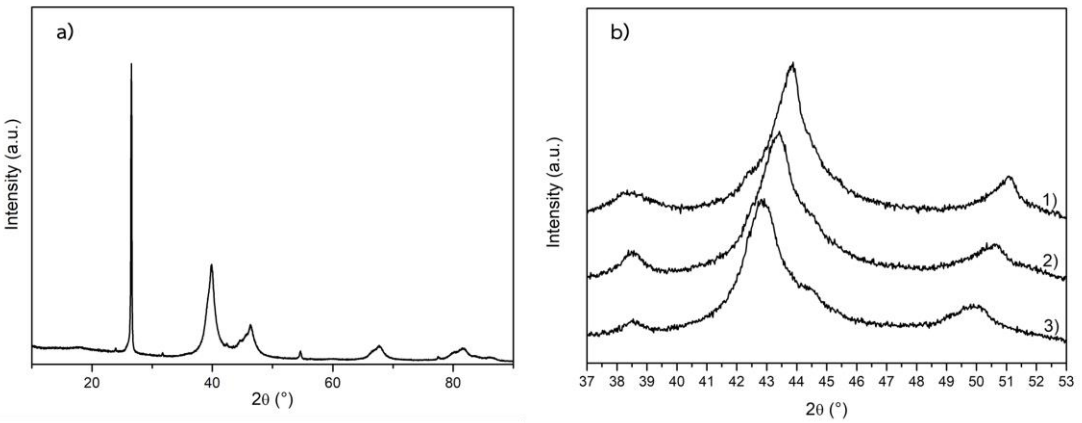

Figure 4.9 XRD patterns of a) Pd/CNHs-4, b.1)NiPd/CNHs-9:1, b.2)NiPd/CNHs 8:2, b.3)NiPd/CNHs-7:3

Pt/CNHs were also studied by XRD and reported in Figure 4.10 (a). The XRD pattern showed diffraction peaks of graphitic carbon and additional peaks at 2θ=39.6°, 46.1°, 67.2°, 81.0°, and 85.4° which were identified as Pt(111), Pt(200), Pt(220), Pt(311), and Pt(222), respectively. For NiPt/CNHs, an alloy formation resulted in peak position shifted from Pt and Ni metal to a new position which were between two initial positions of the metal [83]. The peak position shifted of NiPt/CNHs with different Ni to Pd ratio were presented in Figure 4.10 (b).

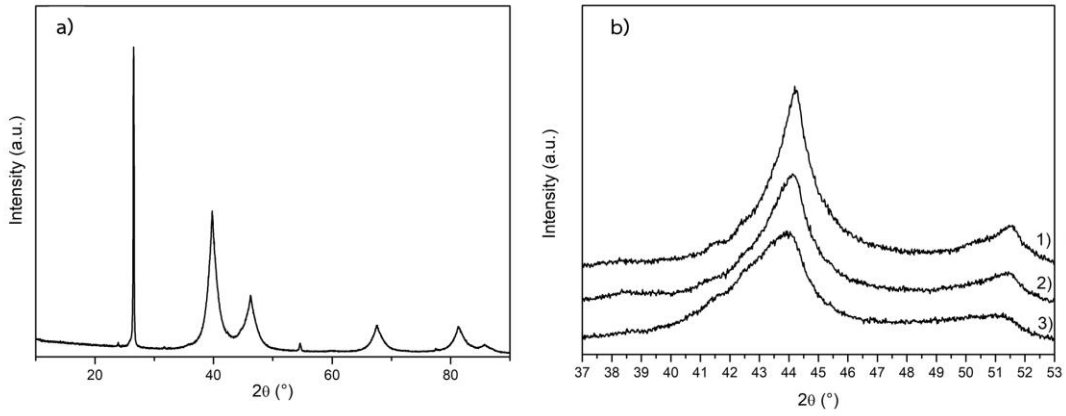

Figure 4.10 XRD patterns of a) Pt/CNHs-4, b.1)NiPt/CNHs-9:1, b.2)NiPt/CNHs 8:2, b.3)NiPt/CNHs-7:3

In case of PdPt/CNHs, the diffraction peak position of Pd and Pt is very close to each other so the PdPt alloy formation is difficult to identify with peak positions. However, the intensity of diffraction peak is differed between Pd and Pt [84, 85]. From Figure 4.11, the intensity of each peak was decreased with an increasing of Pd to Pt ratio. The different in intensity of diffraction peaks can confirmed the PdPt alloy formation in PdPt/CNHs samples.

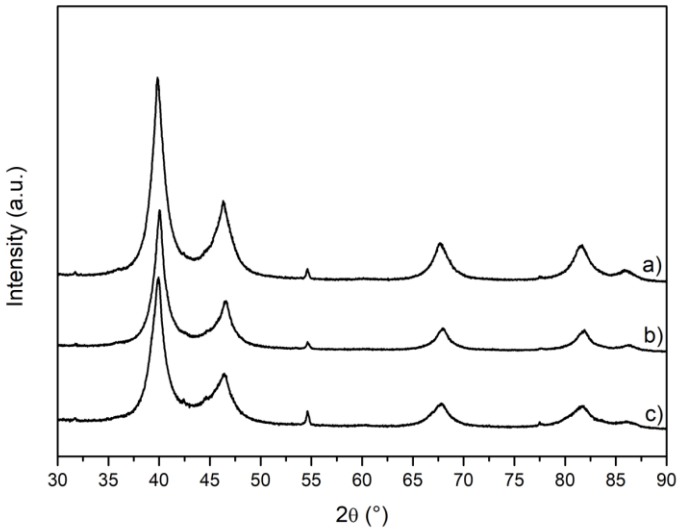

Figure 4.11 XRD patterns of PdPt/CNHs at Pd:Pt = a)1:3, b)2:2, c)3:1

Morphology of all samples was investigated by TEM. TEM have been accepted to be used for measuring the size of nanoparticles (primary particle). TEM images and metal particle size distribution of Ni/CNHs and Cu/CNHs were shown in Figure 4.12 and Figure 4.13, respectively. All samples presented similar morphology which were black particles embedded in CNHs structure. The size of the Ni nanoparticles was increased when the number of Ni wire loading was increased. Similar to the average size of metal nanoparticles, size distribution of Ni nanoparticles was wider when increasing number of Ni wire loading. For Cu/CNHs, similar result was discovered. However, the average size of Ni and Cu nanoparticles was differed from each other with the same number of metal wire. This is due to the different in the evaporation rate of metal and solubility of metal in carbon species. Average size of Ni in Ni/CNHs with Ni wires = 1, 4, 6 and 10 were 4.6, 5.0, 5.6, and 7.5 nm, respectively, while average size of Cu in Cu/CNHs were 4.2, 5.1, 5.2, and 6.6 nm for Cu wires = 1, 4, 6, and 10, respectively. For comparison, the size of the sample measuring by XRD and TEM was in the same magnitude. A similar trend of average size was reported when increasing the metal wire loading for both Ni/CNHs and Cu/CNHs sample. For the reminding, average size which was calculated by Scherrer equation may have some error because this equation is not appropriate to be applied to nanoparticle. According to the above results, size of metal nanoparticles could be depended on metal loading (number of metal wire) in the synthesis process.

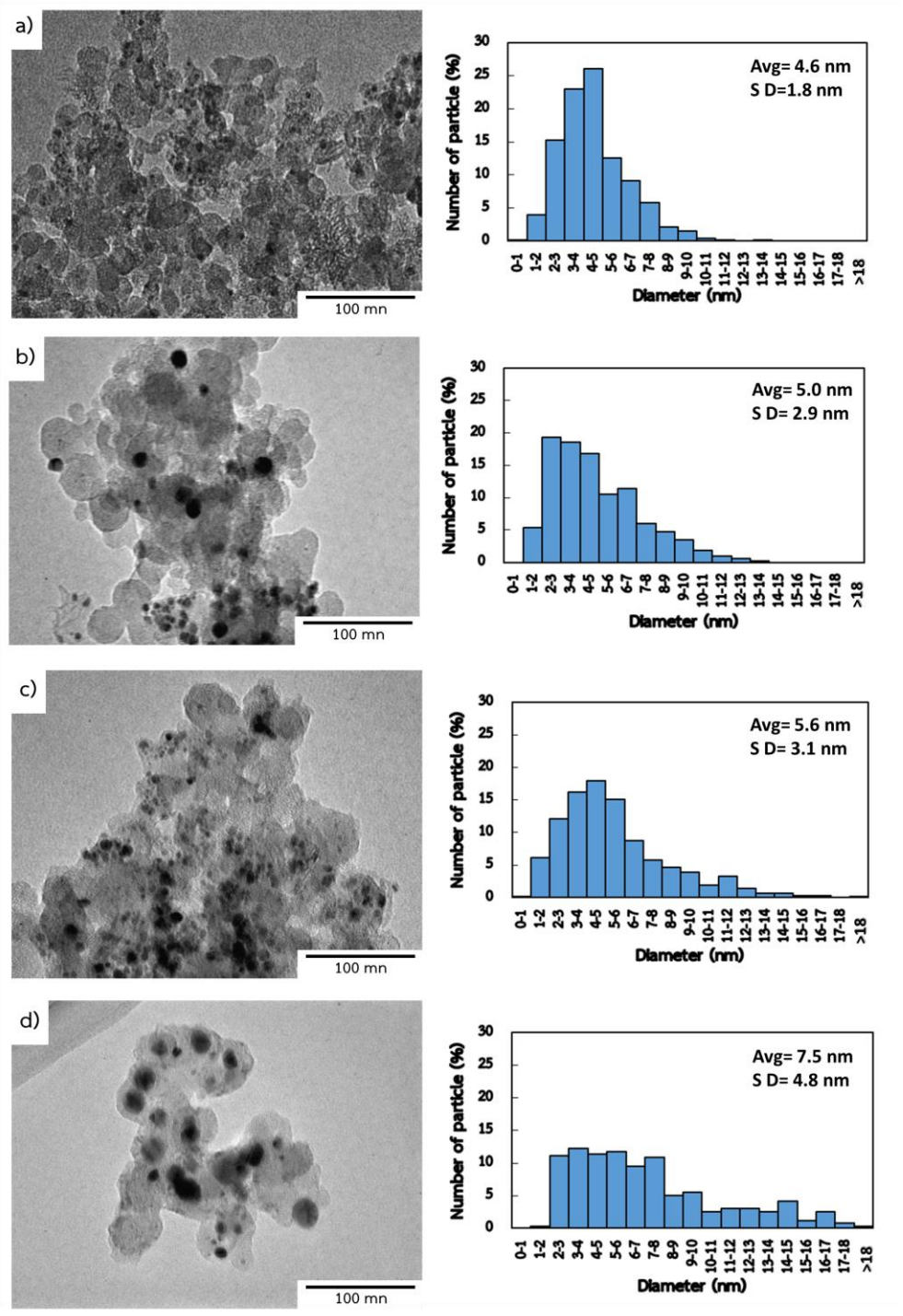

Figure 4.12 TEM images of a)Ni/CNHs-1, b)Ni/CNHs-4, c)Ni/CNHs-6, and d)Ni/CNHs-10

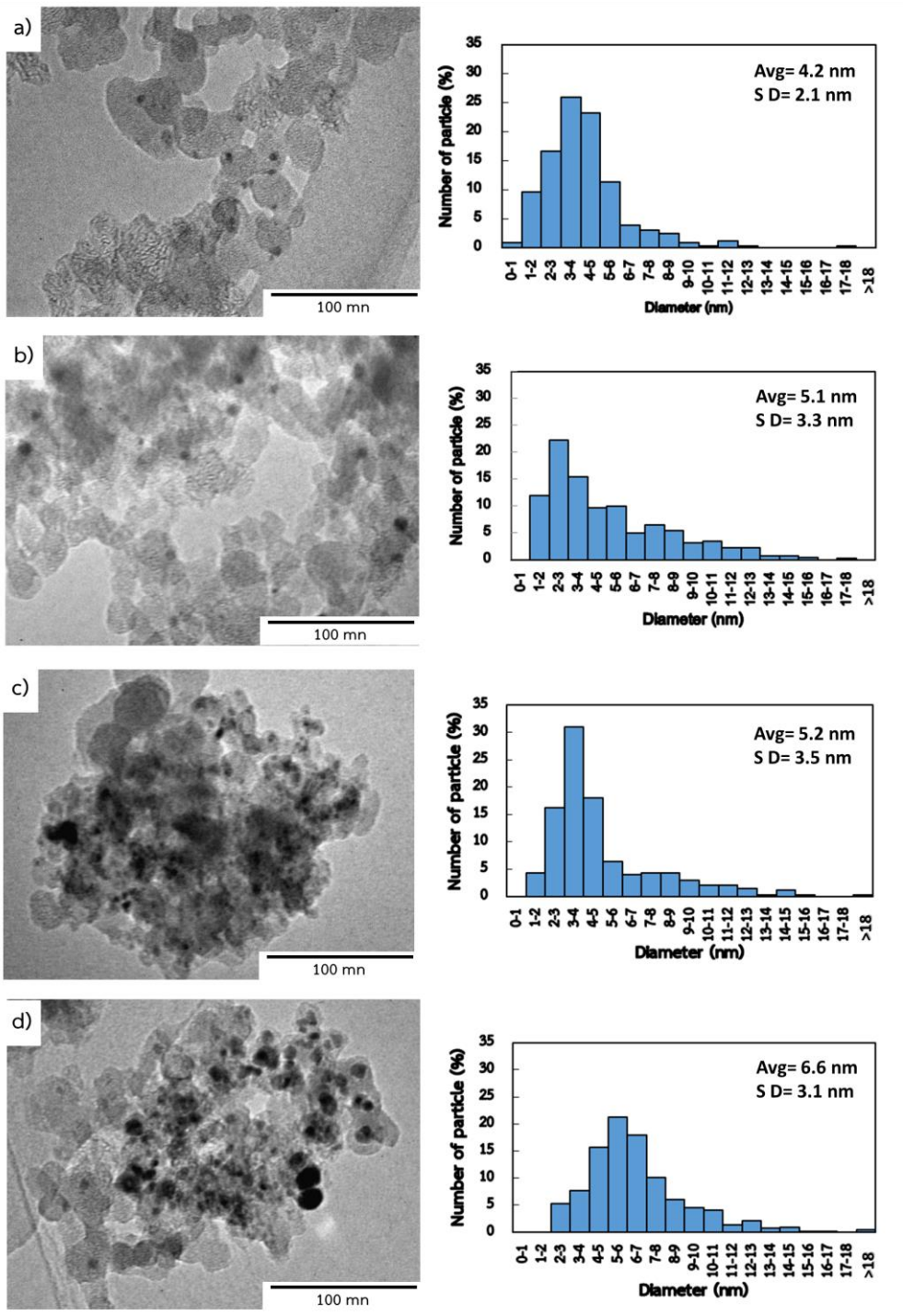

Figure 4.13 TEM images of a)Cu/CNHs-1, b)Cu/CNHs-4, c)Cu/CNHs-6, and d)Cu/CNHs-10

In case of NiCu/CNHs, size of alloy nanoparticles was changed by variation of Ni:Cu ratio (by number of metal wire). TEM images and metal particle size distribution of samples with fix total number of metal wire to 10 wires and varied ratio of Ni:Cu to 8:2, 6:4, 4:6, and 2:8 were reported in Figure 4.14. Average size of alloy nanoparticles was 6.4, 5.0, 4.7, and 4.6 nm for NiCu/CNHs-8:2, 6:4, 4:6, and 2:8. Average size of alloy nanoparticles was decreased when Ni loading was decreased. In addition, average size of NiCu/CNHs-8:2, 6:4, 4:6, and 2:8 were smaller than Ni/CNHs-10 and Cu/CNHs-10. Those results could by caused by the similar structure of Ni and Cu (FCC) resulted in shoving of metal atom which affected to smaller size of alloy nanoparticles [79, 86]. Samples with fix Ni:Cu ratio of 1:1 and vary total number of metal wires (1:1, 2:2, and 4:4,) were also studied by TEM and presented in Figure 4.15. Average diameter size of NiCu alloy nanoparticles in NiCu/CNHs were 6.8, 7.0, and 8.3 nm for NiCu/CNHs-1:1, NiCu/CNHs-2:2, and NiCu/CNHs-4:4, respectively. A wide distribution of average NiCu alloy size was presented in every condition. This could be caused by an increasing of solubility of NiCu in carbon material comparing to the solubility of Cu in carbon material resulted in larger average metal diameter.

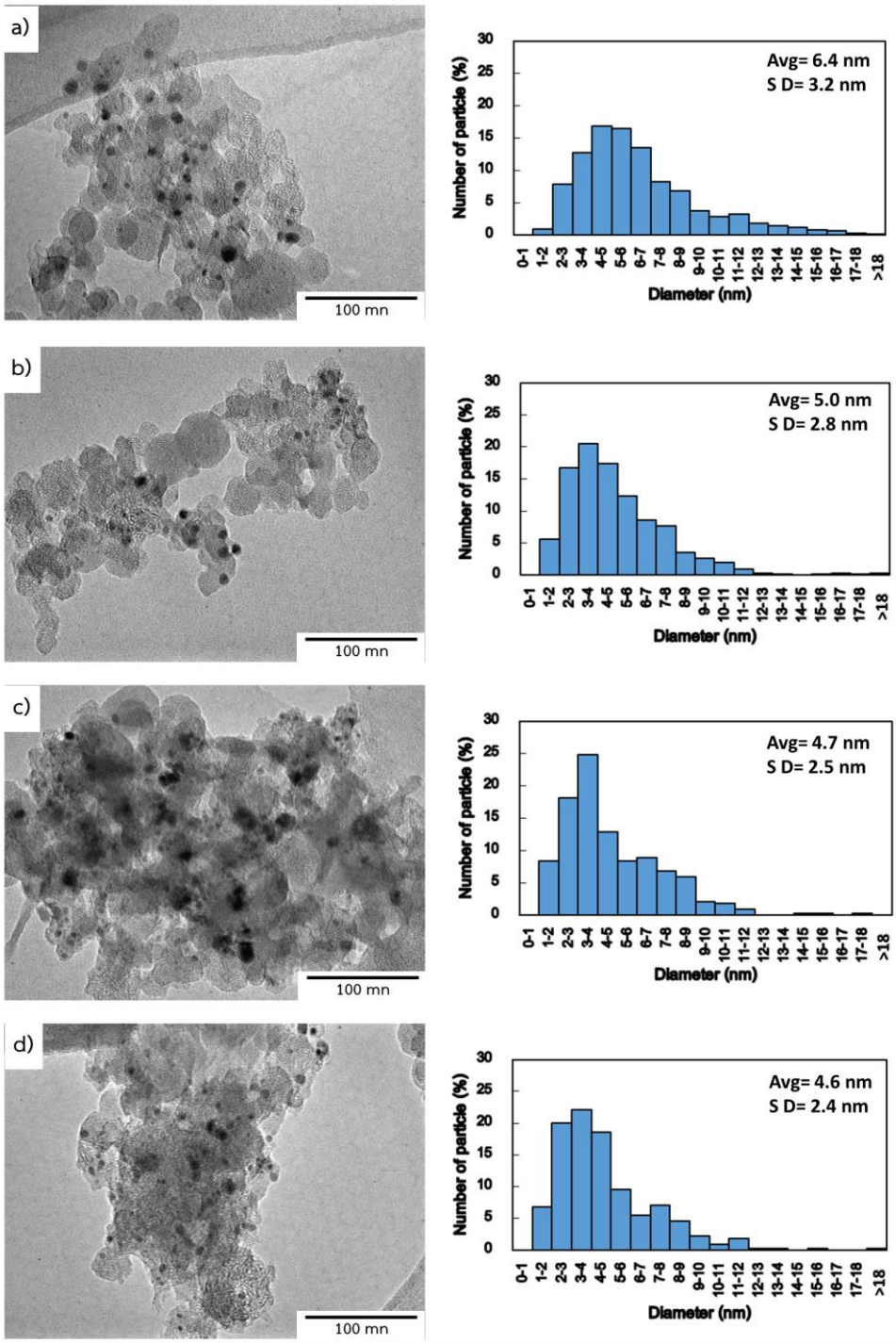

Figure 4.14 TEM images of a)NiCu/CNHs-8:2, b)NiCu/CNHs-6:4, c)NiCu/CNHs-4:6, d)NiCu/CNHs-2:8

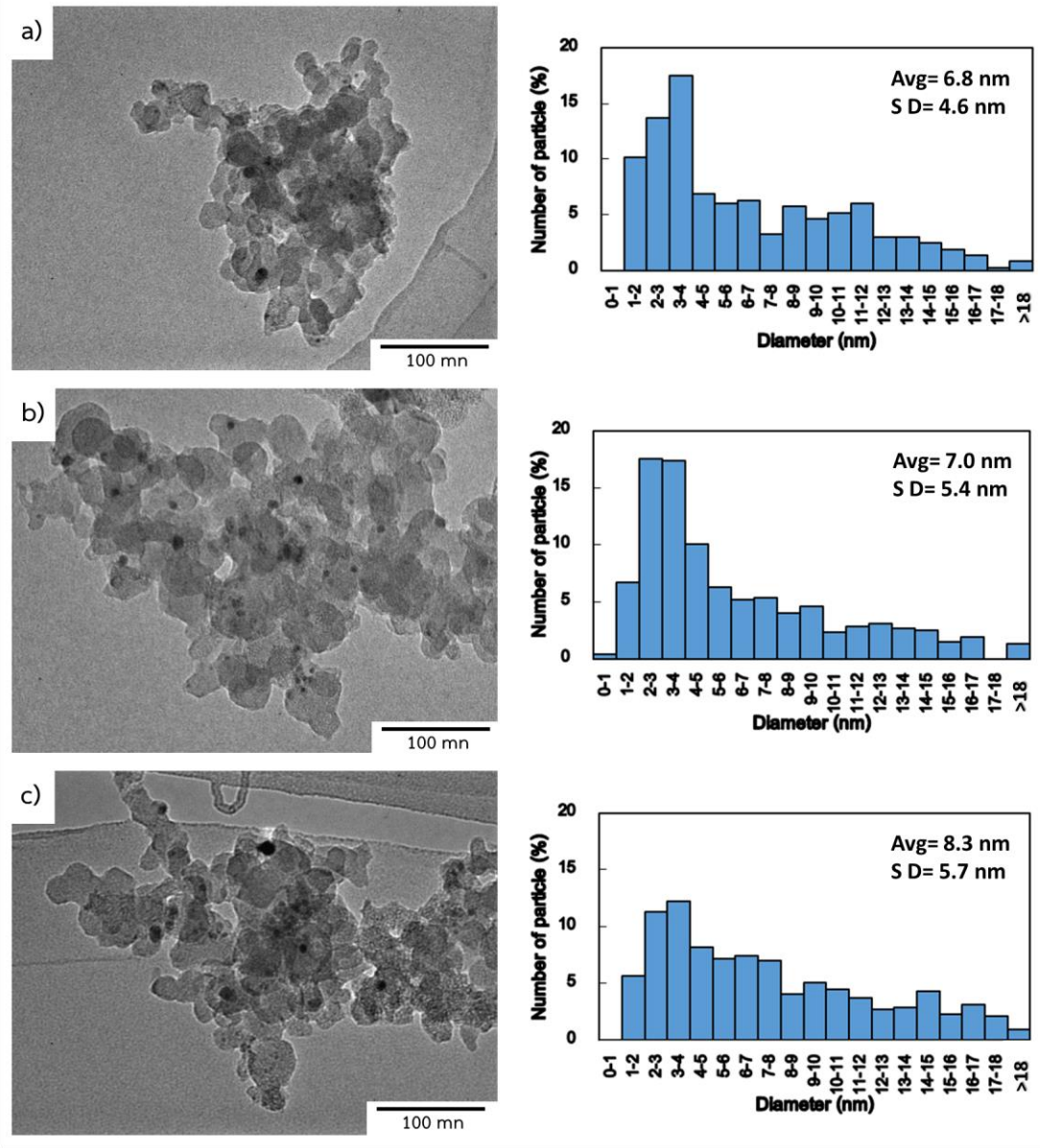

Figure 4.15 TEM images of a)NiCu/CNHs-1:1, b)NiCu/CNHs-2:2, c)NiCu/CNHs-4:4

Morphology of Fe, Pd, Pt hybridized with CNHs were also studied by TEM. A good metal dispersion in CNHs structure was presented in Fe/CNHs-10, Pd/CNHs-4 and Pt/CNHs-4 as shown in Figure 4.16. Average size of Fe, Pd, and Pt in hybridized with CNHs were 6.9, 4.9, and 4.4 nm which differed from each metal due to their properties, evaporation rate and solubility of metal in carbon [87-89]. According to all results, average diameter size of metal/alloy could be depended on the amount of metal loading, type of metal, evaporation rate, and solubility of metal in carbon.

The GI-AIW method started with vaporization of carbon from graphite anode and metal from metal wire to be a vapor of mixture between carbon and metal. These were caused by energy transfer from arc plasma to an anode. After that, the gas mixture was brought to the cooling zone by N_2 gas flow. During the cooling process, the concentration of the vapor gas was reached to the supersaturated point of the mixture and created the nucleus of metal and carbon according to homogenous and heterogeneous nucleation theory, randomly [90-92]. If the metal has a good dissolvability property in carbon, heterogeneous nucleation will be the majority and provide the hybridized material between carbon and metal with high metal loading in the product. On the contrary, if the solubility of metal in carbon is low, the homogeneous nucleation will be the preferable pathway and result in a different product which were composed of a single metal and carbon nanoparticle instead of the hybridized material. Finally, the nucleus were condensed, growth, agglomerate and sinter [93, 94]. In addition, size of metal in the hybridized material was depended on many factors such as concentration of metal in vapor mixture, duration of cooling time (flow rate of N_2 gas), atomic radius of metal, and temperature of arc plasma [90, 95, 96].

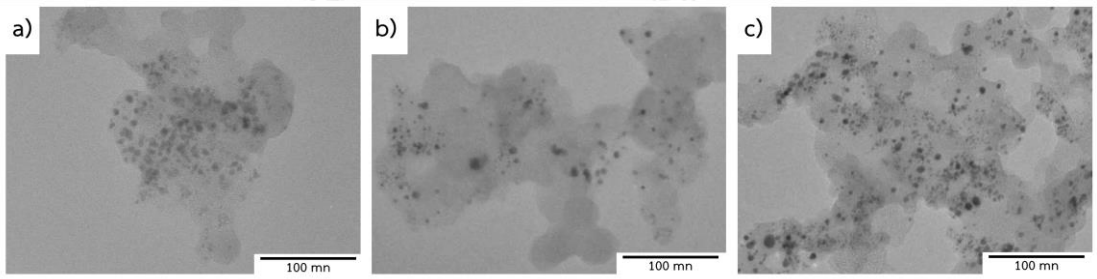

Figure 4.16 TEM images of a)Fe/CNHs-10, b)Pd/CNHs-4, and c)Pt/CNHs-4

The composition and thermal stability of Ni/CNHs and Cu/CNHs were measured by TGA. The compositions of metal in each sample were calculated based on complete oxidation during TGA analysis. For Ni/CNHs, after TGA analysis color of the samples were changed from black to green which is the color of NiO. The Ni content in Ni/CNHs samples were 5.3, 11.3, 14.3, and 15.8 wt% for Ni/CNHs-1, Ni/CNHs-4, Ni/CNHs-6, and Ni/CNHs-10, respectively. Thermal stability of each Ni/CNHs samples were slightly differed in every condition. Weight change of Ni/CNHs samples

changed around 380 °C as seen in Figure 4.17 (a). For Cu/CNHs samples, black powders were obtained after TGA analysis which is the representative of CuO. The content of Cu in Cu/CNHs sample were 3.7, 6.0, 6.4 and 9.2 wt% for Cu/CNHs-1, Cu/CNHs-4, Cu/CNHs-6, and Cu/CNHs-10. From Figure 4.17 (b), weight of Cu/CNHs samples were changed around 350 °C which is lower than Ni/CNHs. Weight changing temperature of Ni/CNHs and Cu/CNHs samples was lower than CNHs. This could be implied that Ni and Cu could help an oxidation process of carbon which resulted in lower decomposition temperature of carbon. In addition, weight of metal in the sample was increased with an increasing of metal wire number.

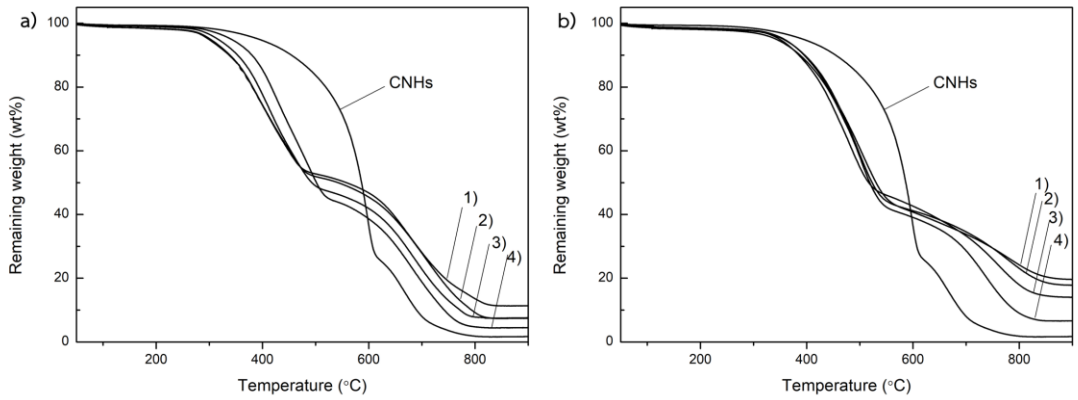

Figure 4.17 TGA curve of Ni/CNHs a.1)Ni/CNHs-10, a.2)Ni/CNHs-6, a.3)Ni/CNHs-4, a.4)Ni/CNHs-1 and Cu/CNHs b.1)Cu/CNHs-10, b.2)Cu/CNHs-6, b.3)Cu/CNHs-4, b.4)Cu/CNHs-1

Compositions of metal/alloy hybridized with CNHs were obtained by EDX and reported in Table 4.3. An increasing of wt% metal was observed with an increasing of metal loading in both Ni/CNHs and Cu/CNHs. For the ratio of alloy component, different results were presented due to the different of metal evaporation rate and the solubility of each metal in carbon [87]. For Ni/CNHs and Cu/CNHs, wt% of Ni was higher than Cu in the products at the same number of metal wire loading. This was due to the lower solubility of Cu in carbon than Ni. However, Ni and Cu system exhibits a complete soluble in each other [97]. According to this explanation, preparation of Cu in form of NiCu alloy could help increase the wt% of Cu in the sample. The solubility of Cu in C is increased when form as NiCu alloy. Mechanism of NiCu/CNHs formation should start with a rapidly evaporation of Ni, Cu and C. Then Ni and Cu dissolved in

each other to form NiCu alloy following with dissolvsion of NiCu in C. After that, NiCu-C were quenched together at the cooling zone. Atomic of NiCu would be condensed and solidified to become nanoparticle which was embedded in CNHs structure as a final product [95]. In addition, Cu (2,562°C) has lower boiling point than Ni (2,913°C) which resulted in Cu provide higher evaporation rate than Ni [98-101]. From this reason, higher wt% of Cu than wt% of Ni in NiCu/CNHs-1:1, 2:2, and 4:4 were reported.

For Fe/CNHs and NiFe/CNHs, wt% of total metal composition in the products was slightly changed between Fe/CNHs and NiFe/CNHs at the same total number of metal wire loading (10 wires). In case of NiPd and NiPt, an increasing of second metal (Pd and Pt) resulted in an increasing of wt% total metal loading in the product due to very high molecular weight compared to C and Ni. On the contrary, due to the large differ of metal properties (melting and boiling point, molecular weight etc.) between Pd and Pt, differentiation of total metal composition in PdPt/CNHs samples were reported as shown in Table 4.3(26-30). From all above evidence not only metal properties but also solubility of metal in carbon both are major factors to control the composition and size of metal in the product [99, 102, 103].

Table 4.3 Composition of the samples by EDX

No.	Samples	Composition by EDX (wt%)					
		C	Ni	Cu	Fe	Pd	Pt
1	Ni/CNHs-1	93.8	6.2	-	-	-	-
2	Ni/CNHs-4	89.6	10.4	-	-	-	-
3	Ni/CNHs-6	86.7	13.3	-	-	-	-
4	Ni/CNHs-10	83.6	16.4	-	-	-	-
5	Cu/CNHs-1	94.1	-	5.8	-	-	-
6	Cu/CNHs-4	91.9	-	8.1	-	-	-
7	Cu/CNHs-6	87.7	-	12.3	-	-	-
8	Cu/CNHs-10	85.8	-	14.2	-	-	-
9	NiCu/CNHs-8:2	79.5	10.6	9.9	-	-	-
10	NiCu/CNHs-6:4	84.5	5.2	10.3	-	-	-

No.	Samples	Composition by EDX (wt%)					
		C	Ni	Cu	Fe	Pd	Pt
11	NiCu/CNHs-4:6	84.6	3.4	12.0	-	-	-
12	NiCu/CNHs-2:8	82.1	2.8	15.1	-	-	-
13	NiCu/CNHs-1:1	90.2	2.2	7.6	-	-	-
14	NiCu/CNHs-2:2	88.3	3.5	8.2	-	-	-
15	NiCu/CNHs-4:4	85.8	5.1	9.1	-	-	-
16	Fe/CNHs-10	75.6	-	-	24.4	-	-
17	NiFe/CNHs-7:3	72.9	19.9	-	7.2	-	-
18	NiFe/CNHs-5:5	77.7	12.9	-	9.5	-	-
19	NiFe/CNHs-3:7	76.7	14.1	-	9.2	-	-
20	NiPd/CNHs-9:1	72.7	20.0	-	-	7.3	-
21	NiPd/CNHs-8:2	63.5	19.3	-	-	17.3	-
22	NiPd/CNHs-7:3	60.2	16.6	-	-	23.2	-
23	NiPt/CNHs-9:1	61.8	19.1	-	-	-	19.1
24	NiPt/CNHs-8:2	64.9	13.2	-	-	-	21.9
25	NiPt/CNHs-7:3	54.6	16.7	-	-	-	28.7
26	Pd/CNHs-4	57.3	-	-	-	42.7	-
27	PdPt/CNHs-3:1	51.5	-	-	-	26.8	21.7
28	PdPt/CNHs-2:2	41.1	-	-	-	25.7	33.3
29	PdPt/CNHs-1:3	57.3	-	-	-	7.8	35.0
30	Pt/CNHs-4	55.8	-	-	-	-	44.2

Specific surface area, total pore volume, and average pore diameter of metal hybridized with CNHs were also studied and presented in Table 4.4. All metal hybridized with CNHs samples had lower specific surface area compared to CNHs (162 m^2/g) due to metal which have smaller surface area attached on CNHs structure. In addition, some of metal nanoparticles could block the space between agglomerated CNHs particles resulted in smaller total pore volume and average pore diameter.

Table 4.4 Specific surface area, total pore volume, and average pore diameter of metal hybridized with CNHs

No.	Samples	Specific surface area (m^2/g)	Total pore volume (cm^3/g)	Average pore diameter (nm)
1	CNHs	162	0.49	12.20
2	Ni/CNHs-10	136	0.44	13.10
3	Cu/CNHs-10	102	0.38	15.05
4	Fe/CNHs-4	125	0.27	8.54
5	Pd/CNHs-4	116	0.31	10.84
6	Pt/CNHs-4	110	0.27	9.83

To scale up the GI-AIW process, many factors have to be considered to provide exact properties with larger production rate. The factors which could have an effect on properties of the products were composed of electrode, gas composition and flow rate, type and amount of energy, geometry of electrode gap, distance between electrodes and so on [90, 95, 96, 104-106]. All factors should be similar to the original one to maintain the product's properties.

4.1.2.2. Oxidation in air

CNHs were oxidized at 380 °C in air to open the pore inside each CNHs. From oxidation process, yield of CNHs was decreased due to the decomposition of carbon. Properties of oxd-CHNs were studied and compared to CNHs.

TEM were used to analyze oxd-CNHs sample and presented Figure 4.18. Structure of CNHs still presented in TEM image. However, the pore opening of CNHs was difficult to observe by TEM.

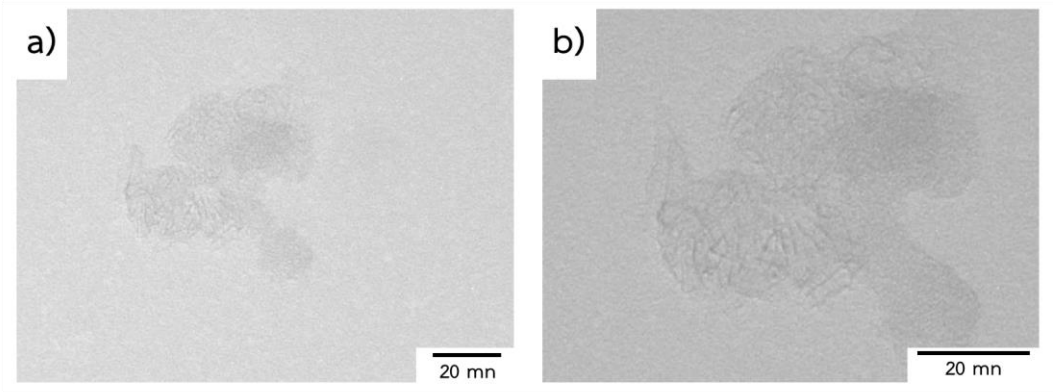

Figure 4.18 TEM images of oxd-CNHs at a)x150k and b)x300k

To confirm the pore opening of CNHs, N_2 sorption was performed. Adsorption -desorption isotherm was presented in Figure 4.19(a). Specific surface area of oxd-CNHs was 418 m^2/g which is almost 2.5 times comparing to CNHs. The increasing of specific surface area was happening due to the pore opening [107-109]. The pore opening process resulted in pore developed in every size of pore as presented in Figure 4.19 (b). Degree of graphitic and disorder carbon of oxd-CNHs was investigated by Raman spectroscopy. Ratio of I_D to I_G of oxd-CNHs was 0.91 which is higher than CNHs. This result supported that amorphous carbons were destroyed during the oxidation process resulted in an increasing of specific surface area.

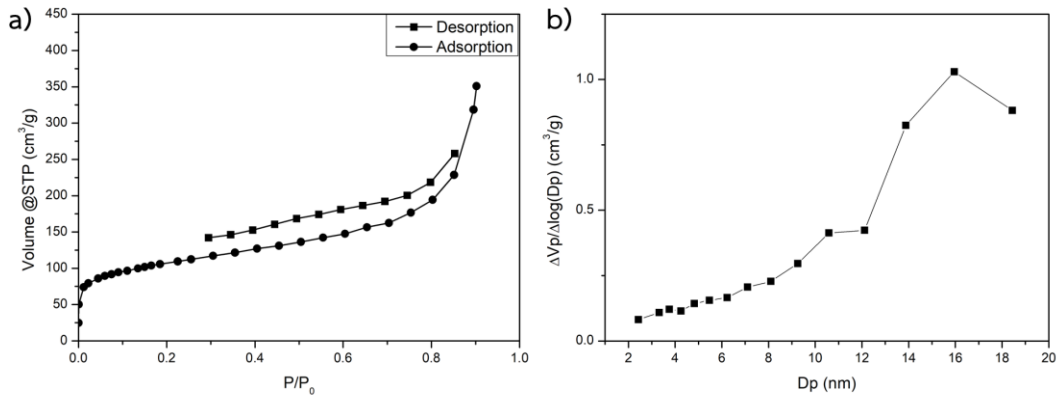

Figure 4.19 a) Adsorption-desorption isotherm of oxd-CNHs, b) pore size distribution of mesopores by BJH

4.1.2.3. Acid treatment

Two different types of acid were used to study the effect of acid treatment on CNHs. Sulfuric acid was chosen due to the very strong acidity property and this acid was normally used in acid treatment of carbon materials. Another acid was acetic acid which is a weak acid. The effect of acid types and treatment time on ultrasonication process were investigated. In addition, acidity and surface functional groups of acid treated CNHs were also measured.

Specific surface area of sulfuric acid treated CNHs (SA-CNHs) and acetic acid treated CNHs (AA-CNHs) were evaluated by N_2 sorption analyzer. Adsorption and desorption isotherm of SA-CNHs and AA-CNHs with different treatment time were presented in Figure 4.20. Adsorption-desorption isotherm shape of SA-CNHs sample were differed from CNHs while adsorption-desorption isotherm shape of AA-CNHs were similar to CNHs. Pore type of SA-CNHs could be identified as a micropore material while pore type of AA-CNHs could be identified as a mesopore material which was similar to CNHs. Specific surface area, total pore volume, and average pore diameter of SA-CNHs and AA-CNHs were shown in Table 4.5. Specific surface area of SA-CNHs was increased with and increasing of ultrasonicating time while insignificantly changed in specific surface area of AA-CNHs at a different ultrasonicating time. This result could be caused by the difference of erosion properties (pK_a) of sulfuric acid and acetic acid.

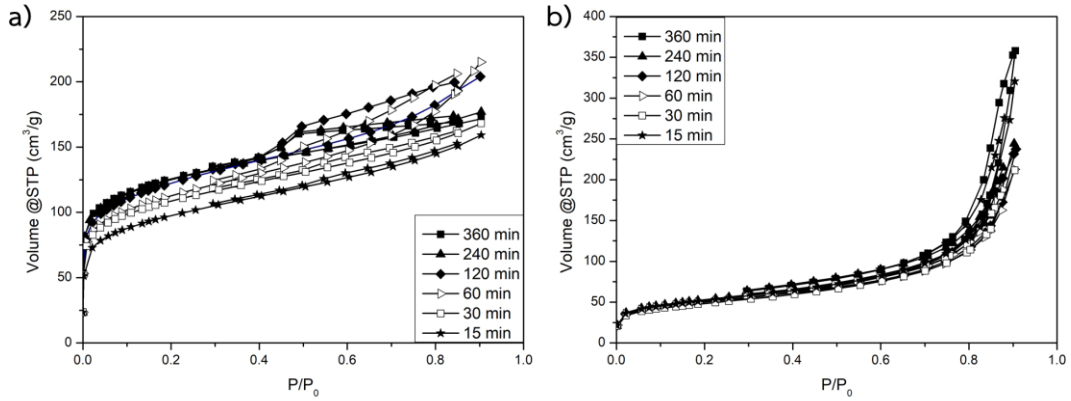

Figure 4.20 Adsorption-desorption isotherm of a) SA-CNHs and b) AA-CNHs

Table 4.5 Specific surface area, total pore volume, and average pore diameter of SA-CNHs and AA-CNHs

No.	Samples	Specific surface area (m^2/g)	Total pore volume (cm^3/g)	Average pore diameter (nm)
1	CNHs	162	0.49	12.17
2	SA-15-CNHs	332	0.35	3.80
3	SA-30-CNHs	367	0.35	3.51
4	SA-60-CNHs	383	0.33	3.30
5	SA-120-CNHs	416	0.32	3.03
6	SA-240-CNHs	420	0.27	2.60
7	SA-360-CNHs	422	0.27	2.52
8	AA-15-CNHs	182	0.50	10.93
9	AA-30-CNHs	169	0.33	7.77
10	AA-60-CNHs	176	0.33	7.50
11	AA-120-CNHs	177	0.37	8.30
12	AA-240-CNHs	187	0.38	8.09
13	AA-360-CNHs	192	0.39	8.04

Degree of graphitic was studied using Raman spectroscopy and reported in Table 4.6. The I_G/I_D of SA-CNHs were 0.90-0.94 while I_G/I_D of AA-CNHs were 0.82-0.88. Due to the increasing of I_G/I_D ratio compared to CNHs (0.80), this can be indicated that acid treatment can also destroy amorphous carbon. Degree of damaging was varied by treatment time and type of acid. Mechanism of acid treatment on CNHs should start with destroying amorphous carbon then destroy the surface of CNHs to make small pore. Moreover, acid treatment could add acid functional groups on the surface and between individual CNHs resulted in coalescence of CNHs [110]. The decreasing of total pore volume and average pore diameter were supported this suggested mechanism.

Table 4.6 I_G to I_D ratio of acid treated CNHs

Ultrasonicating time (min)	Sulfuric acid		Acetic acid	
	I_G/I_D	SD	I_G/I_D	SD
15	0.91	0.001	0.82	0.020
30	0.94	0.017	0.83	0.006
60	0.93	0.003	0.84	0.010
120	0.94	0.010	0.85	0.015
240	0.92	0.018	0.84	0.010
360	0.90	0.014	0.88	0.009

In addition, acid treatment on CNHs can provide acid functional groups on CNHs. Surface functional groups of acid treated CNHs were studied by FT-IR as shown in Figure 4.21. All samples were exhibited hydroxyl (-OH) group which refers to a broad peak at wavenumber of 3200-3600 cm^{-1}. Small peaks around 2700-3000 cm^{-1} are carboxylic groups (-COOH). Peaks around 2800-2900 cm^{-1} are the vibration of C-H stretch bond of carbon materials. In addition, peak around 1600-1700 cm^{-1} and 1100-1200 cm^{-1} show C=O and -C-OH, respectively. These two peaks indicated concentrated acids generate the carboxyl groups on the surface of CNHs which confirmed the success of acid treatment on CNHs [111, 112]. C=C stretch was presented at around 1550 cm^{-1} is the identical peak of hexagonal structure on CNHs. To be noticed, peak at 2300-2400 cm^{-1} is CO_2 [113].

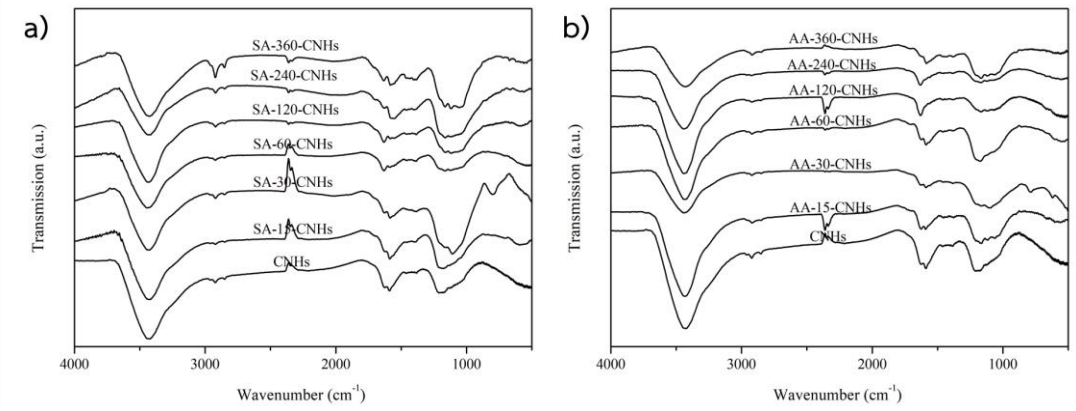

Figure 4.21 FT-IR spectra of acid treated CNHs a)SA-CNHs and b)AA-CNHs

Amount of acidity in the samples was evaluated by NH_3-TPD and reported in Table 4.7. Similar results were presented in SA-CNHs and AA-CNHs. An increasing of ultrasonicating time resulted in an enhancement of acidity of acid treated CNHs. Due to stronger acidity of sulfuric acid, acidity of SA-CNHs was significantly higher than AA-CNHs at the same ultrasonicating time. In addition, both weak (150 – 350 °C) and strong (450 – 700 °C) acid peaks were presented from SA-CNHs while only weak acid peak was observed from AA-CNHs samples. An increasing of acidity was drastically changed at the beginning of treatment period, slowly increasing after a time, then almost the same acidity was reported at a longer treatment time. This is due to the fully occupied of surface which can be functionalized by functional groups.

Table 4.7 Acidity of acid treated CNHs by NH_3-TPD

Ultrasonicating time (min)	Acidity (μmol/g)	
	Sulfuric acid	Acetic acid
0	98	98
15	540	227
30	665	241
60	722	258
120	730	270
240	794	275
360	798	354

4.1.3. Multi-functional groups

4.1.3.1. The thermal treatment (oxidation and reduction) on Ni/CNHs, Cu/CNHs and NiCu/CNHs samples

Metal/alloy nanoparticles in metal/alloy hybridized with CNHs from GI-AIW were embedded in CNHs structure as present in TEM results. To use those samples in catalytic application, the pore opening of carbon was required to allow metal/alloy species (active site) attacked with a reactant. The sample after oxidized process were called oxidized Ni/CNHs-10 (oxd-Ni/CNHs-10), oxidized Cu/CNHs-10 (oxd-

Cu/CNHs-10) and oxidized-NiCu/CNHs-5:5 (oxd-NiCu/CNHs-5:5). However, after the oxidation, metal/alloy nanoparticles were partially oxidized to metal oxide phase as confirmed by XRD pattern (Figure 4.22). To reduce the oxidized samples back to metal phase, reduction process was provided. Samples after reduction process were called reduced-oxidized Ni/CNHs-10 (red-oxd-Ni/CNHs-10), reduced-oxidized Cu/CNHs-10 (red-oxd-Cu/CNHs-10), and reduced-oxidized-NiCu/CNHs-5:5 (red-oxd-NiCu/CNHs-5:5). After reduction process, oxidized form of metal was completely changed to metal/alloy phase as presented in Figure 4.22. In addition, the peak intensity of metal/alloy phase (Ni, Cu, and NiCu) was increased due to the pore opening of carbon and sintering of metal particles due to oxidation and reduction process [30]. Moreover, oxidation and/or reduction process affected to weight reducing of the samples. The weight change of each sample was reported in Table 4.8.

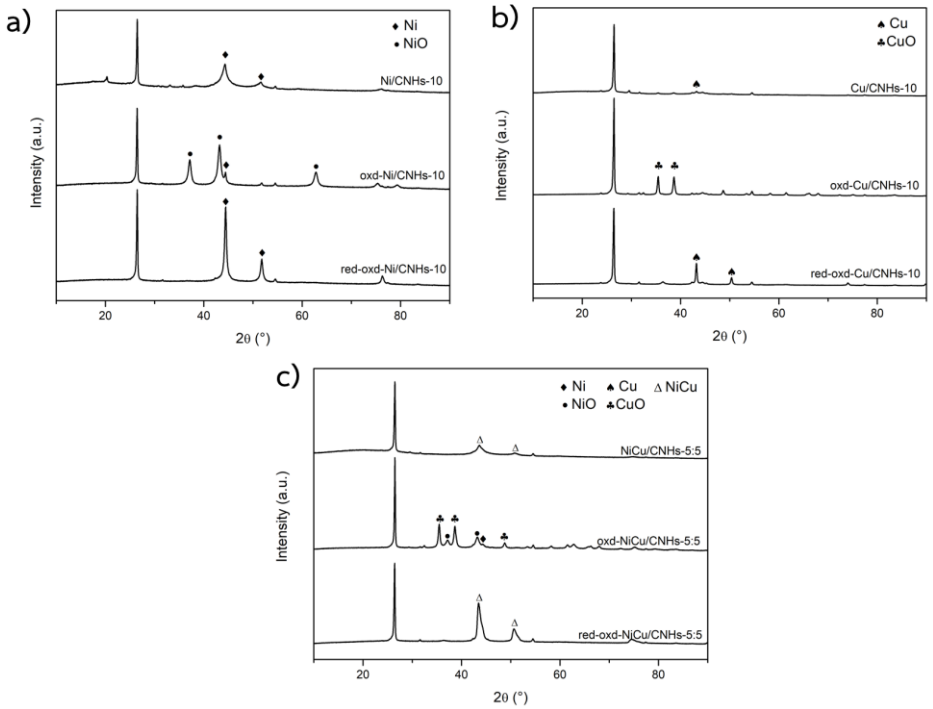

Figure 4.22 XRD patterns of thermal treatment on a)Ni/CNHs-10, b)Cu/CNHs-10, and c)NiCu/CNHs-5:5

Table 4.8 Weight change of samples after thermal treatment process

Samples	Weight change of the sample (%wt)	
	After oxidation	After reduction
Ni/CNHs-10	35	38
Cu/CNHs-10	58	63
NiCu/CNHs-5:5	51	60

4.1.3.2. The acid treatment by sulfuric acid on Pd/CNHs sample

Acid treatment of sulfuric acid on Pd/CNHs sample was studied. The treatment time was set at 1 h of ultrasonicating time. An addition of acid functional groups on surface of CNHs by acid treatment was confirmed in 4.1.2.3 so that similar result could be expected in acid treatment of sulfuric acid on Pd/CNHs (SA-Pd/CNHs).

Phase of SA-Pd/CNHs were studied by XRD and showed in Figure 4.23. The similar diffraction peak pattern was presented in SA-Pd/CNHs comparing to Pd/CNHs. This result suggested that acid treatment did not affect the structure of Pd/CNHs. In addition, degree of graphitic was also measured by Raman spectroscopy. Insignificant change of I_G/I_D was presented in SA-Pd/CNHs (0.87) compared to Pd/CNHs (0.88) which should be caused by an increasing of defected on sp^2 carbon during the acid treatment process [114].

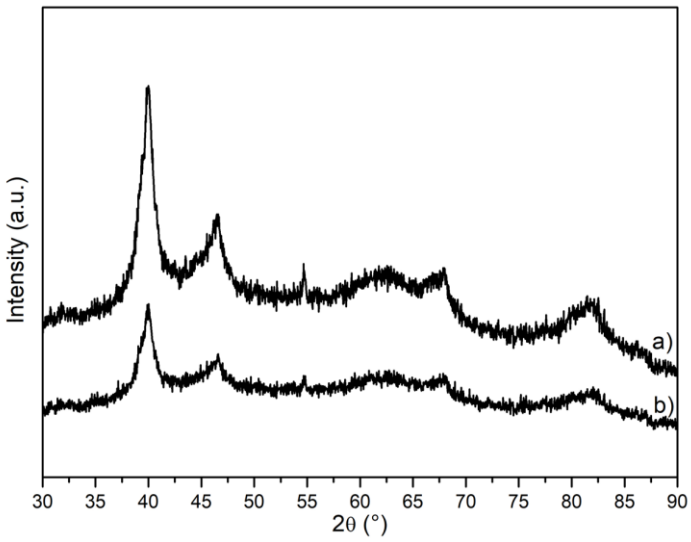

Figure 4.23 XRD patterns of a)Pd/CNHs, b)SA-Pd/CNHs

Specific surface area, total pore volume, and average pore diameter of SA-Pd/CNHs was studied by N_2 sorption through BET method. An increasing of specific surface area while decreasing of total pore volume and average pore diameter were presented in SA-Pd/CNHs as shown in Table 4.9. This result suggested that acid treatment mainly effect on carbon material.

Table 4.9 Specific surface area, total pore volume, and average pore diameter of Pd/CNHs and SA-Pd/CNHs

No.	Samples	Specific surface area (m^2/g)	Total pore volume (cm^3/g)	Average pore diameter (nm)
1	Pd/CNHs	116	0.31	10.845
2	SA-Pd/CNHs	232	0.26	4.51

To confirm leaching of metal after acid treatment, ICP-MS was applied. An acid solution after acid treatment was separated from the suspension by filtration and analyzed by ICP-MS. Less than 0.06 wt% of Pd were presented in the acid solution after the acid treatment. The structure of Pd/CNHs which Pd nanoparticles were embedded in CNHs structure could help protect Pd nanoparticles from acid solution. Moreover, acidity of Pd/CNHs and SA-Pd/CNHs was measured by NH_3-TPD. Acidity of Pd/CNHs was 415 μmol/g and acidity of SA-Pd/CNHs was 1,490 μmol/g. An increasing of acidity after acid treatment were presented. In addition, acidity of SA-Pd/CNHs was higher than SA-CNHs at the same ultrasonicating time. From this result, Pd could have acidity properties and/or could help acid functional groups attached on CNHs surface easier than without Pd.

4.2. Catalysis applications

CNHs and functionalized CNHs were used as a catalyst in three different catalytic reactions. Oxd-CNHs, Ni/CNHs, Cu/CNHs, and NiCu/CNHs were applied in dehydration of xylose. Acid treated CNHs were tested in esterification of ethyl levulinate. Moreover, transfer hydrogenation of methyl levulinate to γ-valerolactone

were catalyzed by Ni/CNHs, Cu/CNHs, and NiCu/CNHs with thermal treatment. The performance of the catalysts was presented in terms of conversion, yield, and selectivity in each reaction.

4.2.1. Dehydration of xylose

Dehydration of xylose is an autocatalytic reaction which could result in the formation of furfural and other derivatives. In the commercial process, mineral acid has been used as Bronsted acid catalyst for the dehydration of xylose to furfural. However, many problems such as instrument corrosion, excessive waste disposal and high investment in catalyst recovery process were reported due to using of homogenous acid catalyst [115]. To overcome such problems, solid acid catalysts would be an alternative way for dehydration of xylose [116]. In addition, the reaction was conducted in water system. Water could perform as an active medium for dehydration of xylose at high temperature, resulting in furfural formation. Water could provide H+ and OH- ions which would efficiently act as acid- and based-catalysts [117, 118]. Two different batch reactors were selected to conduct the reaction.

4.2.1.1. Parr-reactor

Dehydration of xylose was conducted using parr reactor. CNHs and oxd-CNHs were tested in this reaction. In addition, reactions with carbon nanotubes (CNTs) and oxidized CNT (oxd-CNTs) as catalysts were performed for comparing the catalytic performance. CNTs were selected due to their good catalytic property and CNTs also provide the closest morphology to CNHs. Both CNHs and oxd-CNHs can provide a well dispersion of the powder in xylose solution (reactant) due to the absorption of xylose on surface of CNHs. Oxd-CNHs provided the highest xylose conversion (89%) compared to other catalysts as presented in Figure 4.24. Conversion of CNHs and oxd-CNHs were higher than CNTs and oxd-CNTs. CNHs could act as a catalyst to enhance the xylose conversion due to some acid functional groups on the surface which were generated during the synthesis or storage as reported in Figure 4.21. Moreover, after oxidation process, more acid functional groups were added to the surface resulted in an increasing of xylose conversion with oxd-CNHs catalyst. For furfural yield, about 10% of xylose yield were increased when using CNHs and oxd-CNHs as catalysts while 5%

increased when CNTs and oxd-CNTs were used. However, yield of other by-products, especially lactic acid, was significantly increased when using oxd-CNHs as a catalyst. This was caused by the promotion of side reactions which could also be enhanced by acid catalyst [72, 119]. From above results, oxidation process (acidity) had a strong effect on xylose conversion while less effect on furfural yield. However, selectivity of reaction without catalyst was about 2 times higher than using catalysts. Adding a catalyst into the system could promote other side reactions between xylose and furfural. In addition, due to the small pore size of CNHs and oxd-CNHs, mass transfer problem should be considered.

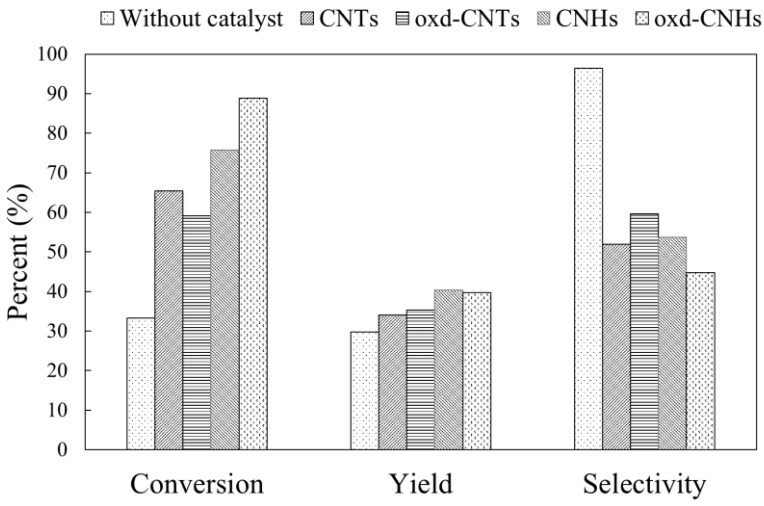

Figure 4.24 Performance of the catalysts in dehydration of xylose in Parr reactor at 170 °C, reaction time=4 h, and initial P=15 bar

4.2.1.2. In-house batch reactor

A smaller size of batch reactor was used to test the catalyst performance of Ni, Cu, NiCu hybridized CNHs. Less amount of catalyst was used in this type of reactor. Performance of each catalyst was reported in Figure 4.25. Xylose conversion, furfural yield and selectivity were slightly decreased when CNHs was used as a catalyst. However, changing a catalyst from CNHs to oxd-CNHs, those values returned to the original. This can be implied that mass transfer problem was occurring when using CNHs as a catalyst and an oxidation process on CNHs could solve this problem. The highest xylose conversion was observed when using oxd-Ni/CNHs-10 as a catalyst.

Thermal treatment on Ni/CNHs had slightly effect on xylose conversion while resulting in a decreasing of furfural yield. Whether, catalysts which were consisted of Ni provided very high xylose conversion, furfural yield was low due to Ni species in Ni/CNHs could help promoted other side reactions. Reaction with Cu/CNHs, oxd-CNH, and red-oxd-Cu/CNHs provided similar xylose conversion and furfural yield to reaction without using a catalyst. All experimental results suggested that the hybridization of Ni, Cu, and NiCu with CNHs would attribute to xylose conversion and also further conversion of furfural to other by-products due to other side reactions. It should be noted that Ni, Cu, and NiCu could act as Lewis acid sites [120]. Weingarten et al. (2011) reported some solid catalysts with a certain number of Lewis acid sites could predominantly enhance conversion of xylose through the dehydration process [121, 122]. In general, most of metal is known as a strong Lewis acid site which could promote other side reactions to convert either xylose or furfural to humin [121]. Therefore, with the presence of Ni/CNHs, selectivity of furfural would be extremely affected, resulting in relatively low yield of furfural though a high conversion of xylose could be achieved. Meanwhile, adding Cu to Ni/CNHs as NiCu/CNHs could play a role in selectively convert xylose to furfural with less side reaction. Many previous works also experimentally confirmed that NiCu could enhance selectivity of Ni catalyst [25, 29, 30]. Therefore, the optimization of Ni to Cu ratio should be a potential approach to enhance the furfural yield from dehydration of xylose or other derivatives [67].

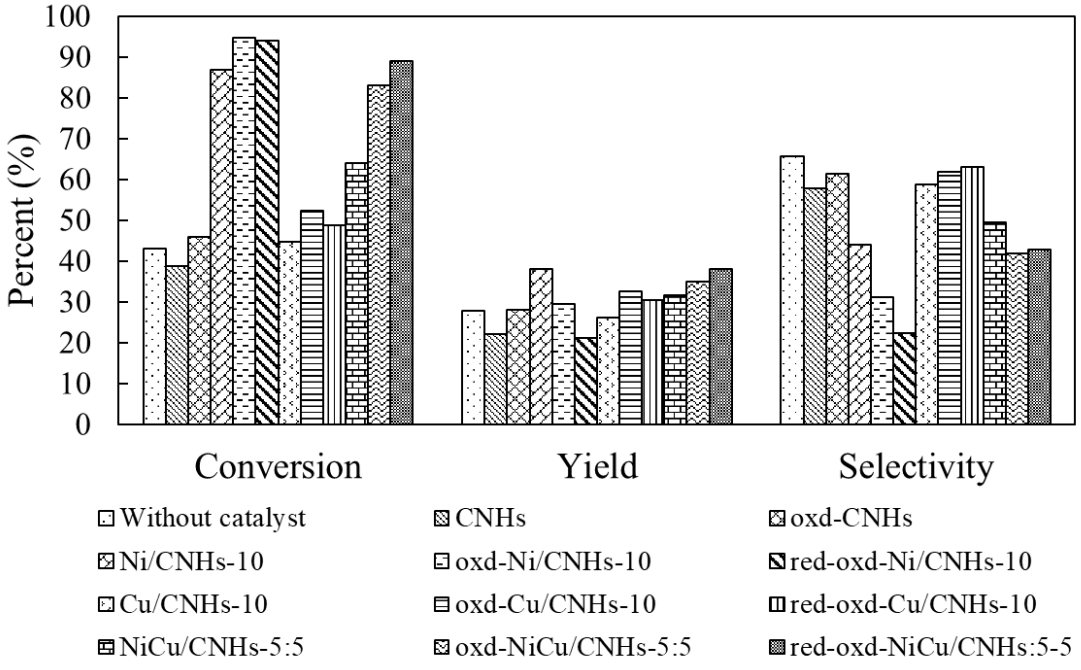

Figure 4.25 Performance of Ni/CNHs Cu/CNHs and NiCu/CNHs with or without thermal treatment catalysts on dehydration of xylose in in-house batch reactor at 170 °C, reaction time=4 h, and initial P=15 bar

4.2.2. Esterification of levulinic acid to ethyl levulinate

Due to the acid catalyst requirement on esterification reaction, sulfuric acid treated CNHs with 60 min of treatment time (SA-60-CNHs) was tested as a catalyst in esterification of levuilnic acid (LA) to ethyl levulinate (EL). Amount of catalyst, reaction temperature and initial molar ratio of LA:EtOH were studied.

Adding a catalyst into the reaction resulted in slightly decreasing of LA conversion and EL yield. On the contrary, selectivity of EL was increased to 98.6% when 15 mg of catalyst was used as reported in Figure 4.26. EL selectivity was increased about 9% compared to the reaction without a catalyst. Due to the micropore structure of catalysts, mass transfer limit could affect the performance of the catalyst resulted in slightly decreasing of conversion via increasing of selectivity of the catalyst [123]. In addition, unclear results of LA conversion and EL yield were presented due to low amount of catalyst loading.

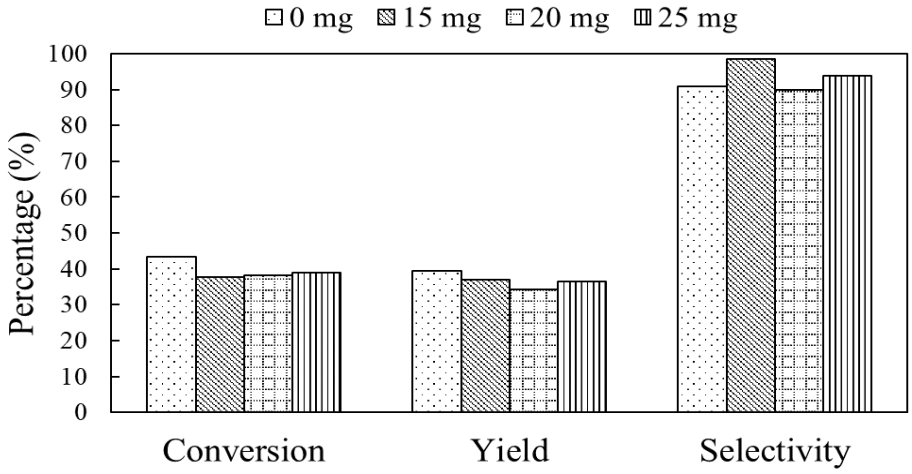

Figure 4.26 Effect of amount of catalyst on esterification of LA to EL at reaction temperature= 140 °C, reaction time = 90 min, initial LA:EtOH=1:5

Effect of temperature was tested by using 15 mg of catalyst. Temperature was varied at 100, 120, and 140 °C. LA conversion and EL yield were increased along with an increasing of reaction temperature from 100 to 140 °C as presented Figure 4.27. For EL selectivity, more than 90% of selectivity was gained in every reaction temperature. Normally, esterification reaction is an exothermic reaction, so that increasing of reaction temperature should increase conversion and yield of the reaction [124, 125]. However, reaction time might not long enough, so low conversion and yield were presented.

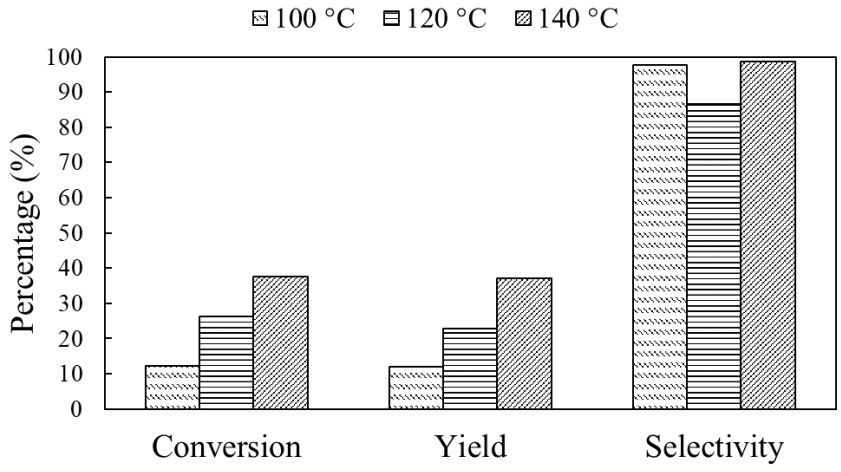

Figure 4.27 Effect of reaction temperature on esterification of LA to EL at 15 mg of catalyst, reaction time = 90 min, initial LA:EtOH=1:5

The influence of molar ratio on esterification of LA to EL was studied and reported in Figure 4.28. The esterification of levulinic acid is a reversible reaction and full conversion of levulinic acid is accomplished through the use of the high volumes of ethanol [126]. Molar ratio of LA to EtOH was set at 1:3, 1:5, and 1:7. The highest selectivity was provided at molar ratio of 1:5. The optimize reaction conditions for esterification of LA to EL in this study were performed at LA:EtOH=1:5, 140 °C for 90 min with 15 mg of catalyst.

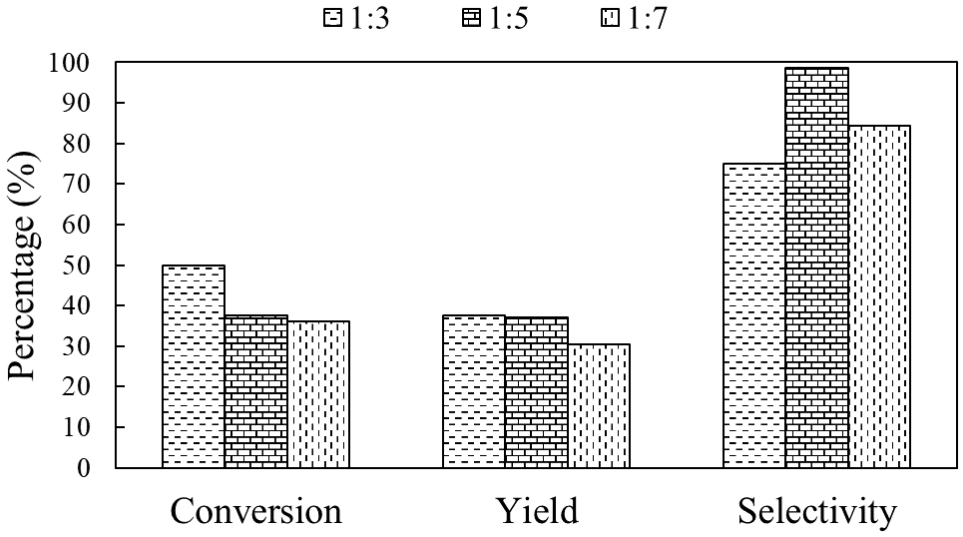

Figure 4.28 Effect of initial LA:EtOH molar ratio on esterification of LA to EL at 15 mg of catalyst, at reaction temperature= 140 °C , reaction time = 90 min

4.2.3. Transfer hydrogenation of methyl levulinate to *γ*-valerolactone

The effect of thermal treatment on Ni/CNHs, Cu/CNHs and NiCu/CNHs on catalyst activity were investigated through transfer hydrogenation of methyl levulinate (ML) to *γ*-valerolactone (GVL). The results were reported in Figure 4.29. Reaction which presented Ni species in the catalyst component provided better conversion compared to other catalysts. Red-oxd-Ni/CNHs-10 showed the highest ML conversion at >90%. Adding Cu in catalyst resulted in low ML conversion which is lower than 20%. Similar to conversion, the highest GVL yield was observed when red-oxd-Ni/CNHs-10 was used as a catalyst. Very low GVL yield was presented with Cu catalysts. Thermal treatment on Ni/CHNs could help increase catalytic performance of

catalysts. Ni active species could expose to the system easier than before the thermal treatment process resulted in the best catalyst performance of red-oxd-Ni/CNHs.

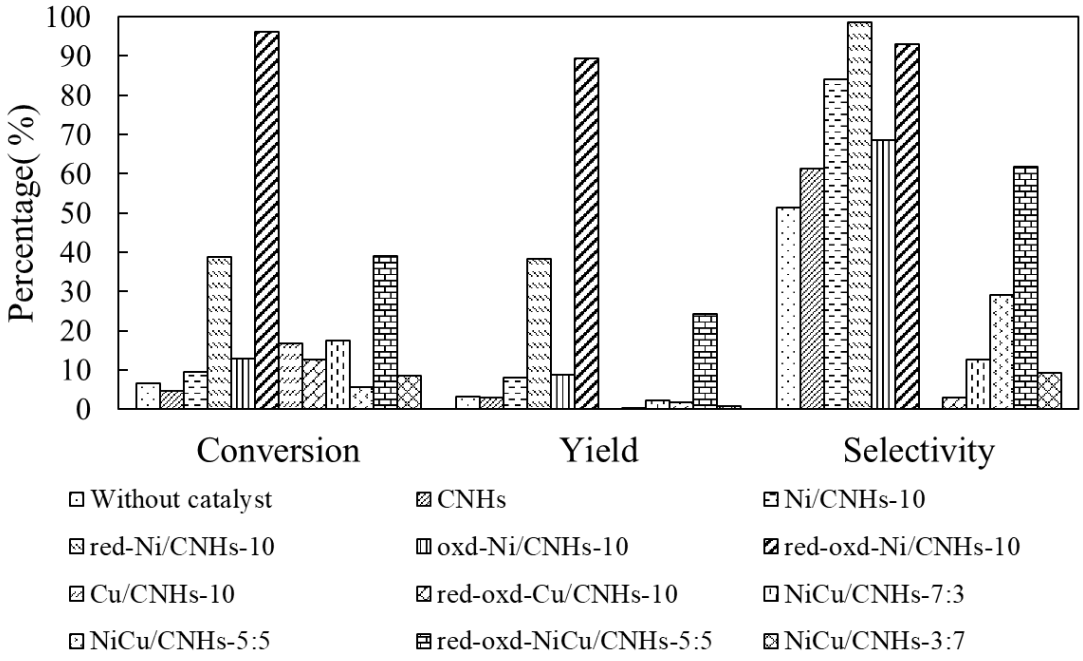

Figure 4.29 Performance of Ni/CNHs Cu/CNHs and NiCu/CNHs with or without thermal treatment catalysts on transfer hydrogenation of ML at 200°C, reaction time=3h

In addition, the effect of reaction temperature on the catalytic performance of red-oxd-Ni/CNHs-10 was shown in Figure 4.30. The red-oxd-Ni/CNH-10 showed extremely low activity (ML conversion below 10%) at the reaction temperature of 140 and 170 °C while the ML conversion was enhanced up to 90% at 200 °C. In addition, the high GVL selectivity suggested that the red-oxd-Ni/CNH-10 could result in very few side reactions. All results based on the increase in the reaction temperature from 140 to 200 °C, which could significantly enhance the ML conversion as well as GVL yield and selectivity, align with an endothermic natural of the transfer hydrogenation of ML to form GVL [127].

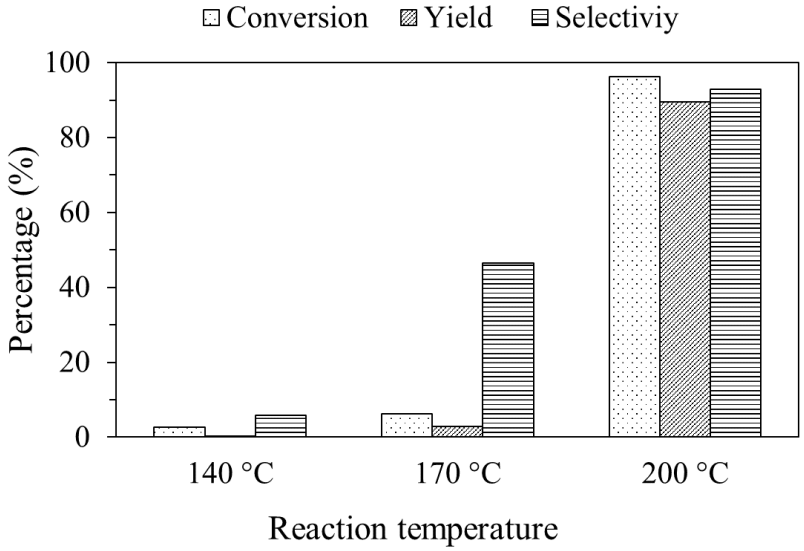

Figure 4.30 Effect of reaction temperature for ML to GVL conversion (reaction time of 3 h, catalyst loading of 0.1 g)

Catalytic reusability of red-oxd-Ni/CNH-10 were also studied for converting ML over 5 repeated cycles and showed in Figure 4.31. Only a slight decline in the conversion of ML was detected while the selectivity of GVL was still higher than 85% after five cycles, suggesting that the red-oxd-Ni/CNHs-10 could exhibit high stability and reusability for GVL production. This was caused by the interaction between CHNs and Ni active species combined with CNHs structure could protect Ni nanoparticles from an agglomeration of Ni nanoparticles which resulting in a good catalyst activity after 5 cycles of the reaction [127].

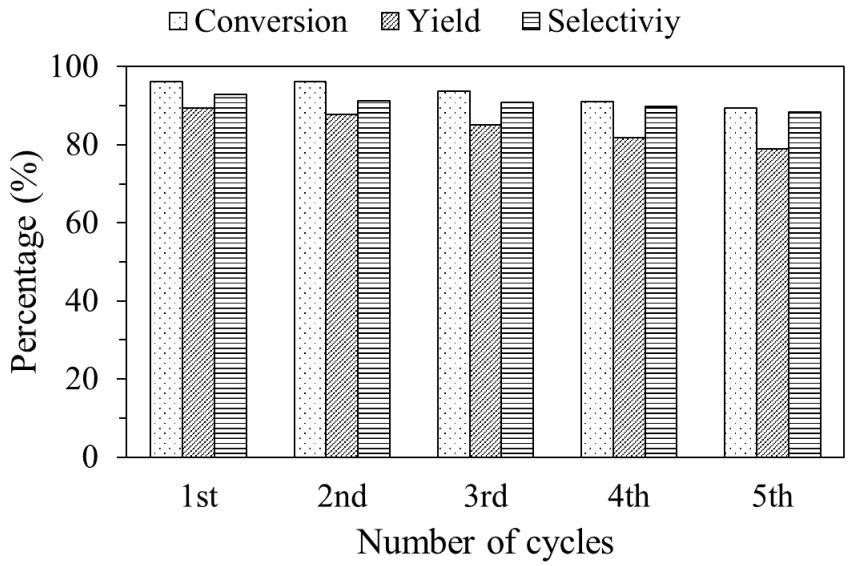

Figure 4.31 Reusability of red-oxd-Ni/CNHs for ML-to-GVL conversion. Reaction conditions: reaction temperature of 200 °C, reaction time of 3 h, catalyst loading of 0.1 g

Chapter V
CONCLUSIONS AND RECOMMENDATIONS

5.1. Conclusions

CNHs could be functionalized by adding metal, alloy, and/or acid functional group into/onto CNHs. Metal and their alloy nanoparticles could be added into CNHs via GI-AIW method which is a single step process resulted in metal their alloy hybridized with CNHs. For metal and their alloy hybridized with CNHs, the amount of metal which could be added onto CNHs was depended on metal properties, evaporation rate and solubility of metal in carbon properties. Differential of metal type could provide a different metal loading and average diameter of metal nanoparticles which were embedded in CNHs structure. Increasing of metal loading resulted in an increasing of average diameter of metal nanoparticles. XRD results could confirm the formation of alloy in CNHs structure. Adding metal into CNHs affected on their properties, especially their thermal stability and specific surface area. On the contrary, acid functional groups could be provided by acid treatment process which could increase specific surface area and acidity of CNHs. In addition, thermal treatment on CNHs could also help increasing of specific surface area of CNHs due to the pore opening process. Interestingly, CNHs could act as a potential barrier to protect metal nanoparticles from strong acid and could reduce a sintering process of metal at high temperature surrounding for metal/alloy hybridized with CNHs as well.

The functionalized CNHs could be applied as a catalyst to convert sugar and their derivatives to valuable bio-chemical products. In dehydration and esterification reaction, an acid catalyst was required to enhance the reaction activity. Oxidized CNHs and acid treated CNHs which had acidity properties could be applied in those reactions. Oxidized CNHs could increase the conversion of dehydration. However, an unclear result was presented in esterification reaction due to inappropriate reaction conditions. In addition, Ni hybridized with CNHs with thermal treatment showed great performance in transfer-hydrogenation of methyl levulinate to γ-valerolactone. Significantly increasing conversion yield and selectivity was reported. Moreover, high stability and reusability of catalysts with 5 cycles were also provided when Ni

hybridized with CNHs with thermal treatment as catalyst due to the interaction between CNHs and Ni active species could increase the stability of the catalyst.

5.2. Recommendations

An increasing in production yield of CNHs and hybridized CNHs should to further investigate. For acid functionalization process, the effect of acid treatment method, type of acid and treatment temperature should be investigated. Lastly, for esterification of levulinic acid, the reaction conditions should be adjusted for example amount of catalyst should be increased or initial concentration of levulinic acid should be decreased.

REFERENCES

[1] B.T. Zhang, X. Zheng, H.F. Li, J.M. Lin, Application of Carbon-Based Nanomaterials in Sample Preparation: A Review, Analytica Chimica Acta, 784 (2013) 1-17.

[2] D. Kasuya, M. Yudasaka, K. Takahashi, F. Kokai, S. Iijima, Selective Production of Single-Wall Carbon Nanohorn Aggregates and Their Formation Mechanism, The Journal of Physical Chemistry B, 106 (2002) 4947-4951.

[3] M.F.L. De Volder, S.H. Tawfick, R.H. Baughman, A.J. Hart, Carbon Nanotubes: Present and Future Commercial Applications, Science, 339 (2013) 535-539.

[4] J.A. Berkmans, M. Jagannatham, R.D. Reddy, P. Haridoss, Synthesis of Thin Bundled Single Walled Carbon Nanotubes and Nanohorn Hybrids by Arc Discharge Technique in Open Air Atmosphere, Diamond and Related Materials, 55 (2015) 12-15.

[5] T. Yamaguchi, S. Bandow, S. Iijima, Synthesis of Carbon Nanohorn Particles by Simple Pulsed Arc Discharge Ignited Between Pre-Heated Carbon Rods, Chemical Physics Letters, 389 (2004) 181-185.

[6] S.A.M. Zobir, Z. Zainal, C.S. Keng, S.H. Sarijo, M. Yusop, Synthesis of Carbon Nanohorn–Carbon Nanotube Hybrids Using Palm Olein as a Precursor, Carbon, 54 (2013) 492-494.

[7] B. Niu, W. Xu, Z. Guo, N. Zhou, Y. Liu, Z. Shi, Y. Lian, Controllable Deposition of Platinum Nanoparticles on Single-Wall Carbon Nanohorns as Catalyst for Direct Methanol Fuel Cells, Journal of Nanoscience and Nanotechnology, 12 (2012) 7376-7381.

[8] S. Iijima, M. Yudasaka, R. Yamada, S. Bandow, K. Suenaga, F. Kokai, K. Takahashi, Nano-Aggregates of Single-Walled Graphitic Carbon Nano-Horns, Chemical Physics Letters, 309 (1999) 165-170.

[9] C. Poonjarernsilp, N. Sano, T. Charinpanitkul, H. Mori, T. Kikuchi, H. Tamon, Single-Step Synthesis and Characterization of Single-Walled Carbon Nanohorns Hybridized with Pd Nanoparticles Using N_2 Gas-Injected Arc-In-Water Method, Carbon, 49 (2011) 4920-4927.

[10] N. Sano, K. Taniguchi, H. Tamon, Gas Flow Rate in the Gas-Injected Arc-in-Water Method as a Critical Factor to Synthesize High-Dispersion Pd-Ni Alloy Nanoparticles in Single-Walled Carbon Nanohorns, Journal of Chemical Engineering of Japan, 47 (2014) 821-826.

[11] N. Sano, Low-Cost Synthesis of Single-Walled Carbon Nanohorns Using the Arc in Water Method with Gas Injection, Journal of Physics D: Applied Physics, 37 (2004) L17.

[12] A. Venezia, R. Murania, G. Pantaleo, G. Deganello, Pd and PdAu on Mesoporous Silica for Methane Oxidation: Effect of SO_2, Journal of Catalysis, 251 (2007) 94-102.

[13] D.S. Su, G. Centi, A Perspective on Carbon Materials for Future Energy Application, Journal of Energy Chemistry, 22 (2013) 151-173.

[14] E. Aryee, A.K. Dalai, J. Adjaye, Functionalization and Characterization of Carbon Nanohorns (CNHs) for Hydrotreating of Gas Oils, Topics in Catalysis, 57 (2013) 796-805.

[15] C. Poonjarernsilp, N. Sano, H. Tamon, Hydrothermally Sulfonated Single-Walled Carbon Nanohorns for Use as Solid Catalysts in Biodiesel Production by Esterification of Palmitic Acid, Applied Catalysis B: Environmental, 147 (2014) 726-732.

[16] Single-Walled Carbon Nanohorn, in, wikipedia.

[17] X. Hu, J. Shi, J. Zhang, W. Tang, H. Zhu, X. Shen, N. Saito, One-Step Facile Synthesis of Carbon-Supported PdAu Nanoparticles and Their Electrochemical Property and Stability, Journal of Alloys and Compounds, 619 (2015) 452-457.

[18] P. Dash, T. Bond, C. Fowler, W. Hou, N. Coombs, R.W.J. Scott, Rational Design of Supported PdAu Nanoparticle Catalysts from Structured Nanoparticle Precursors, Journal of Physical Chemistry C, 113 (2009) 12719-12730.

[19] F. Ruffino, M.G. Grimaldi, Self-Organization of Bimetallic PdAu Nanoparticles on SiO_2 Surface, Journal of Nanoparticle Research, 13 (2010) 2329-2341.

[20] Y.-L. Fang, J.T. Miller, N. Guo, K.N. Heck, P.J.J. Alvarez, M.S. Wong, Structural Analysis of Palladium-Decorated Gold Nanoparticles as Colloidal Bimetallic Catalysts, Catalysis Today, 160 (2011) 96-102.

[21] R. Ferrando, J. Jellinek, R.L. Johnston, Nanoalloys: From Theory to Applications of Alloy Clusters and Nanoparticles, Chemical Reviews, 108 (2008) 845-910.

[22] D.A. Bulushev, S. Beloshapkin, P.E. Plyusnin, Y.V. Shubin, V.I. Bukhtiyarov, S.V. Korenev, J.R.H. Ross, Vapour Phase Formic Acid Decomposition over PdAu/γ-Al_2O_3 Catalysts: Effect of Composition of Metallic Particles, Journal of Catalysis, 299 (2013) 171-180.

[23] D. Li, L. Wang, M. Koike, K. Tomishige, Development of Ni- and Co-based Alloy Catalysts for Steam Reforming of Biomass Tar, Journal of the Japan Petroleum Institute, 56 (2013) 253-266.

[24] K.M.K. Yu, P. Meric, S.C. Tsang, Micelle-Hosted Bimetallic Pd–Ru Nanoparticle for In Situ Catalytic Hydrogenation in Supercritical CO_2, Catalysis Today, 114 (2006) 428-433.

[25] L. De Rogatis, T. Montini, A. Cognigni, L. Olivi, P. Fornasiero, Methane Partial Oxidation on NiCu-based Catalysts, Catalysis Today, 145 (2009) 176-185.

[26] B. Pawelec, R. Mariscal, R.M. Navarro, S. van Bokhorst, S. Rojas, J.L.G. Fierro, Hydrogenation of Aromatics over Supported Pt-Pd Catalysts, Applied Catalysis A: General, 225 (2002) 223-237.

[27] S. Jongpatiwut, Z. Li, D.E. Resasco, W.E. Alvarez, E.L. Sughrue, G.W. Dodwell, Competitive Hydrogenation of Poly-Aromatic Hydrocarbons on Sulfur-Resistant Bimetallic Pt-Pd Catalysts, Applied Catalysis A: General, 262 (2004) 241-253.

[28] X. Zhang, T. Wang, L. Ma, Q. Zhang, Y. Yu, Q. Liu, Characterization and Catalytic Properties of Ni and NiCu Catalysts Supported on ZrO_2–SiO_2 for Guaiacol Hydrodeoxygenation, Catalysis Communications, 33 (2013) 15-19.

[29] M.V. Bykova, D.Y. Ermakov, S.A. Khromova, A.A. Smirnov, M.Y. Lebedev, V.A. Yakovlev, Stabilized Ni-based Catalysts for Bio-oil Hydrotreatment: Reactivity Studies using Guaiacol, Catalysis Today, 220-222 (2014) 21-31.

[30] S.A. Khromova, A.A. Smirnov, O.A. Bulavchenko, A.A. Saraev, V.V. Kaichev, S.I. Reshetnikov, V.A. Yakovlev, Anisole Hydrodeoxygenation over Ni–Cu Bimetallic Catalysts: The Effect of Ni/Cu Ratio on Selectivity, Applied Catalysis A: General, 470 (2014) 261-270.

[31] A.A. Smirnov, S.A. Khromova, O.A. Bulavchenko, V.V. Kaichev, A.A. Saraev, S.I. Reshetnikov, M.V. Bykova, L.I. Trusov, V.A. Yakovlev, Effect of the Ni/Cu Ratio on the Composition and Catalytic Properties of Nickel-Copper Alloy in Anisole Hydrodeoxygenation, Kinetics and Catalysis, 55 (2014) 69-78.

[32] J. Zhang, Y. Wang, R. Ma, D. Wu, Characterization of Alumina-Supported Ni and Ni-Pd Catalysts for Partial Oxidation and Steam Reforming of Hydrocarbons, Applied Catalysis A: General, 243 (2003) 251-259.

[33] Y. Nakagawa, K. Tomishige, Total Hydrogenation of Furan Derivatives over Silica-Supported Ni–Pd Alloy Catalyst, Catalysis Communications, 12 (2010) 154-156.

[34] N. Laosiripojana, W. Sutthisripok, S. Charojrochkul, S. Assabumrungrat, Development of Ni–Fe Bimetallic Based Catalysts for Biomass Tar Cracking/Reforming: Effects of Catalyst Support and Co-Fed Reactants on Tar Conversion Characteristics, Fuel Processing Technology, 127 (2014) 26-32.

[35] H. Liu, T. Chen, D. Chang, D. Chen, D. Kong, X. Zou, R.L. Frost, Effect of Preparation Method of Palygorskite-Supported Fe and Ni Catalysts on Catalytic Cracking of Biomass Tar, Chemical Engineering Journal, 188 (2012) 108-112.

[36] L. Feng, F. Si, S. Yao, W. Cai, W. Xing, C. Liu, Effect of Deposition Sequences on Electrocatalytic Properties of PtPd/C Catalysts for Formic Acid Electrooxidation, Catalysis Communications, 12 (2011) 772-775.

[37] T. Yoshitake, Y. Shimakawa, S. Kuroshima, H. Kimura, T. Ichihashi, Y. Kubo, D. Kasuya, K. Takahashi, F. Kokai, M. Yudasaka, S. Iijima, Preparation of Fine Platinum Catalyst Supported on Single-Wall Carbon Nanohorns for Fuel Cell Application, Physica B: Condensed Matter, 323 (2002) 124-126.

[38] E. Bekyarova, A. Hashimoto, M. Yudasaka, Y. Hattori, K. Murata, H. Kanoh, D. Kasuya, S. Iijima, K. Kaneko, Palladium Nanoclusters Deposited on Single-Walled Carbon Nanohorns, Journal of Physical Chemistry B, 109 (2005) 3711-3714.

[39] T. Itoh, H. Danjo, W. Sasaki, K. Urita, E. Bekyarova, M. Arai, T. Imamoto, M. Yudasaka, S. Iijima, H. Kanoh, K. Kaneko, Catalytic Activities of Pd-Tailored Single Wall Carbon Nanohorns, Carbon, 46 (2008) 172-175.

[40] N. Sano, S.-i. Ukita, One-Step Synthesis of Pt-Supported Carbon Nanohorns for Fuel Cell Electrode by Arc Plasma in Liquid Nitrogen, Materials Chemistry and Physics, 99 (2006) 447-450.

[41] N. Sano, D. Himara, H. Tamon, Simultaneous Enhancement in Porosity and Magnetic Property of Fe-Dispersing Single-Walled Carbon Nanohorns by Oxidation Using CO_2, Chemical Engineering Journal, 271 (2015) 43-49.

[42] R. Arrigo, M. Hävecker, S. Wrabetz, R. Blume, M. Lerch, J. McGregor, E.P.J. Parrott, J.A. Zeitler, L.F. Gladden, A. Knop-Gericke, R. Schlögl, D.S. Su, Tuning the Acid/Base Properties of Nanocarbons by Functionalization via Amination, Journal of the American Chemical Society, 132 (2010) 9616-9630.

[43] R. Chakravarti, M.L. Kantam, H. Iwai, S.S. Al-deyab, K. Ariga, D.-H. Park, J.-H. Choy, K.S. Lakhi, A. Vinu, Mesoporous Carbons Functionalized with Aromatic, Aliphatic, and Cyclic Amines, and their Superior Catalytic Activity, ChemCatChem, 6 (2014) 2872-2880.

[44] M.Q. Tran, C. Tridech, A. Alfrey, A. Bismarck, M.S.P. Shaffer, Thermal Oxidative Cutting of Multi-Walled Carbon Nanotubes, Carbon, 45 (2007) 2341-2350.

[45] A.H. Van Pelt, O.A. Simakova, S.M. Schimming, J.L. Ewbank, G.S. Foo, E.A. Pidko, E.J.M. Hensen, C. Sievers, Stability of Functionalized Activated Carbon in Hot Liquid Water, Carbon, 77 (2014) 143-154.

[46] H. Yu, Y. Jin, F. Peng, H. Wang, J. Yang, Kinetically Controlled Side-Wall Functionalization of Carbon Nanotubes by Nitric Acid Oxidation, The Journal of Physical Chemistry C, 112 (2008) 6758-6763.

[47] N.A. Kumar, S.H. Kim, J.S. Kim, J.T. Kim, Y.T. Jeong, Functionalization of Multi-Walled Carbon Nanotubes with Cysteamine for the Construction of CNT/Gold Nanoparticle Hybrid Nanostructures, Surface Review and Letters, 16 (2009) 487-492.

[48] H.E. Misak, R. Asmatulu, M. O'Malley, E. Jurak, S. Mall, Functionalization of Carbon Nanotube Yarn by Acid Treatment, International Journal of Smart and Nano Materials, 5 (2014) 34-43.

[49] C.H. Zhou, X. Xia, C.X. Lin, D.S. Tong, J. Beltramini, Catalytic Conversion of Lignocellulosic Biomass to Fine Chemicals and Fuels, Chemical Society Reviews, 40 (2011) 5588-5617.

[50] S. Nishimura, N. Ikeda, K. Ebitani, Selective Hydrogenation of Biomass-Derived 5-Hydroxymethylfurfural (HMF) to 2,5-Dimethylfuran (DMF) under Atmospheric

Hydrogen Pressure over Carbon Supported PdAu Bimetallic Catalyst, Catalysis Today, 232 (2014) 89-98.

[51] S. De, B. Saha, R. Luque, Hydrodeoxygenation Processes: Advances on Catalytic Transformations of Biomass-Derived Platform Chemicals into Hydrocarbon Fuels, Bioresource Technology, 178 (2015) 108-118.

[52] S.G. Wettstein, D.M. Alonso, E.I. Gürbüz, J.A. Dumesic, A Roadmap for Conversion of Lignocellulosic Biomass to Chemicals and Fuels, Current Opinion in Chemical Engineering, 1 (2012) 218-224.

[53] E. Lam, J.H.T. Luong, Carbon Materials as Catalyst Supports and Catalysts in the Transformation of Biomass to Fuels and Chemicals, ACS Catalysis, 4 (2014) 3393-3410.

[54] S. Dora, T. Bhaskar, R. Singh, D.V. Naik, D.K. Adhikari, Effective Catalytic Conversion of Cellulose into High Yields of Methyl Glucosides over Sulfonated Carbon Based Catalyst, Bioresource Technology, 120 (2012) 318-321.

[55] T. Komanoya, H. Kobayashi, K. Hara, W.J. Chun, A. Fukuoka, Kinetic Study of Catalytic Conversion of Cellulose to Sugar Alcohols under Low-Pressure Hydrogen, ChemCatChem, 6 (2014) 230-236.

[56] W. Deng, X. Tan, W. Fang, Q. Zhang, Y. Wang, Conversion of Cellulose into Sorbitol over Carbon Nanotube-Supported Ruthenium Catalyst, Catalysis Letters, 133 (2009) 167-174.

[57] E. Lam, J.H. Chong, E. Majid, Y. Liu, S. Hrapovic, A.C.W. Leung, J.H.T. Luong, Carbocatalytic Dehydration of Xylose to Furfural in Water, Carbon, 50 (2012) 1033-1043.

[58] R. Liu, J. Chen, X. Huang, L. Chen, L. Ma, X. Li, Conversion of Fructose into 5-Hydroxymethylfurfural and Alkyl Levulinates Catalyzed by Sulfonic Acid-functionalized Carbon Materials, Green Chemistry, 15 (2013) 2895-2903.

[59] D. Wang, W. Niu, M. Tan, M. Wu, X. Zheng, Y. Li, N. Tsubaki, Pt Nanocatalysts Supported on Reduced Graphene Oxide for Selective Conversion of Cellulose or Cellobiose to Sorbitol, ChemSusChem, 7 (2014) 1398-1406.

[60] A. Takagaki, M. Toda, M. Okamura, J.N. Kondo, S. Hayashi, K. Domen, M. Hara, Esterification of Higher Fatty Acids by A Novel Strong Solid Acid, Catalysis Today, 116 (2006) 157-161.

[61] P.P. Upare, J.-M. Lee, D.W. Hwang, S.B. Halligudi, Y.K. Hwang, J.-S. Chang, Selective Hydrogenation of Levulinic Acid to γ-Valerolactone over Carbon-supported Noble Metal Catalysts, Journal of Industrial and Engineering Chemistry, 17 (2011) 287-292.

[62] L. Negahdar, M.G. Al-Shaal, F.J. Holzhäuser, R. Palkovits, Kinetic Analysis of The Catalytic Hydrogenation of Alkyl Levulinates to γ-Valerolactone, Chemical Engineering Science, 158 (2017) 545-551.

[63] S.H. Shuit, S.H. Tan, Feasibility Study of Various Sulphonation Methods for Transforming Carbon Nanotubes into Catalysts for The Esterification of Palm Fatty Acid Distillate, Energy Conversion and Management, 88 (2014) 1283-1289.

[64] N. Sano, T. Kikuchi, H. Wang, M. Chhowalla, G.A.J. Amaratunga, Carbon Nanohorns Hybridized with a Metal-Included Nanocapsule, Carbon, 42 (2004) 95-99.

[65] N. Sano, K. Taniguchi, H. Tamon, Hydrogen Storage in Porous Single-Walled Carbon Nanohorns Dispersed with Pd–Ni Alloy Nanoparticles, The Journal of Physical Chemistry C, 118 (2014) 3402-3408.

[66] N. Sano, Y. Kimura, T. Suzuki, Synthesis of Carbon Nanohorns by a Gas-Injected Arc-in-Water Method and Application to Catalyst-Support for Polymer Electrolyte Fuel Cell Electrodes, Journal of Materials Chemistry, 18 (2008) 1555.

[67] C. Termvidchakorn, N. Sano, H. Tamon, N. Viriya-Empikul, K. Faungnawakij, T. Charinpanitkul, Conversion of D-Xylose to Furfural via Catalytic Dehydration Using Carbon Nanohorns Hybridized with NiCu Nanoparticles, Journal of the Japan Institute of Energy, 96 (2017) 380-385.

[68] T. Suntornlohanakul, Development of Novel Hydrogen Storage Materials from Single-walled Carbon Nanohorns Dispersed with Fe Nanoparticles, in: Chemical engineering, Kyoto university.

[69] Parr Instrument Company- Series 4560 Mini Reactors, in.

[70] Z.-M. Dang, L. Wang, L.-P. Zhang, Surface Functionalization of Multiwalled Carbon Nanotube with Trifluorophenyl, Journal of Nanomaterials, 2006 (2006) 5.

[71] V. Datsyuk, M. Kalyva, K. Papagelis, J. Parthenios, D. Tasis, A. Siokou, I. Kallitsis, C. Galiotis, Chemical Oxidation of Multiwalled Carbon Nanotubes, Carbon, 46 (2008) 833-840.

[72] C. Termvidchakorn, V. Itthibenchapong, S. Songtawee, B. Chamnankid, S. Namuangruk, K. Faungnawakij, T. Charinpanitkul, R. Khunchit, N. Hansupaluk, N. Sano, H. Hinode, Dehydration of D-xylose to Furfural Using Acid-functionalized MWCNTs Catalysts, Advances in Natural Sciences: Nanoscience and Nanotechnology, 8 (2017) 035006.

[73] Z. Wei, H. Qiao, J. Dai, W. Feng, Q. Wang, W. Li, P. Yan, Preparation and Characterization of Ni Nanopowders Prepared by Anodic Arc Plasma, Transactions of Nonferrous Metals Society of China, 15 (2005) 51-56.

[74] P. Scherrer, Bestimmung der Größe und der inneren Struktur von Kolloidteilchen mittels Röntgenstrahlen, Nachrichten von der Gesellschaft der Wissenschaften zu Göttingen, Mathematisch-Physikalische Klasse, (1918).

[75] M.Z. Kassaee, F. Buazar, E. Motamedi, Effects of Current on Arc Fabrication of Cu Nanoparticles, Journal of Nanomaterials, 2010 (2010) 5.

[76] X.Y. Tao, X.B. Zhang, J.P. Cheng, F. Liu, Synthesis and Characterization of Cu Filled Carbon Nanohorns, Materials Chemistry and Physics, 104 (2007) 210-214.

[77] D. Goranova, G. Avdeev, R. Rashkov, Electrodeposition and Characterization of Ni–Cu Alloys, Surface and Coatings Technology, 240 (2014) 204-210.

[78] E.L. de Leon-Quiroz, D.V.P. Obregon, A. Ponce, M. Jose-Yacaman, L.A. Garcia-Cerda, Synthesis of Magnetic CuNi Nanoalloys by Sol-Gel-Based Pechini Method, IEEE Transactions on Magnetics, 49 (2013) 4522-4524.

[79] J.A. Mary, A. Manikandan, L.J. Kennedy, M. Bououdina, R. Sundaram, J.J. Vijaya, Structure and Magnetic Properties of Cu-Ni Alloy Nanoparticles Prepared by Rapid Microwave Combustion Method, Transactions of Nonferrous Metals Society of China, 24 (2014) 1467-1473.

[80] K. Suwa, T. Nakayama, T. Suzuki, H. Suematsu, W. Jiang, K. Niihara, Synthesis of Ni-Cu Nanoparticles by Pulsed Wire Discharge and their Compositional Distribution, 2008.

[81] J. Zhang, F. Guyot, Experimental Study of the bcc-fcc Phase Transformations in the Fe-rich System Fe-Si at High Pressures, Physics and Chemistry of Minerals, 26 (1999) 419-424.

[82] W.-S. Chang, Y. Wei, J.-M. Guo, F.-J. He, Thermal Stability of Ni-Fe Alloy Foils Continuously Electrodeposited in a Fluorborate Bath, Open Journal of Metal, Vol.02No.01 (2012) 6.

[83] P.V. Vinh, V.-T. Ta, C. Sunglae, Synthesis of NiPt Alloy Nanoparticles by Galvanic Replacement Method for Direct Ethanol Fuel Cell, 2017.

[84] Y. Liu, S. Liu, Z. Che, S. Zhao, X. Sheng, M. Han, J. Bao, Concave Octahedral Pd@PdPt Electrocatalysts Integrating Core-Shell, Alloy and Concave Structures for High-Efficiency Oxygen Reduction and Hydrogen Evolution Reactions, Journal of Materials Chemistry A, 4 (2016) 16690-16697.

[85] X. Li, Y. Zhu, Z. Zou, M. Zhao, Z. Li, Q. Zhou, D.L. Akins, H. Yang, Simple Complexing–Reduction Synthesis of Pd–Pt/C Alloy Electrocatalysts for the Oxygen Reduction Reaction, Journal of The Electrochemical Society, 156 (2009) B1107-B1111.

[86] L.-u. Rahman, R. Qureshi, M.M. Yasinzai, A. Shah, Synthesis and Spectroscopic Characterization of Ag-Cu Alloy Nanoparticles Prepared in Various Ratios, Comptes Rendus Chimie, 15 (2012) 533-538.

[87] R.T. Yang, P.J. Goethel, J.M. Schwartz, C.R.F. Lund, Solubility and Diffusivity of Carbon in Metals, Journal of Catalysis, 122 (1990) 206-210.

[88] J.-M. Aguiar-Hualde, Y. Magnin, H. Amara, C. Bichara, Probing the Role of Carbon Solubility in Transition Metal Catalyzing Single-Walled Carbon Nanotubes Growth, Carbon, 120 (2017) 226-232.

[89] M.J. Climent, A. Corma, S. Iborra, Conversion of Biomass Platform Molecules into Fuel Additives and Liquid Hydrocarbon Fuels, Green Chemistry, 16 (2014) 516.

[90] Z.-q. Wei, T.-d. Xia, J. Ma, W.-j. Feng, J.-f. Dai, Q. Wang, P.-x. Yan, Processing Parameters for Cu Nanopowders Prepared by Anodic Arc Plasma, Transactions of Nonferrous Metals Society of China, 17 (2007) 128-132.

[91] S. Chaitoglou, M.R. Sanaee, N. Aguil-Aguayo, E. Bertran, Arc-Discharge Synthesis of Iron Encapsulated in Carbon Nanoparticles for Biomedical Applications, Journal of Nanomaterials, 2014 (2014) 8.

[92] T. Brar, P. France, P.G. Smirniotis, Heterogeneous versus Homogeneous Nucleation and Growth of Zeolite A, The Journal of Physical Chemistry B, 105 (2001) 5383-5390.

[93] C. Koch, Nanostructured Materials: Processing, Properties, and Applications: Second Edition, 2006.

[94] M. Stein, Synthesis of Metal Nanoparticles by Transferred Arc Discharge, in: Institute of Technology for Nanostructures, University of Duisburg-Essen, 2015.

[95] H. Förster, C. Wolfrum, W. Peukert, Experimental Study of Metal Nanoparticle Synthesis by an Arc Evaporation/Condensation Process, Journal of Nanoparticle Research, 14 (2012) 926.

[96] M. Kundrapu, J. Li, A. Shashurin, M. Keidar, A Model of Carbon Nanotube Synthesis in Arc Discharge Plasmas, 2012.

[97] E.A. Brandes, Smithells metals reference book, 6 ed., Butterworth Publishers,Stoneham, MA, 1983.

[98] H.A. Jones, I.L. r, G.M.J. Mackay, The Rates of Evaporation and the Vapor Pressures of Tungsten, Molybdenum, Platinum, Nickel, Iron, Copper and Silver, Physical Review, 30 (1927) 201-214.

[99] Y. Saito, M. Okuda, T. Yoshikawa, A. Kasuya, Y. Nishina, Correlation between Volatility of Rare-Earth Metals and Encapsulation of Their Carbides in Carbon Nanocapsules, The Journal of Physical Chemistry, 98 (1994) 6696-6698.

[100] A.J. Song, M.Z. Ma, W.G. Zhang, H.T. Zong, S.X. Liang, Q.H. Hao, R.Z. Zhou, Q. Jing, R.P. Liu, Preparation and Growth of Ni–Cu Alloy Nanoparticles Prepared by Arc Plasma Evaporation, Materials Letters, 64 (2010) 1229-1231.

[101] S. Li, J. Lu, M. Teng, Synthesis of Carbon Encapsulated Non-Ferromagnetic Metal Nanoparticles, Diamond and Related Materials, 24 (2012) 88-92.

[102] J.H. Scott, S.A. Majetich, Morphology, Structure, and Growth of Nanoparticles Produced in a Carbon Arc, Physical Review B, 52 (1995) 12564-12571.

[103] J. Jiao, S. Seraphin, Carbon Encapsulated Nanoparticles of Ni, Co, Cu, and Ti, Journal of Applied Physics, 83 (1998) 2442-2448.

[104] Z.-q. Wei, T.-d. Xia, J. Ma, J.-f. Dai, W.-j. Feng, Q. Wang, P.-x. Yan, Growth Mechanism of Cu Nanopowders Prepared by Anodic Are Plasma, Transactions of Nonferrous Metals Society of China, 16 (2006) 168-172.

[105] A. Shashurin, M. Keidar, Factors Affecting the Size and Deposition Rate of the Cathode Deposit in an Anodic Arc Used to Produce Carbon Nanotubes, Carbon, 46 (2008) 1826-1828.

[106] E. Hontañón, J.M. Palomares, M. Stein, X. Guo, R. Engeln, H. Nirschl, F.E. Kruis, The Transition from Spark to Arc Discharge and Its Implications with Respect to Nanoparticle Production, Journal of Nanoparticle Research, 15 (2013) 1957.

[107] N. Karousis, I. Suarez-Martinez, C.P. Ewels, N. Tagmatarchis, Structure, Properties, Functionalization, and Applications of Carbon Nanohorns, Chemical Reviews, 116 (2016) 4850-4883.

[108] D.J. Babu, T. Herdt, S. Okeil, M. Bruns, R. Staudt, J.J. Schneider, Bud Type Carbon Nanohorns: Materials for High Pressure CO_2 Capture and Li-Ion Storage, Journal of Materials Chemistry A, 4 (2016) 14267-14275.

[109] G. Pagona, G. Mountrichas, G. Rotas, N. Karousis, S. Pispas, N. Tagmatarchis, Properties, Applications and Functionalisation of Carbon Nanohorns, International Journal of Nanotechnology, 6 (2009) 176-195.

[110] C.-M. Yang, D. Kasuya, M. Yudasaka, S. Iijima, K. Kaneko, Microporosity Development of Single-Wall Carbon Nanohorn with Chemically Induced Coalescence of the Assembly Structure, 2004.

[111] F.A. Abuilaiwi, T. Laoui, M. Al-Harthi, M.A. Atieh, Modification and Functionalization of Multiwalled Carbon Nanotube (Mwcnt) via Fischer Esterification, Arabian Journal for Science and Engineering, 35 (2010) 37-48.

[112] Rike Yudianti, Holia Onggo, Sudirman, Yukie Saito, Tadahisa Iwata, J.-i. Azuma, Analysis of Functional Group Sited on Multi-Wall Carbon Nanotube Surface, The Open Materials Science Journal, 5 (2011) 6.

[113] S. Gómez, N.M. Rendtorff, E.F. Aglietti, Y. Sakka, G. Suárez, Surface Modification of Multiwall Carbon Nanotubes by Sulfonitric Treatment, Applied Surface Science, 379 (2016) 264-269.

[114] H. Murphy, P. Papakonstantinou, T.I.T. Okpalugo, Raman Study of Multiwalled Carbon Nanotubes Functionalized with Oxygen Groups, Journal of Vacuum Science & Technology B: Microelectronics and Nanometer Structures Processing, Measurement, and Phenomena, 24 (2006) 715-720.

[115] I. Agirrezabal-Telleria, I. Gandarias, P.L. Arias, Heterogeneous Acid-Catalysts for the Production of Furan-Derived Compounds (Furfural and Hydroxymethylfurfural) from Renewable Carbohydrates: A Review, Catalysis Today, 234 (2014) 42-58.

[116] I. Agirrezabal-Telleria, J. Requies, M.B. Güemez, P.L. Arias, Pore Size Tuning of Functionalized SBA-15 Catalysts for the Selective Production of Furfural from Xylose, Applied Catalysis B: Environmental, 115-116 (2012) 169-178.

[117] N. Akiya, P.E. Savage, Roles of Water for Chemical Reactions in High-Temperature Water, Chemical Reviews, 102 (2002) 2725-2750.

[118] N. Mohamad, T.L.K. Yong, Production of Furfural from Oil Palm Frond via Green Chemicals Using Supercritical Ethanol and Formic Acid, Journal of the Japan Institute of Energy, 94 (2015) 835-840.

[119] E. Sairanen, R. Karinen, J. Lehtonen, Comparison of Solid Acid-Catalyzed and Autocatalyzed C5 and C6 Sugar Dehydration Reactions with Water as a Solvent, Catalysis Letters, 144 (2014) 1839-1850.

[120] R.L. Manfro, T.P.M.D. Pires, N.F.P. Ribeiro, M.M.V.M. Souza, Aqueous-phase Reforming of Glycerol Using Ni-Cu Catalysts Prepared from Hydrotalcite-Like Precursors, Catalysis Science & Technology, 3 (2013) 1278-1287.

[121] R. Weingarten, G.A. Tompsett, W.C. Conner Jr, G.W. Huber, Design of Solid Acid Catalysts for Aqueous-Phase Dehydration of Carbohydrates: The Role of Lewis and Brønsted Acid Sites, Journal of Catalysis, 279 (2011) 174-182.

[122] V. Choudhary, S.I. Sandler, D.G. Vlachos, Conversion of Xylose to Furfural Using Lewis and Brønsted Acid Catalysts in Aqueous Media, ACS Catalysis, 2 (2012) 2022-2028.

[123] A. Najafi Chermahini, M. Nazeri, Esterification of the Levulinic Acid with n-Butyl and Isobutyl Alcohols over Aluminum-containing MCM-41, Fuel Processing Technology, 167 (2017) 442-450.

[124] K.Y. Nandiwale, P.S. Niphadkar, S.S. Deshpande, V.V. Bokade, Esterification of Renewable Levulinic Acid to Ethyl Levulinate Biodiesel Catalyzed by Highly Active and Reusable Desilicated H-ZSM-5, Journal of Chemical Technology & Biotechnology, 89 (2014) 1507-1515.

[125] N.A.S. Ramli, N. Hidayah, N.A. Saidina Amin, Esterification of Renewable Levulinic Acid to Levulinate Esters Using Amberlyst-15 as A Solid Acid Catalyst, 2016.

[126] M. Varkolu, V. Moodley, F.S.W. Potwana, S.B. Jonnalagadda, W.E. van Zyl, Esterification of Levulinic Acid with Ethanol over Bio-Glycerol Derived Carbon–Sulfonic-Acid, Reaction Kinetics, Mechanisms and Catalysis, 120 (2016) 69-80.

[127] C. Termvidchakorn, K. Faungnawakij, S. Kuboon, T. Butburee, N. Sano, T. Charinpanitkul, A Novel Catalyst of Ni Hybridized with Single-Walled Carbon Nanohorns for Converting Methyl Levulinate to γ-Valerolactone, Applied Surface Science.

[128] W.G. Cochran, Sampling Techniques. 2nd Edition, John Wiley & Sons, 1963.

APPENDIX

APPENDIX A

BASIC PROPERTIES OF METAL AND ACID

A.1 Basic properties of metal

Table A.1 Basic properties of metal

Species	Mw (g)	Density (g/cm^3)	Melting P (C)	Boiling P (C)
C	12.0	amorphous: 1.8–2.1 graphite: 2.27	3,550	3,825
Ni	58.7	near room temp: 8.91 liquid: 7.81	1,455	2,913
Cu	63.5	near room temp: 8.96 liquid: 8.02	1,085	2,562
Fe	55.8	near room temp: 13.81 liquid: 6.98	1,538	2,862
Pd	106.4	near room temp: 12.02 liquid: 10.38	1,555	2,963
Pt	195.1	near room temp: 21.45 liquid: 19.77	1,768	3,825

A.2 Radius of each metal

Table A.2 Atomic radius of metal

Species	Atomic radius (pm)		
	Empirical radius	Van der Waals radius	Covalent radius
C	sp^3: 77 sp^2: 73 sp: 69	170	No data
Ni	124	163	124
Cu	128	140	132
Fe	126	No data	132-152
Pd	137	163	139
Pt	139	175	136

A.3 Basic properties of sulfuric acid and acetic acid

Table A.3 Basic properties of sulfuric acid and acetic acid

Acid	Formula	Mw (g)	Density (g/cm^3)	Boiling P (C)	Acidity (pK_a)
Sulfuric acid	H_2SO_4	98	1.84	337	-3,1.99
Acetic acid	$C_2H_4O_2$	60	1.05	118	4.76

APPENDIX B
CALIBRATION DATA

B.1 Calibration curve of xylose for HPLC analysis @Nanotechnology center (NSTDA)

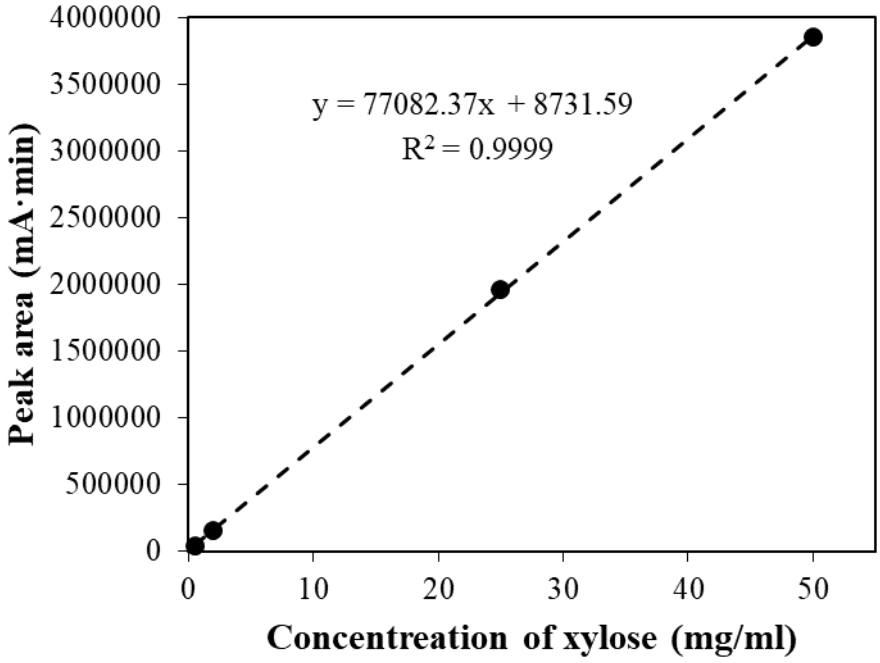

Figure B.1 Calibration curve of xylose for HPLC analysis @Nanotechnology center (NSTDA)

B.2 Calibration curve of furfural for HPLC analysis @Nanotechnology center (NSTDA)

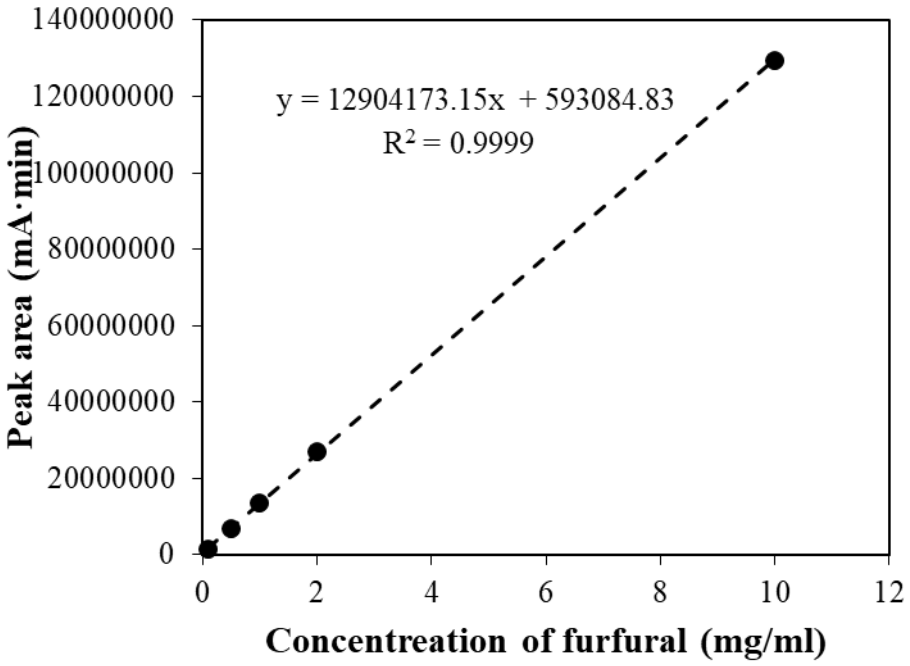

Figure B.2 Calibration curve of furfural for HPLC analysis @Nanotechnology center (NSTDA)

B.3 Calibration curve of xylose for HPLC analysis @Kyoto University

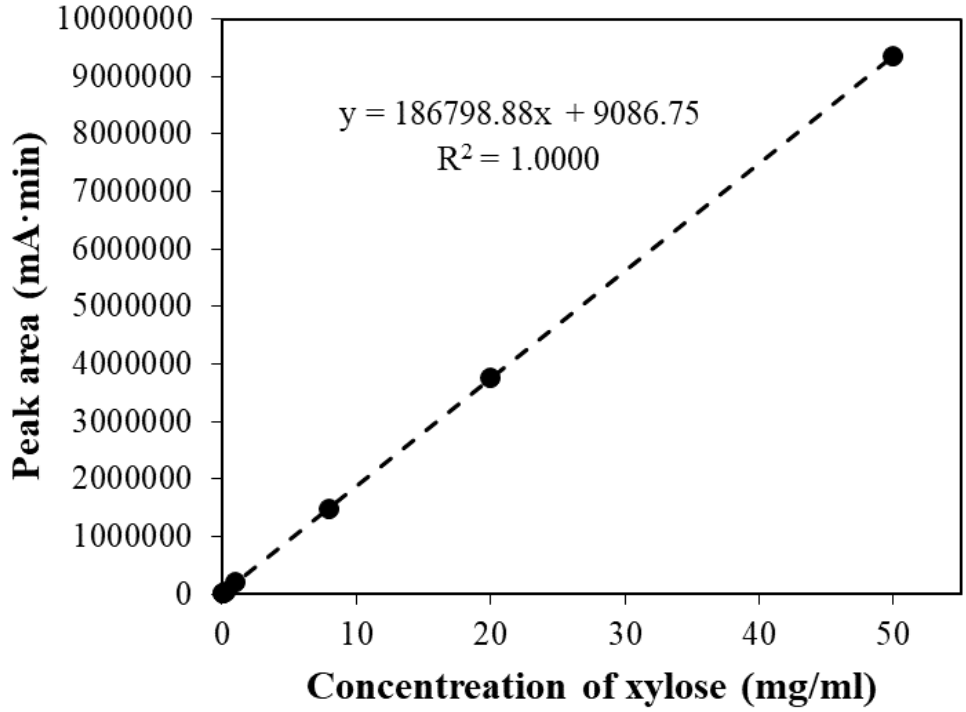

Figure B.3 Calibration curve of xylose for HPLC analysis @Kyoto University

B.4 Calibration curve of furfural for HPLC analysis @Kyoto University

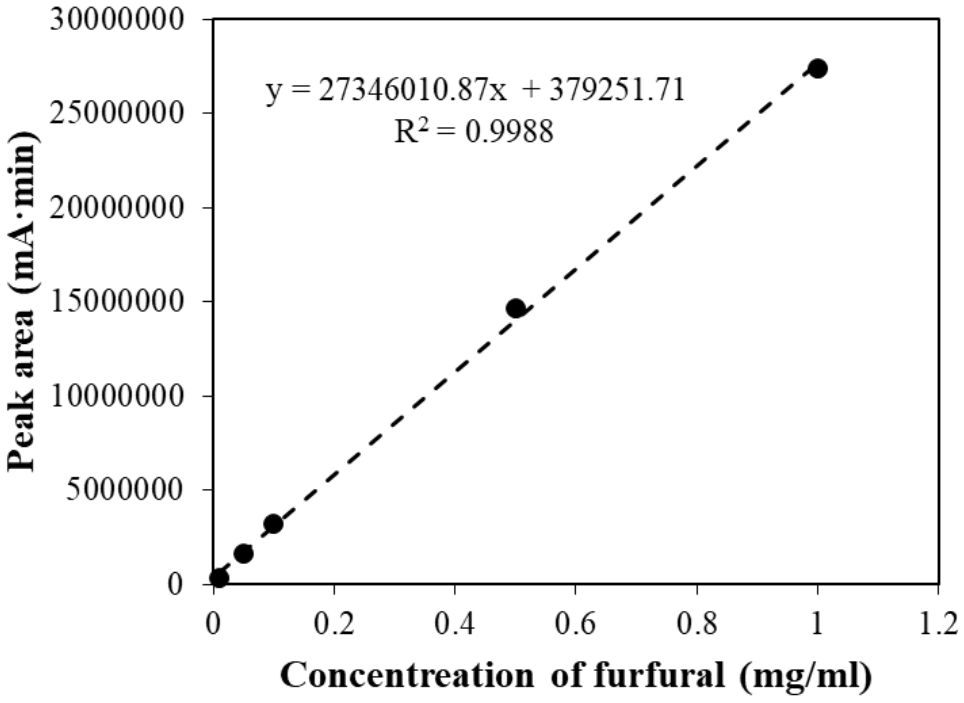

Figure B.4 Calibration curve of furfural for HPLC analysis @Kyoto University

B.5 Calibration curve of methyl levulinate for GC analysis

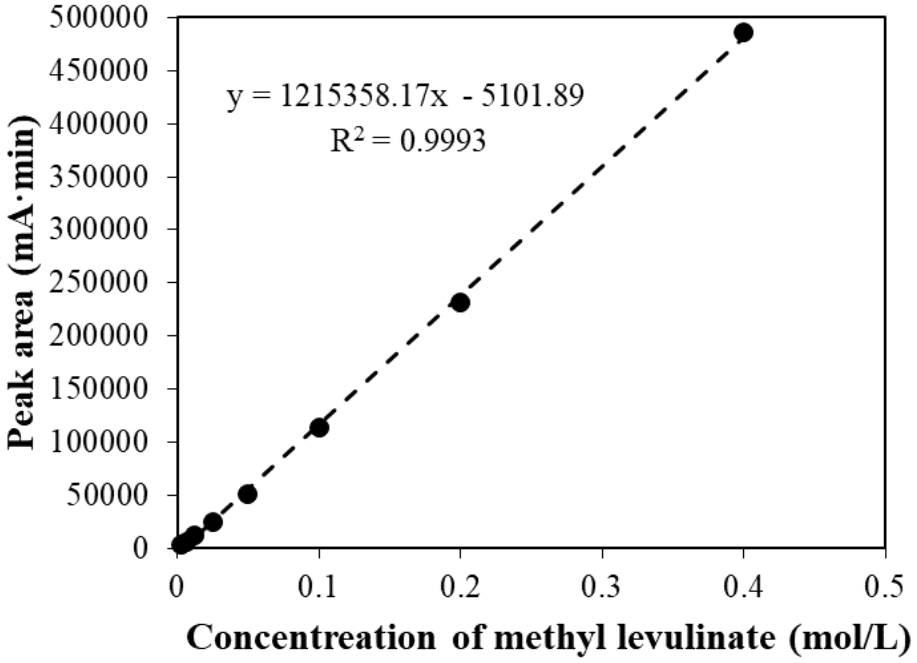

Figure B.5 Calibration curve of methyl levulinate for GC analysis

B.6 Calibration curve of methyl levulinate for GC analysis

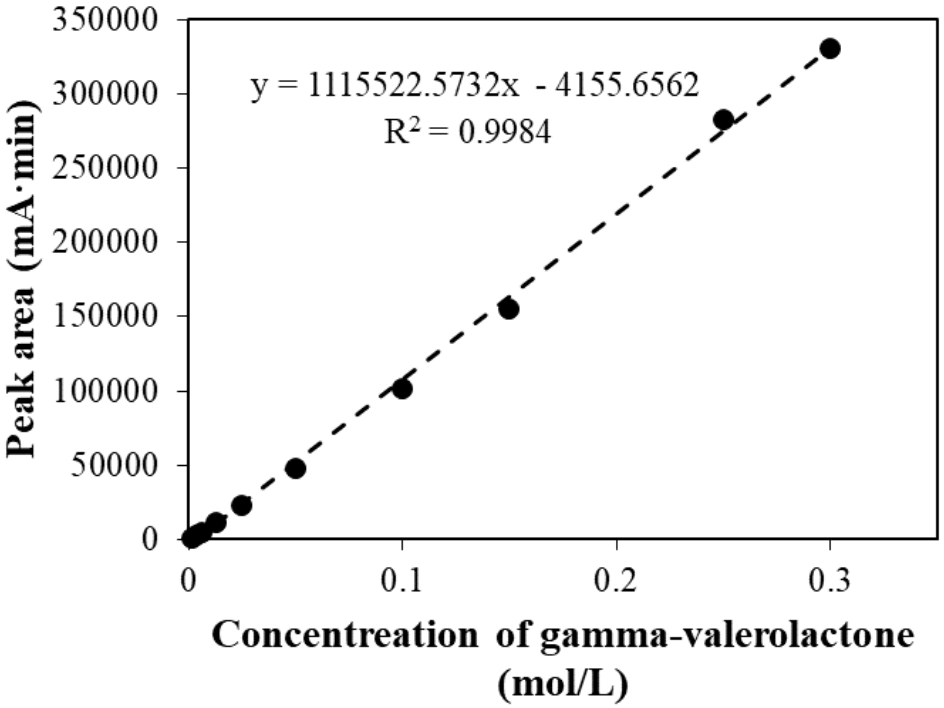

Figure B.6 Calibration curve of methyl levulinate for GC analysis

B.7 Calibration curve of levulinic acid for HPLC analysis

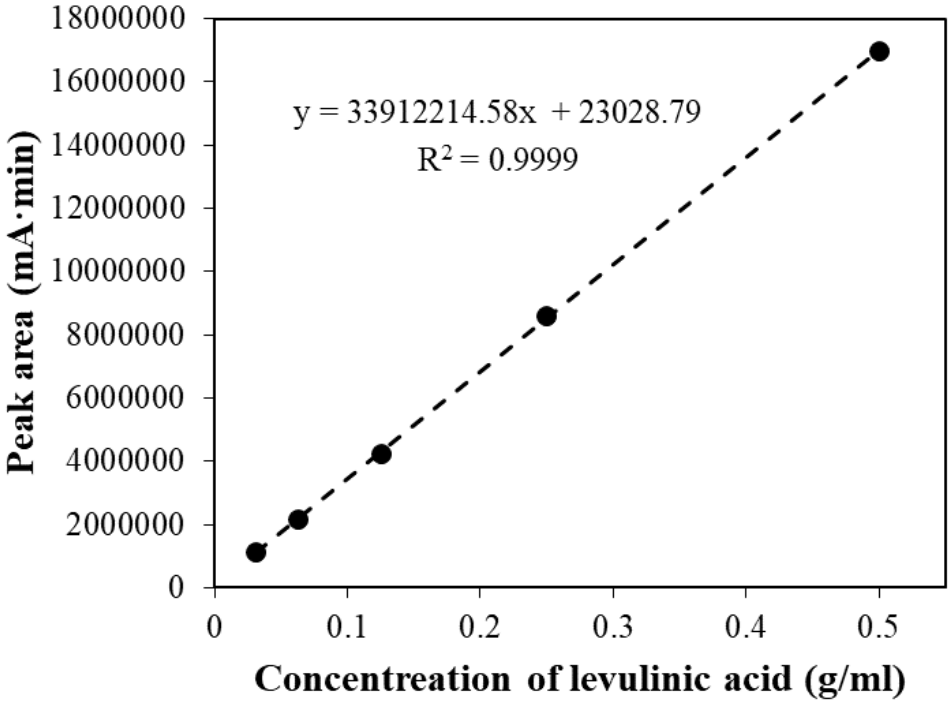

Figure B.7 Calibration curve of levulinic acid for HPLC analysis

B.8 Calibration curve of ethyl levulinate for HPLC analysis

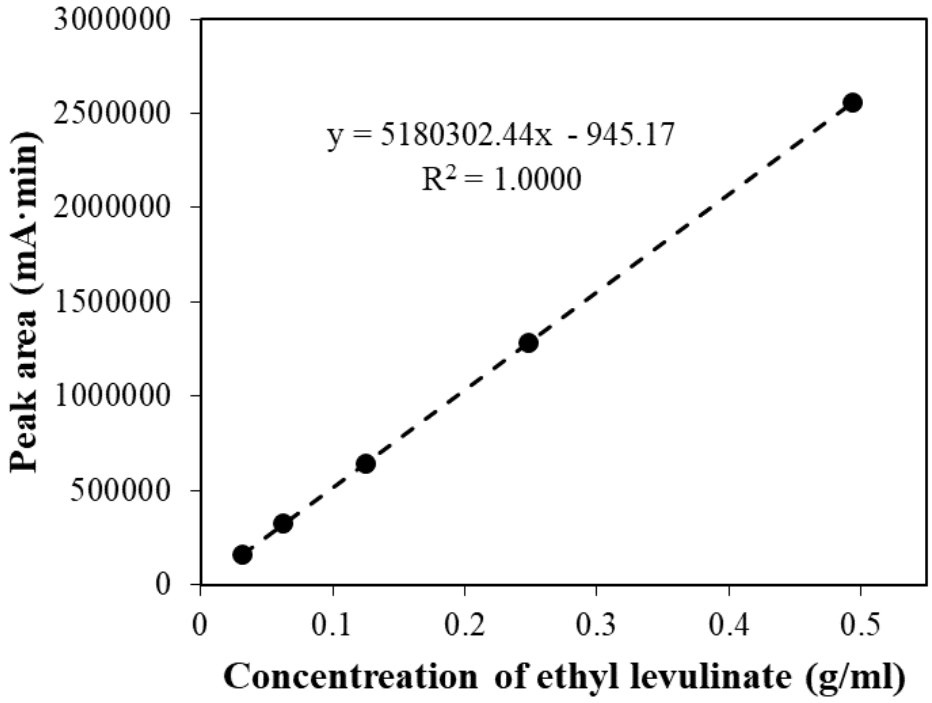

Figure B.8 Calibration curve of ethyl levulinate for HPLC analysis

APPENDIX C
CHROMATOGRAM DATA

C.1 Chromatogram of dehydration of xylose to furfural by HPLC

C.1.1 Chromatogram from UV detector

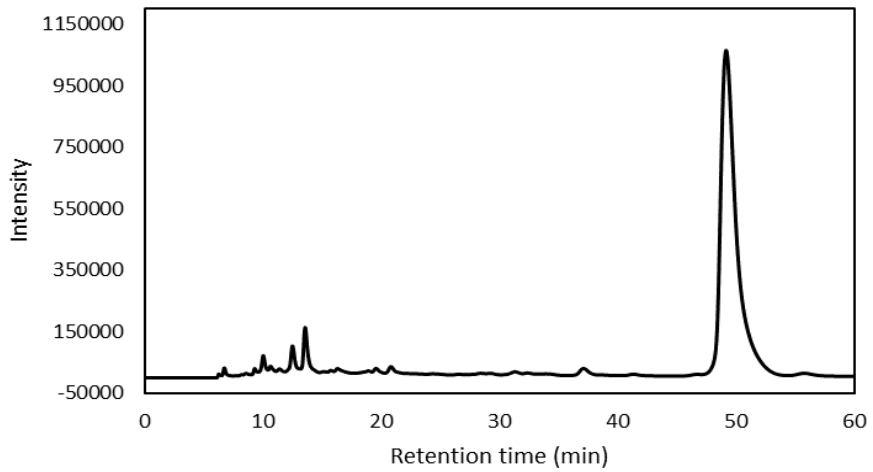

Figure C.1 Chromatogram of dehydration of xylose to furfural by HPLC (UV detector)

C.1.2 Chromatogram from RID detector

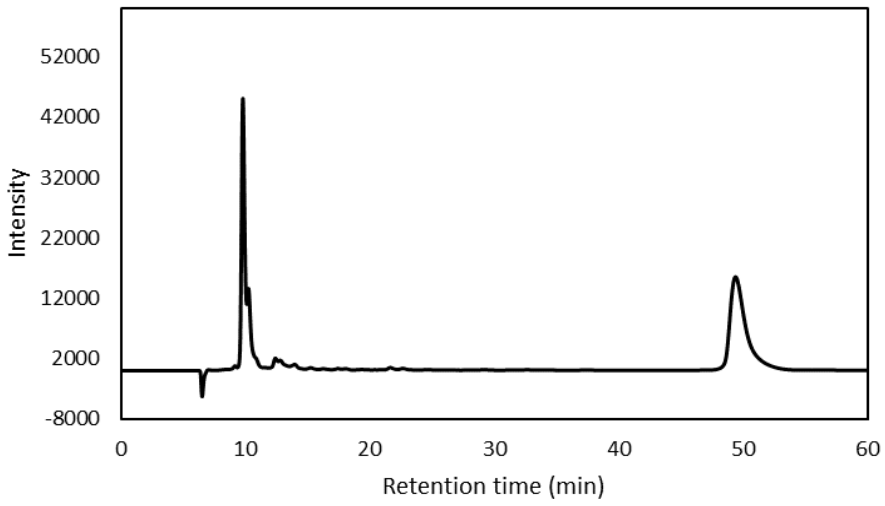

Figure C.2 Chromatogram of dehydration of xylose to furfural by HPLC (RID detector)

C.2 Chromatogram of transfer hydrogenation of methyl levulinate to γ-valerolactone by GC

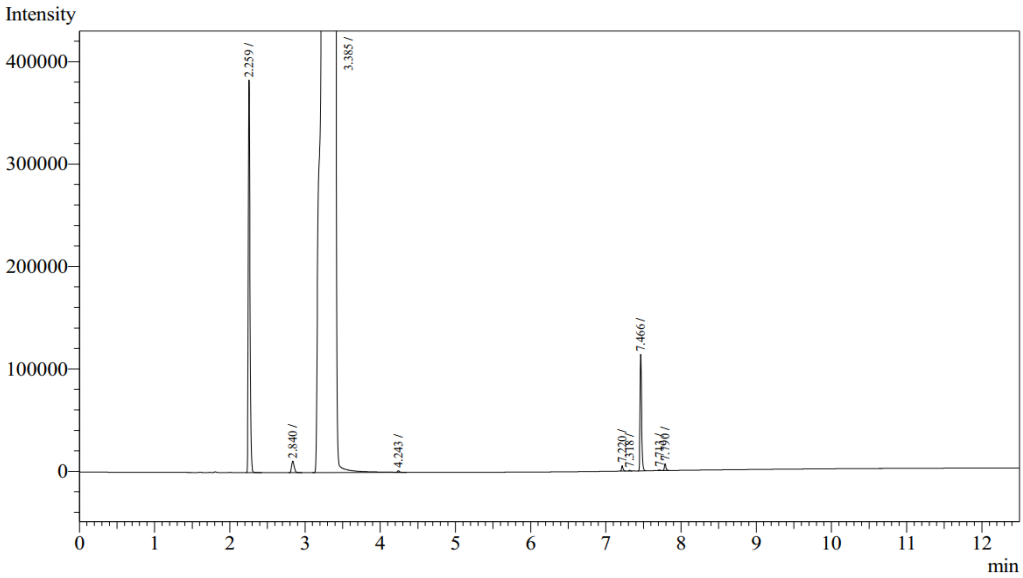

Figure C.3 Chromatogram of transfer hydrogenation of methyl levulinate to γ-valerolactone by GC

C.3 Chromatogram of esterification of levulinic acid to ethyl levulinate by HPLC

C.3.1 Chromatogram from UV detector

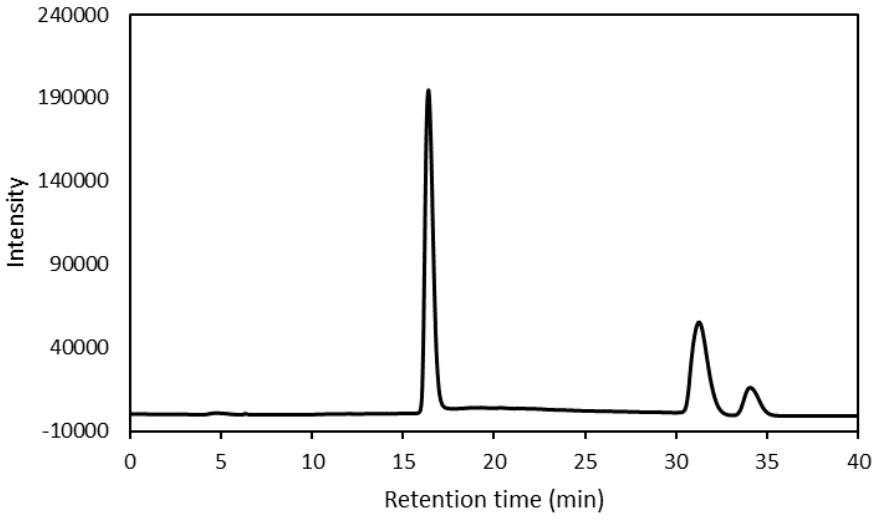

Figure C.4 Chromatogram of esterification of levulinic acid to ethyl levulinate by HPLC (UV detector)

C.3.2 Chromatogram from RID detector

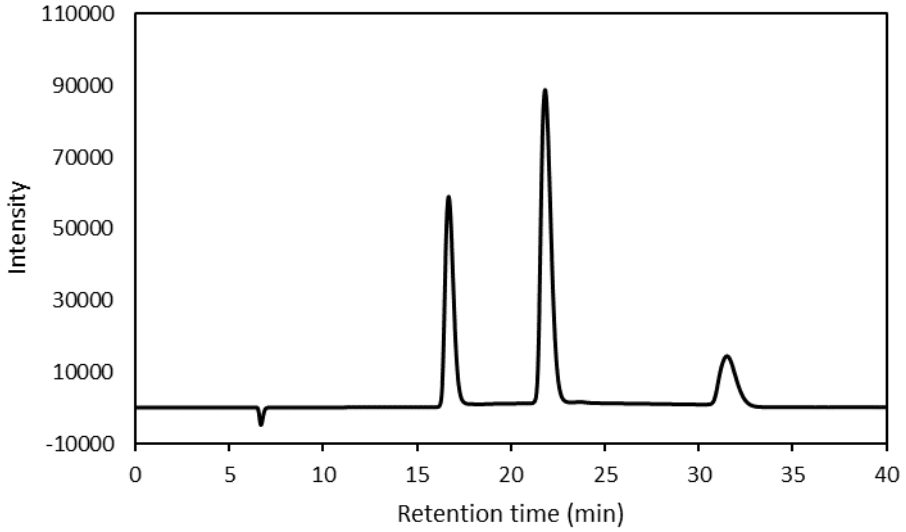

Figure C.5 Chromatogram of esterification of levulinic acid to ethyl levulinate by HPLC (RID detector)

APPENDIX D

RAMAN SPECTRA DATA

D.1 Raman spectra of acid treated CNHs by sulfuric acid (SA-CNHs) with difference ultrasonicating time

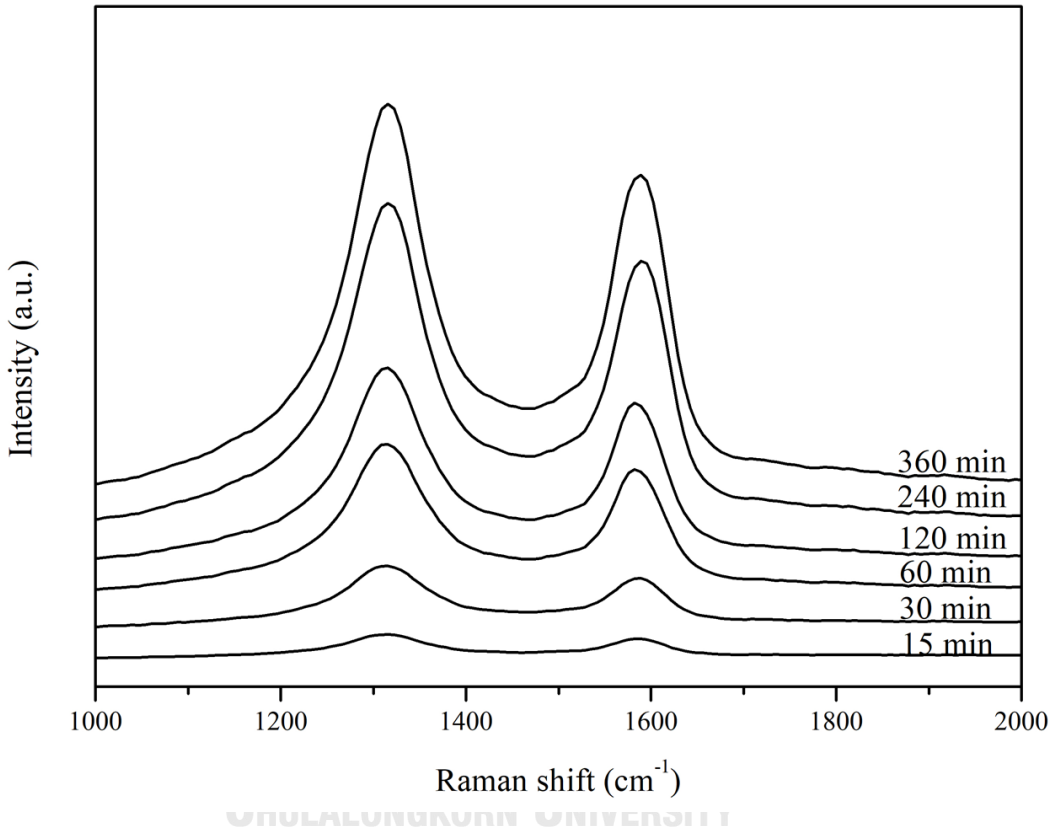

Figure D.1 Raman spectra of acid treated CNHs by sulfuric acid (SA-CNHs) with difference ultrasonicating time

D.2 Raman spectra of acid treated CNHs by acetic acid (AA-CNHs) with difference ultrasonicating time

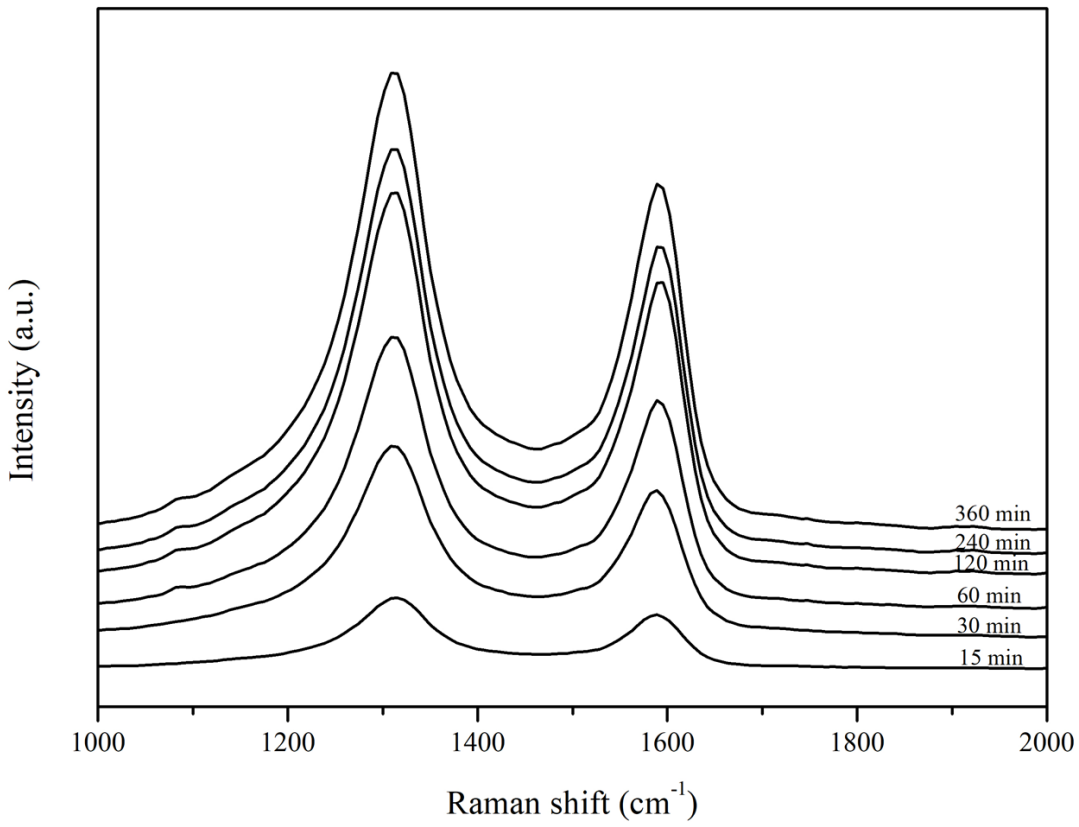

Figure D.2 Raman spectra of acid treated CNHs by acetic acid (AA-CNHs) with difference ultrasonicating time

APPENDIX E

QUANTITATIVE DATA

E.1 Dehydration of xylose in parr reactor at 170 °C, reaction time=4 h, and initial P=15 bar

Table E.1 Dehydration of xylose in parr reactor at 170 °C, reaction time=4 h, and initial P=15 bar

No.	Catalysts	Xylose conversion (%)	Furfural yield (%)	Furfural selectivity (%)
1	Without catalyst	33.3	29.8	96.4
2	CNTs	65.5	34.0	51.9
3	oxd-CNTs	59.2	35.5	59.6
4	CNHs	75.8	40.4	53.7
5	oxd-CNHs	88.9	39.8	44.7

E.2 Dehydration of xylose in in-house batch reactor at 170 °C, reaction time=4 h, and initial P=15 bar

Table E.2 Dehydration of xylose in in-house batch reactor at 170 °C, reaction time=4 h, and initial P=15 bar

No.	Catalysts	Xylose conversion (%)	Furfural yield (%)	Furfural selectivity (%)
1	Without catalyst	43.1	27.9	65.6
2	CNHs	38.7	22.1	57.7
3	Oxd-CNHs	45.8	28.0	61.3
4	Ni/CNHs-10	94.7	29.4	31.1
5	oxd-Ni/CNHs-10	86.8	38.1	44.1
6	red-oxd-Ni/CNHs-10	93.9	21.0	22.4
7	Cu/CNHs-10	44.7	26.2	58.8
8	oxd-Cu/CNHs-10	52.4	32.5	61.9
9	red-oxd-Cu/CNHs-10	48.8	30.3	62.9
10	NiCu/CNHs-5:5	63.9	31.6	49.5
11	oxd-NiCu/CNHs-5:5	83.1	34.8	41.9
12	red-oxd-NiCu/CNHs-5:5	89.1	37.9	42.7

E.3 Transfer hydrogenation of ML to GVL at 200°C, reaction time=3 h

Table E.3 Transfer hydrogenation of ML to GVL at 200°C, reaction time=3 h

No.	Catalysts	ML conversion (%)	GVL yield (%)	GVL selectivity (%)
1	Without catalyst	6.5	3.3	51.4
2	CNHs	4.7	2.9	61.4
3	Ni/CNHs-10	9.5	8	84.1
4	Cu/CNHs-10	16.8	0.0	0.0
5	red-Ni/CNHs-10	38.7	38.2	98.7
6	oxd-Ni/CNHs-10	12.8	8.7	68.5
7	red-oxd-Ni/CNHs-10	96.2	89.4	93.0
8	red-oxd-Cu/CNHs-10	12.6	0.4	2.9
9	NiCu/CNHs-7:3	17.4	2.2	12.7
10	NiCu/CNHs-5:5	5.7	1.6	29.1
11	red-oxd-NiCu/CNHs-5:5	39.1	24.2	61.9
12	NiCu/CNHs-3:7	8.5	0.8	9.2

E.4 Effect of reaction temperature on transfer hydrogenation of ML to GVL, reaction time=3 h

Table E.4 Effect of reaction temperature on transfer hydrogenation of ML to GVL, reaction time=3 h

No.	Reaction temperature (°C)	ML conversion (%)	GVL yield (%)	GVL selectivity (%)
1	140	2.7	0.2	5.8
2	170	6.2	2.9	46.5
3	200	96.2	89.4	93.0

E.5 Reusability of catalyst in transfer hydrogenation of ML to GVL at 200°C, reaction time=3 h

Table E.5 Reusability of catalyst in transfer hydrogenation of ML to GVL at 200°C, reaction time=3 h

Cycles	ML conversion (%)	GVL yield (%)	GVL selectivity (%)
1st	96.2	89.4	93.0
2nd	96.1	87.7	91.2
3rd	93.6	85.0	90.8
4th	91.1	81.8	89.8
5th	89.3	79.0	88.5

E.6 Effect of amount of catalyst on esterification of LA to EL

Table E.6 Effect of amount of catalyst on esterification of LA to EL at reaction temperature= 140 °C, reaction time = 90 min, initial LA:EtOH=1:5

No.	Amount of catalyst (mg)	LA conversion (%)	EL yield (%)	EL selectivity (%)
1	0	43.5	39.4	91.0
2	15	37.6	37.1	98.6
3	20	38.1	34.3	89.9
4	25	38.9	36.5	93.9

E.7 Effect of reaction temperature on esterification of LA to EL

Table E.7 Effect of reaction temperature on esterification of LA to EL at 15 mg of catalyst, reaction time = 90 min, initial LA:EtOH=1:5

No.	Reaction temperature (°C)	LA conversion (%)	EL yield (%)	EL selectivity (%)
1	100	12.3	12.0	97.8
2	120	26.3	22.8	86.6
3	140	37.6	37.1	98.6

E.8 Effect of initial LA:EtOH molar ratio on esterification of LA to EL

Table E.8 Effect of reaction temperature on esterification of LA to EL at 15 mg of catalyst, at reaction temperature= 140 °C, reaction time = 90 min

No.	Reaction temperature (°C)	LA conversion (%)	EL yield (%)	EL selectivity (%)
1	1:3	50.0	37.5	75.0
2	1:5	37.6	37.1	98.6
3	1:7	36.0	30.4	84.4

APPENDIX F
SAMPLING SIZE CALCULATION

Sample size was calculated by Cochran formula [128]:

$$n = \frac{P(1-P)Z^2}{d^2}$$

Where:

n is sample size,

d is the desired level of precision,

P is the proportion of the population which has the attribute in question

In this study,

Confidence level = 95% (Z Score = 1.96).

d = 0.05

P = 0.3

∴ Sample size will be 323 particles

APPENDIX G
PUBLICATIONS

G.1 International journal

1. Chompoopitch Termvidchakorn, Vorranutch Itthibenchapong, Siripit Songtawee, Busaya Chamnankid, Supawadee Namuangruk, Kajornsak Faungnawakij, Hirofumi Hinode. (2017). Dehydration of D-xylose to furfural using acid-functionalized MWCNTs catalysts. Advances in Natural Sciences: Nanoscience and Nanotechnology, 8(3), 035006.

2. Chompoopitch Termvidchakorn, Noriaki Sano, Hajime Tamon, Nawin Viriya-Empikul, Kajornsak Faungnawakij, Tawatchai Charinpanitkul. (2017). Conversion of D-Xylose to Furfural via Catalytic Dehydration Using Carbon Nanohorns Hybridized with NiCu Nanoparticles. Journal of the Japan Institute of Energy, 96(9), 380-385.

3. Chompoopitch Termvidchakorn, Kajornsak Faungnawakij, Sanchai Kuboon, Teera Butburee, Noriaki Sano, Tawatchai Charinpanitkul. A novel catalyst of Ni hybridized with single-walled carbon nanohorns for converting methyl levulinate to γ-valerolactone, Applied Surface Science, In Press.

G.2 International conference

1. Chompoopitch Termvidchakorn, Patipat Supina, Buratouch Chonvirachkul, Nawin Viriya-empikul, Kajornsak Faungnawakij and Tawatchai Charinpanitkul. “Modification of MWCNT Surface for Supporting Pd Catalyst to be used in Hydrodeoxygenation of Octanoic acid”, The 3rd Joint Conference in Renewable Energy and Nanotechnology (JCREN 2014), December 22-23, 2014, Kanchanaburi, Thailand

2. Chompoopitch Termvidchakorn, Nawin Viriya-empikul, Kajornsak Faungnawakij, Noriaki Sano, and Tawatchai Charinpanitkul. “Catalytic activity of sulfonated carbon nanotubes in dehydration of xylose”, The 4th Joint Conference on

Renewable Energy and Nanotechnology (JCREN 2015), December 5-7, 2015, Matsuyama, Japan

3. Chompoopitch Termvidchakorn, Noriaki Sano, Hajime Tamon, Nawin Viriya-empikul, Kajornsak Faungnawakij, and Tawatchai Charinpanitkul. "Conversion of xylose to furfural via catalytic dehydration using carbon nanohorns hybridized with NiCu alloy", The 5th Joint Conference in Renewable Energy and Nanotechnology (JCREN 2016), December 8-9, 2016, Kuala Lumpur, Malaysia

4. Chompoopitch Termvidchakorn, Kajornsak Faungnawakij, Sanchai Kuboon, Noriaki Sano, and Tawatchai Charinpanitkul. "Novel Catalysts of Ni, NiCu, and Cu Hybridized with Single-Walled Carbon Nanohorns for converting Methyl Levulinate to γ-Valerolactone", The 10th International Conference on Advanced Nano Materials, September 11-13, 2017, Guildford, England

5. Chompoopitch Termvidchakorn, Kajornsak Faungnawakij, Noriaki Sano, and Tawatchai Charinpanitkul. "Effect of Ultrasonicating Time on Sulfonated Single-Walled Carbon Nanohorns", The 6th Joint Conference in Renewable Energy and Nanotechnology (JCREN 2017), October 12-14, 2017, Bangkok, Thailand

VITA

Miss Chompoopitch Termvidchakorn was born on June 18th, 1991 in Bangkok, Thailand. She graduated primary education from Somthavil school and secondary education from Horwang school. She obtained her Bachelor in Chemical Engineering from Chulalongkorn University with second class honors in 2013. She continuously conducted her Ph.D. in Center of Excellence in Particle Technology (CEPT), Department of Chemical Engineering, Faculty of Engineering, Chulalongkorn University. During her Ph.D. study, she got an opportunity for research aboard for one year at Kyoto University, Kyoto, Japan under financial support from Overseas Research Experience Scholarship for Graduate Student, Chulalongkorn University. She received financial support from Doctoral Degree Chulalongkorn University 100th Year Birthday Anniversary scholarship from Chulalongkorn University throughout her doctoral period as well.